SINGLE-MOLECULE FLUORESCENCE MICROSCOPY STUDIES OF FLUORESCENT PROBES IN THIN FILMS AND ON NANOPARTICLE SURFACES

A Thesis Submitted to the College of

Graduate Studies and Research

In Partial Fulfillment of the Requirements

For the Degree of Doctor of Philosophy

In the Department of Chemistry

University of Saskatchewan

Saskatoon

By

YIN LU

PERMISSION TO USE

In presenting this thesis in partial fulfillment of the requirements for a postgraduate degree from the University of Saskatchewan, I agree that the libraries of the University may make it freely available for inspection. Permission for copying of this thesis in any manner, in whole or in part, for scholarly purposes may be granted by the professor or professors who supervised my thesis work or, in their absence, by the Department or the Dean of the College in which my thesis work was done. It is understood that any copying or publication or use of this thesis or parts thereof for financial gain shall not be allowed without my written permission. It was also understood that proper recognition shall be given to me and to the University of Saskatchewan in any scholarly use which may be made of any material in my thesis.

Requests for permission to copy or to make other use of material in this thesis in whole or part should be address to:

Head of Department of Chemistry

University of Saskatchewan

110 Science Place

Saskatoon, Saskatchewan (S7N 5C9)

ABSTRACT

Single-molecule (SM) fluorescence spectroscopy has become a useful and important experimental approach for investigating the optical properties of chemical systems. In this thesis, four subprojects in the field of SM fluorescence spectroscopy are presented in which SM spectroscopy has provided invaluable experimental insight into the systems of interest.

In the first project, the photophysical properties of Calcium-Green 1 (CG-1), a calcium-ion indicator, were studied at both the ensemble and SM levels. CG-1 is non-fluorescent in the absence of Ca^{2+} and becomes strongly fluorescent when bound to Ca^{2+}. In the ensemble measurements, the absorption and fluorescence spectra were collected under various Ca^{2+} concentrations. In addition, the fluorescence lifetime of CG-2 was also studied as a function of $[Ca^{2+}]$. From SM measurements, the photobleaching time and fluorescence intensity distributions of CG-1 were studied both in the presence and in absence of Ca^{2+}. The results were compared with those obtained for the dual-fluorophoric variant, Calcium-Green 2 (CG-2), whose photophysical properties have been investigated by previous researchers. The experimental results reveal that CG-1 can exist in two different forms: a highly-quenched form due to the occurrence of photoinduced electron transfer (PET) in the absence of Ca^{2+}, and a strongly fluorescent form when bound to Ca^{2+}.

The second project is a continuation of a previous study on CG-2. In the dual-chromophore CG-2 system, energy transfer between chromophores is controlled by the orientation and spatial separation between chromophores. Dual polarization fluorescence microscopy was used to determine the relative conformation of the two fluorophores in the emissive form of CG-2. Distributions of fluorescence polarization of individual CG-2 molecules were collected for both Ca^{2+}-free and Ca^{2+}-saturated conditions. The experimental polarization results were compared to those calculated from a simple geometric model based on randomly-orientated fluorescent dimers. The results show good agreement with previous calculations of the molecular conformation of CG-2. This indicates that the dual polarization imaging approach has significant potential as a general tool for characterizing chromophore orientation in coupled-fluorophore systems.

In the third project, Nile Red (NR), a solvatochromic lipid stain, was incorporated into phase separated Langmuir-Blodgett (LB) films composed of arachidic acid (AA) and perfluorotetradecanoic acid (PA). According to previous studies by atomic force microscopy (AFM), two types of separated domains are formed in the LB films: micron-sized hexagonal discontinuous domains that are exclusively comprised of AA, and the surrounding continuous domains which are enriched in PA. The photophysical properties of NR were characterized in the two physically and chemically distinct domains via bulk and SM fluorescence measurements. In addition to fluorescence microscopy, fluorescence confocal spectromicroscopy was also applied in the ensemble measurements to determine the spectral properties of NR in different sub-environments. Experimental results indicated that a small sub-population of dye molecules localize on the perfluorinated regions of the sample, but this sub-population is spectroscopically indistinguishable from that associated with the hydrogenated domains. Contrast in images was primarily due to preferential accumulation of the hydrophobic dye on the hydrophobic regions of the LB films.

In the final project, the fluorescence quenching behavior of a strongly fluorescent probe Alexa Fluor 514 (AF514) was investigated when it was covalently bound to gold metal protected clusters (AuMPC) with negligible plasmon bands. The fluorescence emission of the dye-AuMPCs system was characterized at different dye/Au MPC loading ratios with a combination of steady state and time-resolved ensemble spectroscopic measurements. It was found that the extent of fluorescence quenching in the system was small. After correction of inner filter effects, the results from bulk measurement demonstrate that the weak quenching is due to static quenching of the dye by the AuMPCs. SM measurements provided further support for the bulk measurements, with the fluorescence intensity of coupled AF514 molecules being comparable with that of unconjugated molecules. The photobleaching of the dye-AuMPC conjugates took place as a series of consecutive photobleaching events, without additional blinking dynamics within the time resolution of the experiment. These results suggest that the fluorophores on the AuMPCs are either entirely quenched, or remaining unquenched, as is consistent with the ensemble measurements.

ACKNOWLEDGEMENTS

I would like to express my gratitude to all whose guidance and advice allowed me to grow, and without whom this work would have never been possible. It has been a wonderful experience to work under the supervision of Dr. Matthew F. Paige, whose guidance, patience, and enthusiasm helped me get through the periods of frustration association with ups and downs of this work. My thanks and gratitude to him for his constant inspiration and supports are beyond words.

My sincere thanks also go to my present and past committee members Dr. Richard. Bowles, Dr. Ian Burgess, Dr. Ronald Steer, Dr. Jeremy Lee for their invaluable suggestion and advice. I further would like to express my sincere thanks to Dr. Sophie Brunet for giving me the permission to use instrumental facilities and to Dr. Robert Scott for his advice on gold nanoparticle synthesis and characterization.

I would also like to thank the present and past members of my research group Shatha Qaqish, J. Valiani, Zahid Islam, Sunish Sugunan, Jaclyn O'Brien, Terri Thunder, Hessam Younesi Arghi, and Ala' Eftaiha for their support and cooperation. I am also thankful to all the collaborators Robyn Porterfield (Concordia University) for her great efforts on the single molecule study of Nile Red, Adam Leontowich, Christina Calver, and Mita Dasog (Dr. Scott's group) for their amazing work on gold nanoparticle synthesis. My appreciation also goes to my dearest friends both inside and outside Canada: Mintang Liu, Josiah Obiero, Eshwari Addala, Alessia Guo, Wenbo Hou, Ivan Wang, Gaozhen Liu, and Dragon.

I would like to thank NSERC and University of Saskatchewan for granting the research project (to Dr. Matthew F. Paige) and financial assistance without which the work would not been possible to carry out.

Finally, I thank my family for their love and support. My love goes out to my mom Baoling Dai and my sister Iris Lu, who have always stood by me throughout my life. Finally my deepest love goes to my husband De Li. I would like to express my heartiest gratitude for his company, sharing tough and happy moments and constant encouragement.

Dedicated

To my parents,

Late Yulin Lu

&

Baoling Dai

With love.

TABALE OF CONTENTS

LIST OF TABLES

LIST OF FIGURES

LIST OF ABBREVIATIONS

AA	Arachidic acid
AF514	AlexaFluor 514
AFM	Atomic force microscopy
APDs	Avalanche photodiodes
AuMPC	Gold metal protected cluster
BAPTA	1,2-bis (2- aminophenoxy) ethane-N,N,N',N'-tetra acetic acid
CG-1	Calcium-Green 1
CG-2	Calcium-Green 2
CCD	Charge coupled device
FIM	Field ion microscopy
Gly-CSA	Glycine-cysteamine
IC	Internal conversion
ICP-MS	Inductively-coupled-plasma mass-Spectrometry
ICT	Intramolecular charge transfer
ISC	Intersystem conversion
IVR	Internal vibrational relaxation
LB	Langmuir-Blodgett
MCP	Multichannel plate
MMFF	Merck molecular force field
NA	Numerical aperture
NR	Nile Red
NSOM	Near field scanning optical Microscopy
PA	Perfluorotetradecanoic acid
PET	Photoinduced electron Transfer
PMTs	Photomultiplier tubes
R6G	Rhodamine 6G
S_1	Singlet first excited state
SM	Single-molecule
SNARF	Seminaphtorhodafluor
SNR	Signal-to-noise ratio
STM	Scanning tunneling Microscopy
T_1	Triplet first excited state
TCSPC	Time-correlated single-photon counting
TICT	Twisted intramolecular charge transfer
TIRF	Total internal reflection fluorescence microscopy
USAF	United State Air Force
UV-vis	Ultraviolet-visible
1D	One-dimensional
2D	Two-dimensional

CHAPTER 1

INTRODUCTION

1.1 Single-molecule Techniques

The goal of single-molecule (SM) measurements is to directly or indirectly "visualize" an individual molecule, and collect information about the molecule in the absence of ensemble averaging. Through SM measurements, the behavior of an individual molecule can be measured and analyzed. In contrast with ensemble or bulk studies where only average characteristics can be observed, SM techniques allow the construction of a frequency histogram of values for an experimental parameter. The new information that the distribution provides (i.e. the shape of the full distribution) can provide opportunities for probing various properties and processes which could not be fully understood from bulk measurements.

Many techniques have the ability to observe one molecule or one particle at a time. An example of this is the "patch-clamp" technique, which was one of the earliest means of detecting single molecules.[1] The rapid development of microscopic imaging has enabled the detection of molecules or atoms on material surfaces via scanning tunneling microscopy (STM) and field ion microscopy (FIM).[2,3] In addition, other approaches including atomic force microscopy (AFM) and atom trapping, by either optical or magnetic tweezers, are also well suited for SM measurements, especially in biological and biochemical systems.[4-6]

Of particular recent interest is the SM approach known as SM fluorescence microscopy, and this is the general subject of this thesis. In 1989, the fluorescence signal of an individual molecule in condensed phase was first successfully observed by Moerner et al.[7] Since then, SM fluorescence imaging has become one of the most convenient and widespread techniques to observe individual molecules.[8-12] In single-molecule fluorescence measurements, an individual photoexcited fluorophore will emit fluorescence photons, which are discriminated from any unwanted background emission and collected by an ultra-sensitive detector. Time-dependent

dynamical studies at the SM level allow one to probe the unexpected fluctuations, heterogeneities, or stochastic changes in a number of photophysical parameters, such as fluorescence intensities, photobleaching times, spectral diffusion, and fluorescence polarization.

The overall objective of this thesis is to use SM spectroscopy as a tool to probe the fluorescence emission of individual molecules and to characterize how emission is affected by molecular conformation, charge transfer, and energy exchange. Serving as an important addition to conventional ensemble spectroscopy measurements, the major practical benefit of the SM measurements is that they can provide invaluable complementary information which is generally obscured by ensemble averaging.

1.2 Single-molecule Fluorescence Spectroscopy

Fluorescence detection has been widely applied as an ultrasensitive measurement technique long before it was applied to SM studies. The basic principle of fluorescence is well known (and is illustrated in the Jablonski diagram, Figure 1-1): when a molecule absorbs a photon in the UV-vis range, it can be excited from the ground state (S_0) into an electronic excited state S_n ($n \geq 1$, usually S_1). The excited molecule will relax back to the ground state by either non-radiative or radiative decay. The radiative decay from S_1 to S_0 is called fluorescence emission. There are a number of possible fates for a photoexcited molecule that do not lead to fluorescence emission, including fluorescence quenching (non-radiative decay to the ground state), and intersystem crossing (ISC) when the excited molecule converts to its triplet excited state. Fluorescence quenching can be trigged by a variety of molecular interactions including excited-state reactions, molecular rearrangements, energy transfer, and ground-state complexation. The energy of the emitted photon is usually smaller than the excitation photon. This can be attributed to the energy loss during the internal vibrational relaxation (IVR) process, whereby the energy is dissipated through interaction with solvent molecules. As a result, one often observes a spectral red shift of the fluorescence emission spectra in comparison to the absorption spectra (Stokes shift).

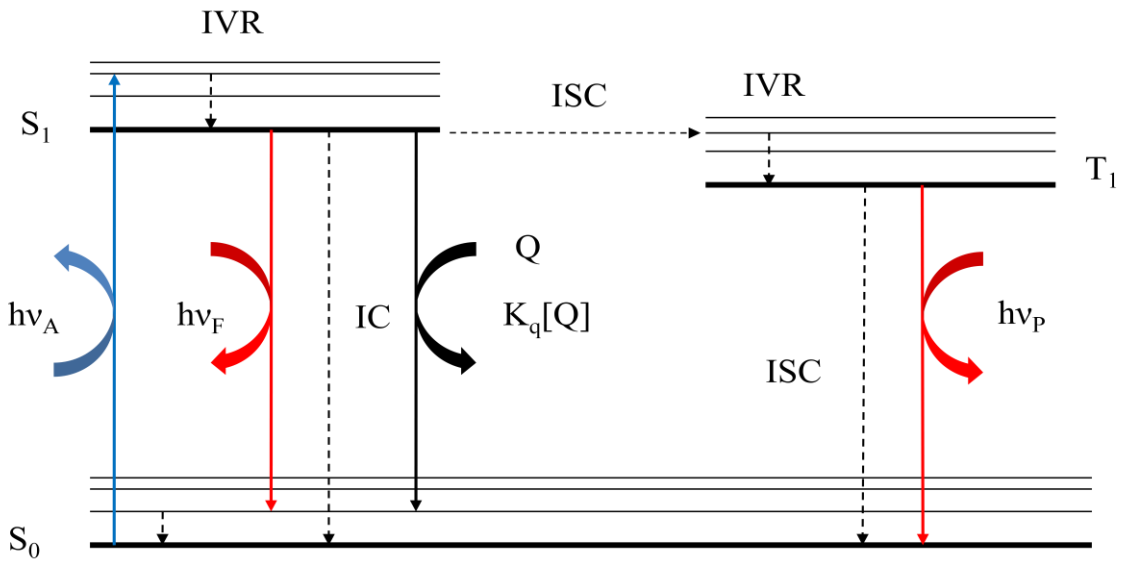

Figure 1-1. Jablonski diagram with collisional quenching, where IVR represents for internal vibrational relaxation, IC stands for internal conversion, ISC is intersystem crossing, S_0 and S_1 refer to the singlet ground state and first excited state, respectively, T_1 is the triplet first excited state, and Q represents the presence of a quencher.

1.2.1 Basic review of key fluorescence parameters

There are several important variables that serve as criteria for the performance of a fluorophore in SM measurements, such as absorption cross section, quantum yield, fluorescence lifetime, to name a few. In the following sections we review these performance parameters in further detail.

(A) Absorption cross section

The absorption cross section is a measure of the probability of photon absorption. When light penetrates through a solution of absorbing molecules, and the number of photons absorbed between the distance dx along the path of the beam is the product of total number of photons (N), the concentration of absorbing molecules (n) and the absorption cross section (σ_A):

$$\frac{dN}{dx} = -Nn\sigma_A \qquad (1\text{-}1)$$

Absorption cross section is the probability of a molecule absorbing a photon of a particular wavelength and polarization. The general expression for the cross section of a randomly oriented molecule is:

$$\sigma_A = 2\pi\left(\frac{\lambda}{2\pi}\right)^2\left(\frac{\gamma_r}{\Gamma_{tot}}\right) \quad (1\text{-}2)$$

where λ is the light wavelength, γ_r the spontaneous fluorescence rate, and Γ_{tot} the total frequency width of the absorption.

A simpler way to determine the absorption cross section (in unit of cm^2) of a molecule at room temperature is through the Equation (1-3):

$$\sigma = 2.303\varepsilon/N_A \quad (1\text{-}3)$$

where ε is the molar extinction coefficient (in $cm^{-1}\cdot M^{-1}$) at the desired wavelength, and N_A is the Avogadro constant. Typically, a dye molecule in solution at room temperature will have a molar extinction coefficient of ~ 50,000 $cm^{-1}\cdot M^{-1}$, so that the absorption cross section of a single dye molecule is on the order of 10^{-16} cm^2, a value comparable to the molecule size.

(B) Quantum yield

As shown in Figure 1-1, in a simplified two-level system, an excited fluorophore will relax back to the ground state via either radiative or non-radiative decay processes. The fluorescence quantum yield refers to the probability of an excited molecule de-exciting through fluorescence emission, which is given by:

$$\phi_F = \frac{\gamma_r}{\gamma_r + k_{nr}} \quad (1\text{-}4)$$

where γ_r and k_{nr} represent the radiative and non-radiative rate constants, respectively. A strongly fluorescent probe usually exhibits a large fluorescence quantum yield. A typical fluorescent labeling reagent, Rhodamine 6G, exhibits a quantum yield of ~ 0.90 in ethanol,[13] which indicates that the overwhelming majority of the photoexcited molecules decay through fluorescence emission.

(C) Fluorescence lifetime

Fluorescence lifetime is the average time a molecule spends in its excited state before emitting a photon. In the two-level system, fluorescence intensity typically follows a first-order exponential decay (Equation (1-5)):

$$I_t = I_0 e^{-t/\tau} \tag{1-5}$$

where, I_t is the fluorescence intensity at time t, I_0 is the initial fluorescence intensity and τ is the fluorescence lifetime. Fluorescence lifetime is one of the most important fluorescence characteristics as it determines the time available for the excited fluorophore to interact or diffuse in its environment and hence the information available from its emission. Thus, fluorescence lifetime is regarded as an important parameter to monitor any conformational changes of the dye upon excitation, or any possible electron and energy exchange between the dye and its surrounding. Furthermore, the fluorescence lifetime also strongly affects the size of the fluorescence signal. In general, the steady-state intensity (I_{SS}) is proportional to the fluorescence lifetime.[14]

$$I_{SS} = \int_0^\infty I_0 e^{-t/\tau} dt = I_0 \tau \tag{1-6}$$

(D) Typical fluorescent substances

From the photophysical point of view, a good fluorescence emitter should have a large absorption cross section, high quantum yield (close to 1), strong photo-stability, and resist photobleaching. These strongly fluorescent molecules often have some structural similarities. As shown in Figure 1-2, typical fluorescence emitters usually possess rigid aromatic rings and a large number of de-localized electrons, which will reduce the possibility of internal conversion and intersystem crossing, or any other types of energy loss through non-radiative decay.

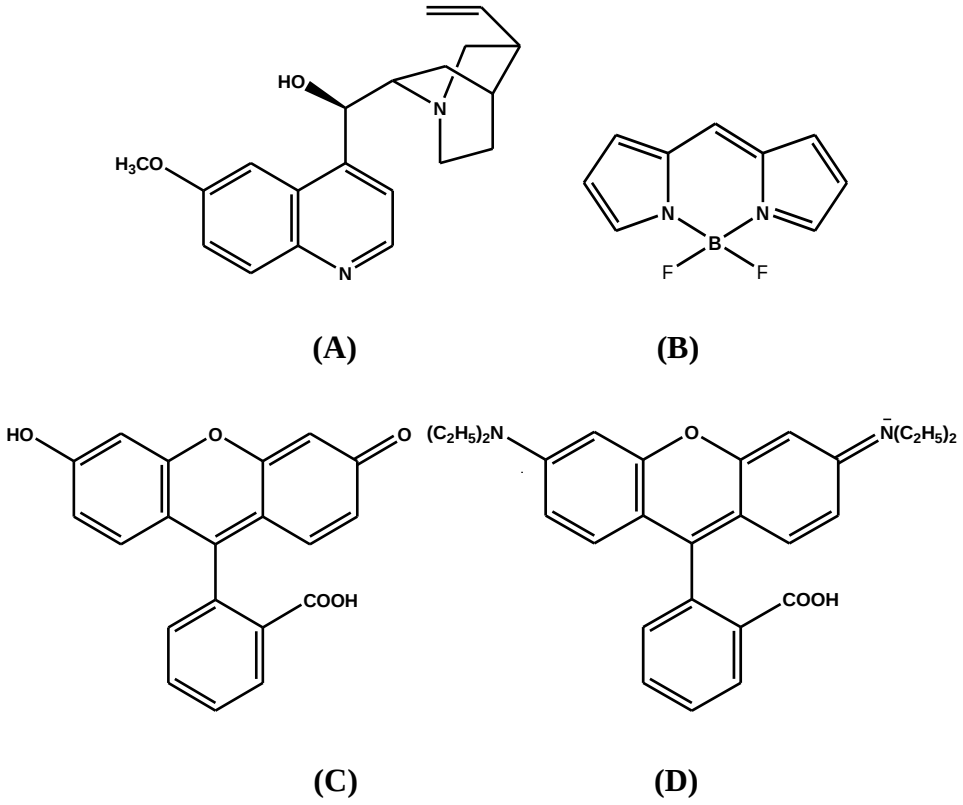

Figure 1-2. Chemical structures of some strongly fluorescent probes (A) Quinine, (B) BODIPY, (C) Fluorescein, and (D) Rhodamine-B

1.2.2 Factors controlling signal size in SM fluorescence measurements

One of the most challenging parts of any SM fluorescence measurement is attaining a sufficiently large signal-to-noise ratio (SNR) to allow both basic detection and a meaningful analysis. Optimizing the SNR in these measurements involves an obvious two-fold of strategy: 1) maximizing the signal, and 2) minimizing the noise.

To enlarge the fluorescence signal, one attempts to improve both the fluorescence photon generation and collection processes. The former is dependent on the excitation conditions and the photophysical properties of the fluorophore; the latter relies on the performance of the detection optics and electronics, which will be discussed in detail in the following section.

(A) Optical Saturation

To maximize the fluorescence emission rate during the excitation process, it is necessary to maximize the probability of pumping the molecule to its excited state. Theoretically, increasing incident photon flux will result in a greater excitation rate and hence a greater photon emission rate. However, when the excitation power reaches a critical value, optical saturation of the transition will take place. Once the incident photon flux is so high that it has exceeded the rate at which photoexcited molecules relax back to the ground state, the ability of the molecule to absorb photons (absorption cross section) will sharply decrease. Further increasing the incident photon flux will only increase background signals from scattering which will lead to a decrease in the SNR. The characteristic saturation intensity (I_S) for a molecule approximates a two level system is given by Equation (1-7).[14] Therefore, optimization of the pumping power is crucial for SM fluorescence measurements.

$$I_S = h\nu/(2\sigma_A\tau) \qquad (1\text{-}7)$$

(B) Photobleaching

In ideal cases, a good fluorescent probe is capable of emitting ~ 10^6 photons at room temperature before photobleaching.[10] The total number of emitted photon will be limited by the occurrence of photobleaching, which will stop the fluorophore from further emission by irreversible photochemical destruction. The precise mechanism for photobleaching is complicated and currently remains unclear. In many cases, the photobleaching process is enhanced by the presence of atmospheric dioxygen. This could be attributed to the interaction between the excited state of the fluorophore and triplet state O_2, which results in the formation of non-fluorescent species.[15] The average time that the fluorophore remains emissive prior to photobleaching is inversely proportional to excitation density and dependent on the local environment. For instance, covering fluorophores with polymer films can significantly decrease the rate of photobleaching by preventing oxygen from reaching the dye.[16,17]

In other cases, photobleaching has been attributed to nonlinear photochemical pathways, such as two-photon absorption, which lead to the non-radiative relaxation of the dye molecules to the ground state. Given that the lifetime of the T_1 state (first triplet excited state) is substantially longer than the S_1 state (first singlet excited state), the multi-photon photochemistry proceeds

predominantly through the triplet manifold via triplet-triplet absorption.[18] This process results in a highly reactive excited state from which irreversible photo-destruction can occur.

To summarize, optical saturation in combination with the photobleaching act to limit the maximum photon absorption rate and maximum number of photons emitted.

1.2.3 Signal-to-noise and signal-to-background issues

The "signal" of a photodetector in SM measurements (as demonstrated in Figure 1-3) is generally comprised of the detector offset and dark counts, the background and the signal from the fluorescence emission. "Dark counts" refers to the output signal of a photodetector in the absence of the excitation source, and it contains the bias count (normally a constant number that the producer of the CCD camera adds to each pixel to get non-zero counts) as well as the count from thermally released electrons. "Background" is usually derived from photons that may arrive at the detector from any source other than the molecule of interest, such as residual excitation light, scattered photons and impurities in the sample.

In the context of this thesis, "noise" refers to fluctuation in the signal that comes from a variety of sources such as background, and shot noise (known as an intrinsic fluctuation in signals due to photon or electron quantization). The SNR due to shot noise is equal to the square root of the average number of photons collected. This limits the ultimate SNR to be $N^{1/2}$ (shot-noise limit). However, in real samples, this shot-noise limit is rarely reached and background contributions often limit the overall SNR. In general, to minimize the noise level, the background photons derived from both excitation and emission processed need to be suppressed.

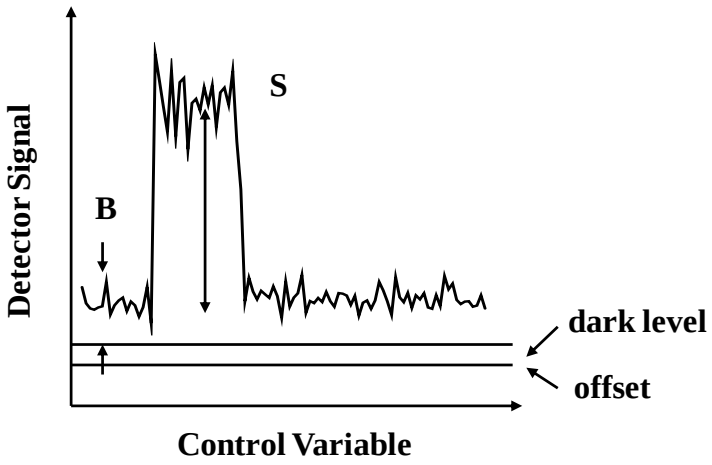

Figure 1-3. A hypothetical signal (S) with control variable shown on the horizontal axis. The definition of the offset, dark level, and background level (B) are shown.

The excitation-induced background is mainly due to both Rayleigh and Raman scattering at the air-sample interface. Rayleigh scattering is an elastic process which only alters the propagating direction of the photon without any energy loss, and therefore the energy of the scattered photon that arrives at the detector is the same as the excitation energy. This can generally be removed through the use of carefully selected optical filters aimed at removing excitation light. Raman scattering usually involves energy loss from the incident photon, and as such, the scattered photon exhibits a spectral red-shift. Raman scattered light may have similar wavelengths to the fluorescence emission of interest, and is difficult to remove from the overall detected signal.

In addition to scattering of the excitation light, impurities in the sample matrix (polymer, solvents, coverslips) can also contribute to the background level in SM measurements. Impurities at low concentrations may even exhibit SM features which could be mistaken for the molecule of interest. Thus the sample preparation is crucial for the success of SM fluorescence measurement. First of all, ultra-clean and scratch-free glass substrates should be chosen during the sample preparation in order to effectively minimize the background due to Rayleigh scattering. Furthermore, any possible source of fluorescent contaminant in the host medium should also be avoided or minimized. Control samples that contain all components of the test sample (i.e. spin-cast solvent, polymer film on the glass coverslip) but the dye molecule is

usually prepared and examined to ensure that there are no significant fluorescence impurities observed under SM imaging conditions. The other effective solution for minimizing the noise level of SM measurements is the application of emission filters, which is discussed in the following section.

In total, the SNR is determined by all the factors listed in the semi-empirical equation (Equation (1-8))[10],

$$SNR = \frac{D\phi_F(\frac{\sigma_A}{A})\frac{P_0}{h\nu}T}{\sqrt{\left(\frac{D\phi_F\sigma_A P_0 T}{Ah\nu}\right)+C_b P_0 T+N_d T}} \quad (1\text{-}8)$$

where ϕ_F is the fluorescence quantum yield of the molecule of interest, σ_A is the absorption cross section, T refers to the detector counting interval, A the beam area, $P_0/h\nu$ the number of incident photon per second, C_b the background count rate (W^{-1}), and N_d the dark count rate. D refers to the instrument-dependent factor which will be discussed later.

1.2.4 Instrumental approaches to SM fluorescence measurements

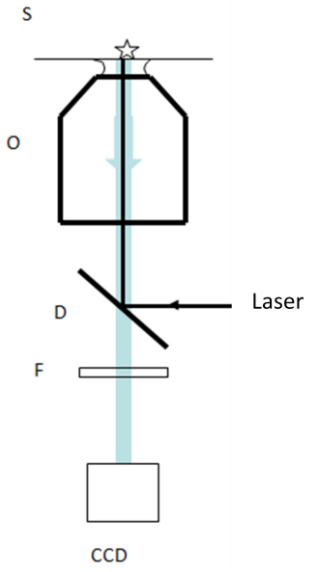

Figure 1-4. General schematic of a microscope system. S: sample, O: microscope objective, D: dichroic beamsplitter, F: long-pass emission filter (s), CCD: CCD photodetector

Significant efforts have been made to enhance the performance of standard fluorescence microscopes to achieve the sensitivity and spatial resolution needed for SM measurements. These enhancements have created great diversity in the microscope configurations used in SM measurements. The two main branches of microscope types include wide-field and scanning microscopes. In wide-field microscope techniques, the sample is excited with a collimated laser beam and all the fluorescence emission within the illumination area is projected onto a high-sensitivity CCD detector. Epifluorescence microscopy and total internal reflection fluorescence microscopy (TIRF) are common examples of wide-field microscope techniques. The scanning methods, such as near field scanning optical microscopy (NSOM) and confocal microscopy, usually involve illumination of the sample with the smallest spot possible and then scanning either the illumination spot or the sample itself. In scanning approaches, the image is constructed by point-to-point scanning. Once the position of a molecule is identified, it can be selectively excited by positioning the laser spot directly over the molecule. Unlike wide-field measurements, the scanning method does not allow the parallel excitation of several isolated molecules. However, with a smaller volume of illuminated sample, SM measurements via the scanning method can yield a higher SNR. Furthermore, by selective exciting a spot of interest, the scanning method can be used to conduct point spectroscopy and lifetime measurements.

Generally speaking, a typical SM fluorescence microscope is composed of an excitation light source (usually a laser), a microscope objective, a sensitive photodetector, and optics such as long-pass filters and dichroic beamsplitter to remove the background scattering. In addition, for near-field or confocal approaches, a sample or beam-scanning stage is also required in the instrumental setup. As noted previously, the signal size does not only depend on the emission intensity from the sample, but is also closely related to the collection efficiency of the instrument. The overall collection efficiency (defined in terms of instrument-dependent factor, D, Equation (1-9)) is determined by each component in the optical train of the microscope:

$$D = \eta_{obj} \times \eta_{opt} \times \eta_{filter} \times \eta_{det} \qquad (1\text{-}9)$$

where $\eta_{obj,}$ $\eta_{opt,}$ $\eta_{filter,}$ and η_{det} represent the collection efficiency of the microscope objective, optics, filter and photodetector, respectively. Typical values of D are in the range of 1%-8% for most modern systems.

(A) Detector

Detecting SM fluorescence requires a device that can detect single photon arrivals with minimal dark noise. This necessitates that the quantum efficiency of the detector be as high as possible for detection of fluorescence emission from a single molecule before it undergoes irreversible photobleaching. There are two classes of detectors that are commonly used in SM fluorescence microscopy: single-element detectors and two-dimensional array detectors. The former is used in near-field and confocal microscopes, and the latter is widespread in wide-field fluorescence microscopes. The capability and characteristics of each class of detectors for the SM measurements will be discussed in the subsequent paragraphs.

Single-element detectors are designed to count the number of photon arrivals in a given counting interval, and then convert this to an electronic signal. Single-elements detectors are designed for conducting the experiments that require maximum sensitivity and temporal resolution. In addition, parameters such as detection area, level of dark counts, as well as the quantum efficiency at the wavelength of interest, are also considered very important criteria for judging the performance of a single-element detector. Microchannel plate photomultiplier tubes (PMTs) and avalanche photodiodes (APDs) are both good representatives of single-element detectors that are commercially available for SM measurements. PMTs usually have a large area of detection, often on the order of 1 cm^2, with the dark count rates in the range of 10-100 counts/s. With much smaller active sensing area (usually in the mm^2 scale), the APD detectors can have dark counts to the level as low as 25 counts/s. However, compared to APDs (with a quantum efficiency of >60% across the visible spectrum), PMTs suffer from low quantum efficiency for visible light (<20%), and often require several additional pieces of low-noise electronics to efficiently detect single photons. As a result, the APD is often more desirable and used more commonly than PMTs for near-field and confocal SM fluorescence measurements.

For wide-field fluorescence imaging, two-dimensional array detectors (usually ultrasensitive CCD cameras) are capable of recording a series of sequential images of fluorescence emissions at rapid acquisition rates. CCD detectors allow the entire sample illumination area to be imaged onto the CCD chip, which in turn allows the fluorescence emission from many molecules to be imaged simultaneously. Using this approach, large sets of data can be acquired reasonably rapidly. However, the readout process of the CCD detectors is usually slower than the single-

element detectors, and the time resolution of CCD-based measurements is usually lower than those taken with single-element detectors. (A fast APD can have a nanosecond scale time resolution, which is compared to a millisecond scale time resolution for CCD detectors[19,20])

One of the most sensitive two-dimensional array detectors is the intensified frame transfer Si-based CCD camera. The high degree of sensitivity is achieved by placing a multichannel plate (MCP) between the photocathode and phosphor screen to enable signal amplification. However, intensified CCD photodetectors are relatively expensive and since signal amplification takes place before the detector chip (photon amplification), there is a significant risk of the camera being damaged by exposure to excess light. Recently, a new class of CCD camera with so-called "on-chip" multiplication gain has been created. With these cameras, signal amplification takes place after photons reach the detector chip (electron amplification), and there is no risk of detector damage from over-exposure. Cameras with on-chip multiplication gain are capable of SM sensitivity with relatively high image acquisition speed (usually as high as ~ 30 ms per frame). This new type of camera is commercially available from several manufactures (Cascade, Roper Scientific; iXon, Andor), and these have been employed in the majority of SM experiments described in this thesis.

(B) Microscope objective, optics and emission filters

In SM measurements, the microscope objective is used to gather the light from the fluorophores being observed and to focus the light to produce an image. Its performance is usually characterized by a series of parameters including magnification, color correction, numerical aperture (NA) and so forth. The most important parameter for SM applications is the numerical aperture, which is a measure of the light collecting efficiency of the lens. As shown in Equation (1-10), NA is related to both the refractive index of the medium between the objective lens and sample (n) and the half angular aperture (θ) of the objective lens.

$$NA = n\sin\theta \qquad (1\text{-}10)$$

In SM fluorescence detection, oil immersion microscope objectives (NA ~ 1.4) are highly preferred (shown in Figure 1-5). With oil immersion lenses, a small droplet of oil is placed on the lens, and since the immersion oil has a higher refractive index than air, this provides high-efficiency light collection during fluorescence measurements.

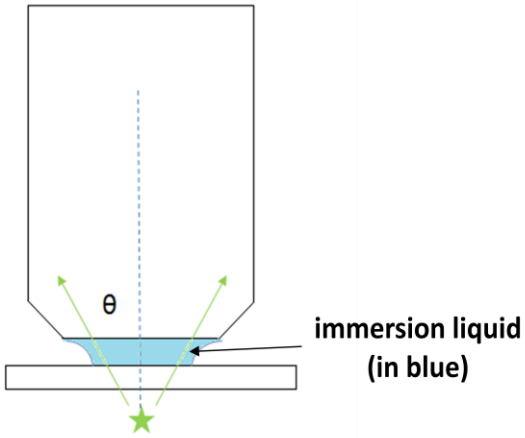

Figure 1-5. Schematic illustration showing geometry of oil immersion lens operation, and θ is the half-angle aperture.

In addition to the microscope objective lens, a number of optics are typically used to change the optical properties of the excitation beam, including its alignment, intensity, spatial profile and polarization. For example, a dichroic beamsplitter is used to split the beams of excitation and emission into two orthogonal directions: the excitation light is reflected into the microscope objective, and the fluorescence emission (at longer wavelengths) is allowed to pass through into the detector. An effective dichoroic beamsplitter could reflect over 90% of the excitation light, and let 80% of the photons at higher wavelength go through. In addition, several emission filters are also employed to suppress the background during SM detection. These emission filters, typically Raman notch filters, long-pass filters, and band-pass filters, are selected to attenuate any residual scattered excitation light, while allowing fluorescence emission to reach the photodetector.

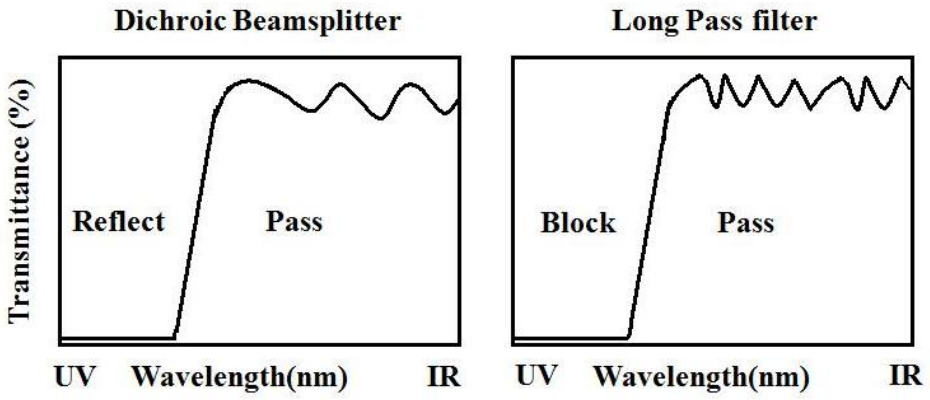

Figure 1-6. The transmission curves for (A) a dichroic beamsplitter, and (B) a long-pass emission filter[10] (Reproduced with the permission from Review of Scientific Instruments **2003**, 74, 3602. Copyright 2003 American Institute of Physics)

Careful selection of these filters can significantly affect the SNR ratio for the experiment and the overall quality of the fluorescence imaging. For example, a SM fluorescence measurement is carried out with the excitation intensity of 1 kW/cm^2 and the illumination area of ~ 1 μm^2 at the wavelength of 500 nm. Under these conditions, the incident photon flux is ~ 2.5×10^{21} photon/(s·cm^2). For a fluorophore with an absorption cross section of 10^{-16} cm^2, there would be ~ 2.5×10^5 excitations/s occurring. If the instrument-dependent factor (D) is 6%, ~ 1.5×10^4 photons/s can be detected. If unwanted reflections off optical interfaces in the microscope system could direct ~ 1% of photons from the pump laser to be detector, the resulting count rate will be 2.5×10^{11} photon/s, which indicates that the real fluorescence signal (1.5×10^4 photons/s) would be swamped out by the scattered photons. As a result, the excitation light needs to be attenuated by ~ 10^{10} fold in order to make the SM signal detectable. Moreover, as each filter will have a <100% transmission efficiency even for wavelengths they are designed to transmit (shown in Figure 1-6), care must be taken to avoid over-filtering of light in the microscope.

1.3 Detailed Review of SM Fluorescence Microscopy Techniques Used in This Thesis

Several microscope configurations have been used in the SM fluorescence studies in this thesis, including epifluorescence microscopy, dual-polarization fluorescence microscopy, and spectromicroscopy via a confocal microscope design. In the following section, we briefly describe the design and performance principles underlying these microscope configurations.

1.3.1 Epifluorescence microscopy

The epifluorescence microscope is arguably the simplest and most common microscopy setup for wide-field SM fluorescence imaging. A typical setup is shown in Figure 1-7.[21] A CW laser with the desired wavelength is directed through a Glan-Thompson polarizing prism and a quarter waveplate to make the beam circularly-polarized before reaching the sample. A focusing lens is used to focus the incident laser onto the back focal plane of the microscope objective. After propagating through the objective, the beam becomes collimated and is then directed onto the sample which was usually pre-deposited onto a glass coverslip. The fluorophores are excited by the incident beam, and the resulting fluorescence photons will be transferred to the ultrasensitive CCD camera. The illumination area is usually on the order of ~ 10 micrometer in diameter (area can be adjusted through selection of focusing lens with different focal lengths), where there are usually several molecules in the field of view at a time. The spatial resolution d, measured as the smallest resolvable distance between two specimen points) of an epifluorescence microscope is proportional to wavelength of the light being observed (diffraction-limited), and inversely proportional to the numerical aperture (NA) of the microscope.

$$d = \frac{0.5\lambda}{NA} \qquad (1\text{-}11)$$

The size of a single-molecule in a diffraction-limited image could be calculated from Equation (1-11), where λ is the excitation wavelength, and NA is the numerical aperture of the microscope objective. Given that the typical NA is ~ 1.4 for a SM epifluorescence setup, the size of a SM spot is comparable to approximately half of the excitation wavelength.

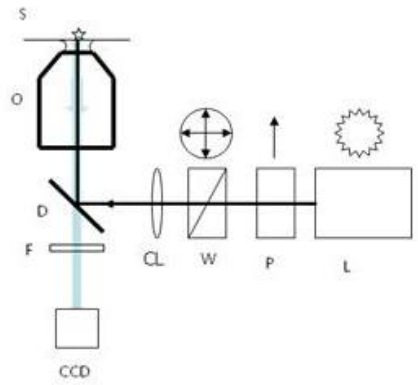

(A)

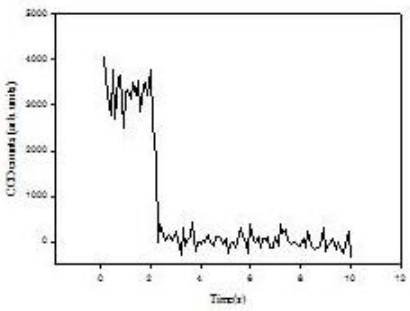

(B) (C)

Figure 1-7. (A) Schematic diagram of a typical SM epifluorescence microscope. L: laser, P: Glan-Thompson polarizing prism, W: quarter waveplate, CL: focusing lens, S: sample, O: microscope objective, D: Dichroic beamsplitter, F: long-pass emission filter(s), CCD: CCD photodetector (reproduced with the permission from Canadian Journal of Chemistry **2005**, 83, 437. Copyright 2005 NRC Canada), (B) a typical SM fluorescence image, and (C) the fluorescence time trajectory of single-molecule fluorescence emission

With a large depth of focus (~ 300-500 nm), the epifluorescence microscope always illuminates a relatively large total volume (up to 100 μm^3). The size of the total excitation volume is always closely related to the level of the background. As a result, epifluorescence microscopy is not the most sensitive SM fluorescence image technique. However, it can still provide SM sensitivity and perform useful measurements of photophysical properties. Dynamic

studies at SM level are carried out via acquisition of series of images by the CCD detector. The isolated emission events of each molecule are recorded and then converted into fluorescence time trajectories, plots showing the intensity variation of a fluorophore as a function of time. By measuring several hundreds of molecules, frequency histograms of values of the experiment parameters (such as fluorescence intensity and photobleaching time) can be constructed. Typical fluorescence emission of a single molecule exhibits single-step photobleaching in its fluorescence time trajectory, which in combination with the diffraction limited spot size, is considered the signature of a SM signal.

1.3.2 Dual-polarization fluorescence microscopy

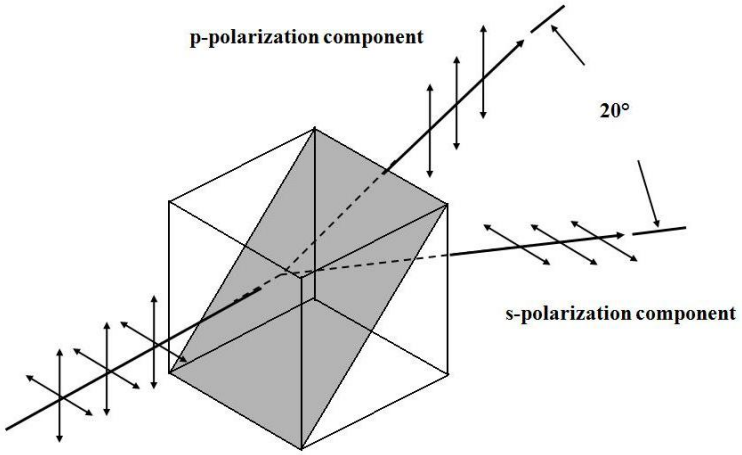

Figure 1-8. Schematic diagram of the Wollaston prism

The fluorescence emission of an individual molecule is highly polarized, and by measuring the polarization of emitted light, one can gain useful information about the spatial orientation of a fluorophore.[22-28] One method of gathering polarization information about an individual molecule is to use a dual-polarization measurement. In dual-polarization measurements, a SM fluorescence emission image from a regular epifluorescence microscope configuration is split into two orthogonal polarization images, and the intensity ratio between the images provides information on the orientation of the fluorophore(s) in the molecule of interest.[29,30] As shown in Figure 1-9, the dual-polarization fluorescence microscope is modified from the epifluorescence

setup by inserting a polarizing beamsplitter (Wollaston prism in our system) in front of the CCD detector. The Wollaston prism splits the fluorescence image into two constituent polarization components: p (horizontal) and s (vertical) polarization component, with their electric fields lying along the axis within or orthogonal to the plane of incidence, respectively. As shown in Figure 1-8, the s and p polarization components are transmitted through the polarizer, with a divergence angle of 20 °.[31] Therefore, the fluorescence emission from the same specimen will be separated into two images (represents s and p polarization respectively) on the CCD detector.

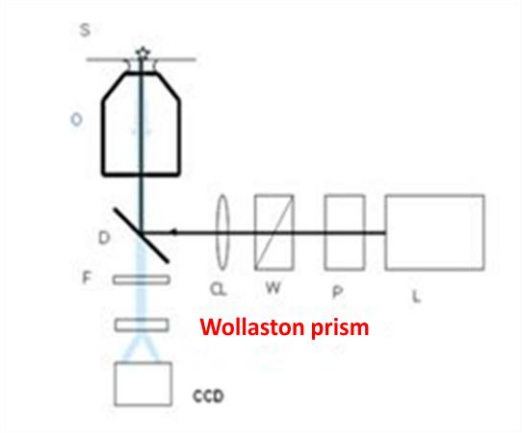

(A)

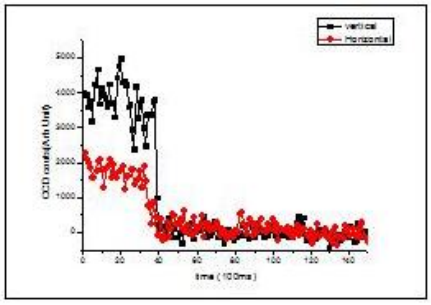

(B) (C)

Figure 1-9. (A) Schematic diagram of the dual-polarization fluorescence microscopy, (B) typical dual-polarization fluorescence image of SM emission, and (C) fluorescence time trajectories of the vertical and horizontal polarization components of a single-molecule fluorescence emission

Similar to epifluorescence imaging, the circularly polarized excitation laser is utilized to excite all the fluorophores with projections of their absorption transition dipoles on the x-y plane. However, the different orientations of the molecule will certainly result in a distribution of effective absorption cross-sections, which is considered a primary reason for intensity variations among different individual molecules. The fluorescence emission of each molecule is then split into two separate images which correspond to the intensity of the vertical and horizontal polarization components in the fluorescence emission (referred to as $I_{\parallel}$, $I_{\perp}$, respectively). The fluorescence polarization (P) is simply given by,

$$P = \frac{I_{\parallel} - I_{\perp}}{I_{\parallel} + I_{\perp}} \qquad (1\text{-}12)$$

By measuring the frequency histograms of the distribution of P, we can obtain additional information regarding the orientation and conformation of the fluorophore. In our study of Calcium Green-2 (Chapter 3), this approach has been used in the study of the relative orientation of fluorophores inside a multi-fluorophoric probe.

1.3.3 Spectromicroscopy with a confocal microscope

The confocal microscope is a scanning method for SM fluorescence measurements. In the setup used in this thesis, a laser is first directed into a spatial filter and re-collimated by a focusing lens. After the beam is circularly-polarized with a quarter waveplate, the collimated beam is then directed into the back of the microscope and then focused down to the smallest spot possible (ideally diffraction limited) at the sample plane. Only a very small volume of the sample is excited by the laser spot, and the resulting photons (including both fluorescence emissions and the background scattering photon) are passed through a pinhole (diameter of 75 μm) to remove any light from out of focus parts of the sample. One of the advantages of the confocal setup is that it allows a smaller excitation volume and suppresses the overall background, which results in a highly-sensitive measurement. The existence of pinhole whose diameter determines the depth of focus for confocal imaging can spatially reject the out-of-plane light and give rise to high axial resolution in the SM measurements. In addition, the APD detector exhibits a better temporal resolution than CCD cameras used in wide-field fluorescence imaging, which allows for faster data acquisition in dynamic and time-dependent measurements.

The fluorescence emission will either reach the APD and be used to generate a confocal fluorescence image, or be reflected by means of a mirror into a spectrograph and then collected by another CCD detector (iXon, Andor Technology) and converted into an emission spectrum. As shown in Figure 1-10, the configuration of the microscope could be converted between the confocal to the epifluorescence setups by simply adding a focusing lens in front of the back focal plane of the microscope. While the focusing lens is out, the collimated beam will be directed into the microscope as in the confocal microscope; while it is in, the collimated beam will be focused on to the back focal plane and therefore converted into the wide-field configuration.

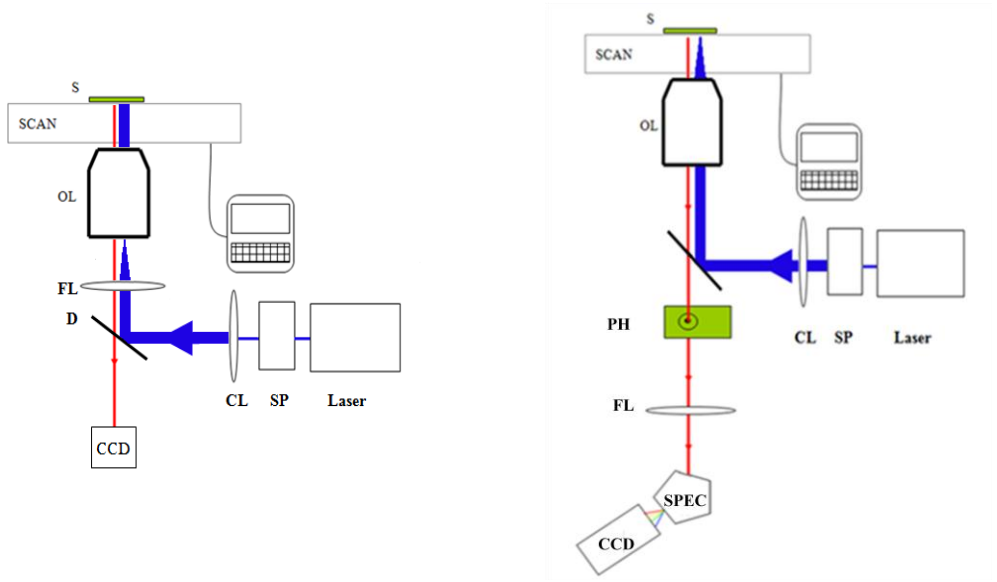

(A) (B)

Figure 1-10. Schematic diagrams of (A) epifluorescence microscope system and (B) fluorescence confocal spectromicroscopy system. SP: spatial filter, CL: collimating lens, D: dichroic beamsplitter, PH: pinhole, FL: focusing lens, SPEC: spectrograph, CCD: CCD camera, OL: objective lens, SCAN: sample scan stage, S: sample)

1.4 Overviews of Sub-projects in This Thesis

A number of different areas of spectroscopy and photophysics have been investigated during the course of this PhD program using SM fluorescence techniques. SM fluorescence studies have demonstrated that molecules are very sensitive to changes in their local environment. This sensitivity can be exploited to gain insight into a variety of process regarding any possible intra and intermolecular energy or electron transfer processes. Useful spectroscopic properties, such as fluorescence intensity, photobleaching time, molecular orientation, and spectral diffusion, can be detected and characterized with proper instrumental configurations. This section briefly reviews the subprojects of my PhD thesis regarding the SM studies of several fluorescent systems.

1.4.1 Photoinduced electron transfer in Calcium-Green 1 (CG-1)

Calcium-Green 1 (CG-1, structure shown in Figure 2-1) is a fluorescent ion-indicator that undergoes significant changes in fluorescence emission intensity upon binding with the target ions. These ion-indicators have found numerous applications, including detection and qualification of harmful inorganic analytes in environmental analysis, as well as to visualize, through high-sensitivity fluorescence imaging, localized ion-dependent processes in live cells and tissues.[32-36] Among all ion-sensors, the fluorescence-based Ca^{2+} ion-indicators are arguably the most important and widely used types of indicators because of the great importance of intercellular Ca^{2+} in biological signalling.[37,38] CG-1 is composed of a fluorophore and a BAPTA group (1,2-bis(2-aminophenoxy) ethane-N,N,N',N'-tetra acetic acid) for chelating Ca^{2+}. As a calcium-ion sensor, its fluorescence intensity responds linearly as a function of the concentration of Ca^{2+} in solution. In a Ca^{2+}-free environment, the fluorescence emission is strongly quenched. The mechanism of fluorescence quenching in CG-1 has been attributed to the process of photoinduced electron transfer (PET).[39,40] During PET, rapid electron transfer from the BAPTA group to the photoexcited fluorophore takes place and results in quenching of fluorescence. The electron transfer process between the BAPTA group (donor, D) and the fluorophore (acceptor, A) can be simplified into the following redox reaction:

$$D + A \overset{h\nu}{\rightarrow} D^{+\cdot} + A^{-\cdot} \qquad (1\text{-}13)$$

The thermodynamic criterion of this reaction is expressed in the Rehm-Weller equation:

$$\Delta G^{\circ} = -nF\left(E^{o}_{\frac{A}{A^{-\cdot}}} - E^{o}_{\frac{D^{+\cdot}}{D}}\right) - \Delta E_{0,0} + \omega_P \qquad (1\text{-}14)$$

where ΔG° is the change in standard Gibbs free energy for the PET process, n is the number of electrons transferred, F is Faraday's constant, E° represent the standard reduction potentials for both donor and acceptor, $\Delta E_{0,0}$ is the equalized excitation energy, and ω_P is the Coulombic work requires to bring the donor and acceptor to within the electron transfer distance.

Upon chelating Ca^{2+}, the oxidation potential of the donor (BAPTA group) will increase, which results in the increase of ΔG° into a positive value, which indicates that the PET process becomes thermodynamically unfavorable. Thus, the fluorophore becomes emissive due to the retardation of the PET process. To simplify, the Ca^{2+} serves as a molecular switch, which can turn fluorescence emission "on" and "off". The increase in fluorescence intensity as a function of the concentration of calcium ion could be ascribed to the increase in the number of emissive fluorophore in the solution upon chelating.

The goal of this subproject was to characterize the emission behavior of CG-1 using a combination of ensemble and SM spectroscopy measurements. Both ensemble and SM observations of CG-1 were compared with the previous work done on its close variant, Calcium-Green 2 (CG-2) whose basic spectroscopic properties (both ensemble and single-molecule) are well understood.[41] As another Ca^{2+} sensor from the Calcium Green family, CG-2 consists of a BAPTA moiety combined with two identical fluorophores. Similar to CG-1, the fluorescence intensity of CG-2 responds to the concentration of calcium ion in solution, which was related to the excitonic coupling between the two fluorophores in a single CG-2 molecule. It was found that in the absence of Ca^{2+}, CG-2 adopts a conformation in which the two fluorophores are parallel and facing each other. This gives rise to the formation of an intramolecular exciton and a corresponding "self-quenching" of the fluorescence emission. When the BAPTA group binds to Ca^{2+}, the relative separation and orientation of the constituent fluorophores are altered and the excitonic coupling between two fluorphores is disrupted. This results in a large increase in fluorescence emission intensity and an accompanying spectral shift in the absorption spectrum of CG-2. Thus, it is anticipated that there will be some similarities between CG-1 and CG-2 in

terms of their basic spectroscopic and photophysical properties, while the differences between the two will provide further insight into the mechanism of operation of both dyes.

In the steady state measurements, the absorption spectra of CG-1 were collected at different [Ca^{2+}]. Unlike CG-2, no significant spectral changes were observed from CG-1 before and after chelating Ca^{2+}. This provides additional support that the spectral shift observed for CG-2 is due to the excitonic coupling between the two constituent fluorophores. As observed in CG-2 samples, the lifetime measurements of CG-1 showed two chemical forms of the dye with significantly different lifetimes coexisting in the solution. Furthermore, varying [Ca^{2+}] causes a change in the relative proportions of the two species, which can be assigned to the Ca^{2+} bound form and the Ca^{2+} free form of CG-1, respectively.

During the SM measurements, frequency histograms of emission intensities and photobleaching time for single CG-1 molecules both in presence and in absence of Ca^{2+} were constructed. There were no significant differences in the distributions in both intensity and photobleaching time, which strongly support the PET mechanism presented by previous researchers. Further comparisons between SM results from CG-1 and CG-2 indicated that a single CG-2 molecule is around twice as bright as the CG-1 molecule on average. This is another expected result, simply because CG-2 will have an absorption cross-section that is approximately twice as large as the monomeric CG-1.[42]

1.4.2 Fluorophore orientation in Calcium-Green 2 via dual-polarization microscopy

Modification of an epifluorescence microscope enables the detection of emission polarization of a molecule, which can provide insight into the orientation and conformation of fluorescence probes. In this subproject, dual-polarization fluorescence microscopy was used to determine the relative orientation of the two fluorophores in CG-2. As noted previously, in the absence of Ca^{2+}, CG-2 adopts a self-quenching conformation in which the two fluorophores are approximately coplanar. Such molecular conformation will be disturbed if CG-2 forms a complex with Ca^{2+}. SM measurements indicate that the Förster energy transfer can take place between the two fluorophores at a rate that exceeds the rate of fluorescence, which gives rise to the collective photobleaching of both fluorophores upon formation of a damaged (trap) state.[41,43] This indicates that the fluorescence emission from both fluorophores of CG-2 molecule could only be switched

"on" and "off" spontaneously, which has been confirmed by the appearance of collective photobleaching in the SM measurements.

The relative orientation of the constituent fluorophores in the multifluorophoric system like CG-2 is an important parameter that controls the extent of energy transfer between fluorophores. Previous molecular mechanics calculation indicated that the two emission transition dipoles in a CG-2 molecule tend to form a ~ 120 ° angle when chelating with Ca^{2+}.[41] However, the epifluorescence setup used in these original measurements cannot determine the angle and relative orientation between the fluorophores. This information can be quantitatively determined in the dual-polarization fluorescence microscope by obtaining the polarization distribution of randomly oriented CG-2 molecules. The dual-polarization imaging approach was first tested on a randomly orientated single fluorophore system (Rhodamine 6G), and the SM results were compared to the mathematical model of the polarization distribution of randomly orientated 1D transition dipoles. The main features in the calculated distributions were observed in the experimental data, which proved that the approach of dual-polarization image worked well and could be reliably applied to the more complicated dual-chromophore system.

The SM observations of CG-2 were also compared to the calculated polarization distribution of the dual-transition dipole system with the angle between the two dipoles fixed at 120 °. The shapes of polarization distributions of SM CG-2 both in the presence and absence of Ca^{2+} were comparable, indicating that the relative orientations of the transition dipoles in Ca^{2+}-bound and Ca^{2+}-free samples were essentially the same. In addition, both showed good agreement to the calculated model, which indicates that the angle between two transition dipoles in the "emissive" CG-2 is ~ 120 °. Furthermore, the shape of the polarization distribution was found to be very sensitive to the angle between two transition dipoles, which suggests that this technique can be used to determine fluorophore orientation in other multi-fluorophoric systems.[30]

1.4.3 Probing local environments in phase-separated lipid films via Nile Red emission

The fluorescence emission of a molecule is highly dependent on its local chemical and physical environment. In our studies, the polarity sensitive dye Nile Red (NR) was incorporated into phase-separated lipid films that contained two significantly different chemical and physical environments. As a lipid stain, NR was chosen as a probe for the local environment because of the strong dependence of its fluorescence emission upon the polarity of its local environment

(solvatochromism).[44-46] In polar matrices, NR emission is strongly quenched, but in non-polar environments, the fluorophore becomes strongly emissive with a blue shift in both excitation and emission maxima. In addition to the solvatocharomism, another key feature of NR staining that would affect the contrast in fluorescence images is the general affinity of the dye for its matrix. If the dye molecules preferably accumulate in one region of the sample, a stronger fluorescent signal could be observed simply because the local concentration of the fluorophore is higher. Our goal is to use both epifluorescence imaging and the spectromicroscopy to probe both the spectral dispersion and the fluorescence intensity variation of NR in different part of the lipid film and determine whether a strong fluorescence signal can be attributed to a highly emissive form of dye (due to its solvatochromism), accumulation of dye in the area of interest, or a combination of both.

In these studies, the lipid film is composed of a phase-separated Langmuir-Blodgett (LB) monolayer with both continuous and discontinuous domains.[47,48] The discrete, hexagonal-shaped discontinuous domains are exclusively comprised of non-polar hydrocarbons. The surrounding continuous domain is enriched with fluorocarbons. When the LB film was stained with NR, sharp contrast was observed in terms of the relative fluorescence intensities of both domains. The hydrocarbon dominated domains exhibited much stronger fluorescence emission in comparison to the surrounding continuous domain. These results could be either caused by the variation in emission behaviors of the NR molecules in different polarities or to the difference in affinity of the dye to the two different domains during the staining process.

The emission spectra collected by the spectromicroscopy indicate a significant spectral shift of NR emission in the two chemically different domains. Additional information was obtained from the intensity distributions of NR in the SM measurements. Instead of getting a double-peaked distribution in the histogram, a single-peak distribution was obtained, indicating that the emissive properties of NR were comparable in both domains. Thus, the generation of contrast in fluorescence emission in two different domains is mainly due to the selective accumulation of NR in the hexagonal (hydrocarbon) domain over the surrounding continuous domain.[49]

1.4.4 Investigation of a fluorophore-nanoparticle conjugate system that exhibits minimal fluorescent quenching

Fluorescence quenching is often induced by energy transfer or electron transfer between an excited fluorophore and an acceptor. In this sub-project, we have performed an investigation of fluorescence quenching of fluorophores that are covalently bound to a gold metal protected cluster (AuMPC) with negligible plasmon band. The system was characterized using a combination of steady state and time-resolved ensemble spectroscopic measurements in conjunction with single-molecule fluorescence microscopy. By examining the spectroscopic properties of these labeled fluorescent probes, information about the extent of fluorescent-labeling, degree of fluorescence quenching, as well as the influence of AuMPCs on excited-state lifetime and most importantly, the SM emission behaviors has been obtained, and the quenching mechanism has been investigated.

Briefly, the system is comprised of small-sized AuMPCs (<2 nm) coupled to strongly fluorescent molecules through covalent bonds.[50,51] The presence of the covalent bond will limit the distance between the fluorophore and the gold surface in a well-defined fashion. The bulk measurements in fluorescence emission spectra of the dye-AuMPC conjugates only exhibited minimal quenching at low loading ratios. During the fluorescence lifetime measurements, the dye showed negligible change upon conjugation to the gold surface. The SM measurements were conducted on the samples with different dye/AuMPC ratios. The emission intensities of several fluorophores attached to the same gold particle were collected and imaged into the same fluorescence spot. As a result, an “unusual” double-step photobleaching was observed in approximately half of the samples at all loading ratios with a small sub-population exhibiting more than two photobleaching steps. Photobleaching was observed without additional blinking dynamic events. Emission intensities of the coupled fluorophores were comparable with those measured of dye molecules in absence of AuMPCs. This suggests that the statically quenched fluorophores are entirely non-emissive, while the remaining dyes are essentially unquenched.

1.5 References

1. Neher, E.; Sakmann, B.; Steinbach, J. H. *Pflugers Archiv-European Journal of Physiology* 1978, *375*, 219-228.
2. Binning, G.; Rohrer, H.; Gerber, C.; Weibel, E. *Physical Review Letters* 1982, *49*, 57-61.
3. Muller, E. W. *Science* 1965, *149*, 591-&.
4. Roiter, Y.; Minko, S. *Journal of the American Chemical Society* 2005, *127*, 15688-15689.
5. Moffitt, J. R.; Chemla, Y. R.; Smith, S. B.; Bustamante, C. *Annual Review of Biochemistry* 2008, *77*, 205-228.
6. Gosse, C.; Croquette, V. *Biophysical Journal* 2002, *82*, 3314-3329.
7. Moerner, W. E.; Kador, L. *Physical Review Letters* 1989, *62*, 2535-2538.
8. Moerner, W. E. *Journal of Physical Chemistry B* 2002, *106*, 910-927.
9. Moerner, W. E.; Orrit, M. *Science* 1999, *283*, 1670-1676.
10. Moerner, W. E.; Fromm, D. P. *Review of Scientific Instruments* 2003, *74*, 3597-3619.
11. Ambrose, W. P.; Goodwin, P. M.; Jett, J. H.; Van Orden, A.; Werner, J. H.; Keller, R. A. *Chemical Reviews* 1999, *99*, 2929-2956.
12. *Single Molecule Optical Detection, Imaging and Spectroscopy*; Basche, T.; Moerner, W. E.; Orrit, M.; Wild, U. P., Eds.; Verlag-Chemie: Munich, 1997.
13. Kubin, R. F.; Fletcher, A. N. *Journal of Luminescence* 1982, *27*, 455-462.
14. Lakowicz, J. *Principles of fluorescence spectrosopy*; 2nd ed.; Kluwer Academic: New York, 1999.
15. Zondervan, R.; Kulzer, F.; Orlinskii, S. B.; Orrit, M. *Journal of Physical Chemistry A* 2003, *107*, 6770-6776.
16. Talhavini, M.; Atvars, T. D. Z. *Journal of Photochemistry and Photobiology a-Chemistry* 1999, *120*, 141-149.
17. Andrew, T. L.; Swager, T. M. *Macromolecules* 2008, *41*, 8306-8308.
18. Xie, X. S.; Trautman, J. K. *Annual Review of Physical Chemistry* 1998, *49*, 441-480.
19. Li, L. Q.; Davis, L. M. *Review of Scientific Instruments* 1993, *64*, 1524-1529.
20. Spring, K. R.; Fellers, T. J.; Davidson, M. W.; http://www.microscopyu.com (accessed Oct 2010).

21. Bagh, S.; Paige, M. F. *Canadian Journal of Chemistry-Revue Canadienne De Chimie* 2005, *83*, 435-442.
22. Sosa, H.; Peterman, E. J. G.; Moerner, W. E.; Goldstein, L. S. B. *Nature Structural Biology* 2001, *8*, 540-544.
23. Schade, S. Z.; Jolley, M. E.; Sarauer, B. J.; Simonson, L. G. *Analytical Biochemistry* 1996, *243*, 1-7.
24. Hopkins, S. C.; Sabido-David, C.; Corrie, J. E. T.; Irving, M.; Goldman, Y. E. *Biophysical Journal* 1998, *74*, 3093-3110.
25. Sosa, H. J.; Peterman, E. J. G.; Moerner, W. E.; Goldstein, L. S. B. *Biophysical Journal* 2001, *80*, 572A-572A.
26. Chen, C. S.; Chen, W. N. U.; Zhou, M. J.; Arttamangkul, S.; Haugland, R. P. *Journal of Biochemical and Biophysical Methods* 2000, *42*, 137-151.
27. Forkey, J. N.; Quinlan, M. E.; Goldman, Y. E. *Progress in Biophysics & Molecular Biology* 2000, *74*, 1-35.
28. Chung, I.; Shimizu, K. T.; Bawendi, M. G. *Proceedings of the National Academy of Sciences of the United States of America* 2003, *100*, 405-408.
29. Kinosita, K.; H. Itoh, S. I.; Hirano, K.; Nishizaka, T.; Hayakawa, T. *Journal of Cell Biology* 1991, *115*, 67-73.
30. Lu, Y.; Bowles, R. K.; Paige, M. F. *Chemphyschem* 2008, *9*, 1947-1953.
31. ThorLabsWeb.; http://www.thorlabs.com (accessed Oct 2010).
32. Kao, J. P. Y. In *Methods in Cell Biology, Vol 40* 1994; Vol. 40, p 155-181.
33. Berridge, M. J.; Lipp, P.; Bootman, M. D. *Nature Reviews Molecular Cell Biology* 2000, *1*, 11-21.
34. Bootman, M. D.; Collins, T. J.; Peppiatt, C. M.; Prothero, L. S.; MacKenzie, L.; De Smet, P.; Travers, M.; Tovey, S. C.; Seo, J. T.; Berridge, M. J.; Ciccolini, F.; Lipp, P. *Seminars in Cell & Developmental Biology* 2001, *12*, 3-10.
35. Brini, M.; Carafoli, E. *Cellular and Molecular Life Sciences* 2000, *57*, 354-370.
36. Knot, H. J.; Laher, I.; Sobie, E. A.; Guatimosim, S.; Gomez-Viquez, L.; Hartmann, H.; Song, L. S.; Lederer, W. J.; Graier, W. F.; Malli, R.; Frieden, M.; Petersen, O. H. *Molecular Interventions* 2005, *5*, 112-127.
37. Dominguez, D. C. *Molecular Microbiology* 2004, *54*, 291-297.

38. Thomas, A. P. *Nature Cell Biology* 2000, *2*, E126-E128.
39. de Silva, A. P.; Gunaratne, H. Q. N. *Journal of the Chemical Society-Chemical Communications* 1990, 186-188.
40. de Silva, A.; Gunnlaugsson, T.; Rice, T. *Analyst* 1996, *121*, 1759-1762.
41. Bagh, S.; Paige, M. F. *Journal of Physical Chemistry A* 2006, *110*, 7057-7066.
42. Lu, Y.; Paige, M. F. *Journal of Fluorescence* 2007, *17*, 739-748.
43. Lounis, B.; Deich, J.; Rosell, F. I.; Boxer, S. G.; Moerner, W. E. *Journal of Physical Chemistry B* 2001, *105*, 5048-5054.
44. Greenspan, P.; Fowler, S. D. *Journal of Lipid Research* 1985, *26*, 781-789.
45. Golini, C. M.; Williams, B. W.; Foresman, J. B. *Journal of Fluorescence* 1998, *8*, 395-404.
46. Greenspan, P.; Mayer, E. P.; Fowler, S. D. *Journal of Cell Biology* 1985, *100*, 965-973.
47. Qaqish, S. E.; Paige, M. F. *Langmuir* 2007, *23*, 2582-2587.
48. Qaqish, S. E.; Paige, M. F. *Langmuir* 2007, *23*, 10088-10094.
49. Lu, Y.; Porterfield, R.; Thunder, T.; Paige, M. F. *Spectrochimica Acta Part a-Molecular and Biomolecular Spectroscopy* 2010.
50. Leontowich, A. F. G.; Calver, C. F.; Dasog, M.; Scott, R. W. J. *Langmuir* 2010, *26*, 1285-1290.
51. Lu, Y.; Dasog, M.; Leontowich, A. F. G.; Scott, R. W. J.; Paige, M. F. *Journal of Physical Chemistry C* 2010, *114*, 17446-17454.

CHAPTER 2

AN ENSEMBLE AND SINGLE-MOLECULE FLUORESCENCE SPECTROSCOPY INVESTIGATION OF CALCIUM GREEN 1, A CALCIUM-ION SENSOR

This Chapter is a slightly modified copy of an article published in *Journal of Fluorescence* in November 2007. (Reproduced with permission from Journal of Fluorescence **2007**, 17, 739-748.

Calcium ion plays an important role in a diverse range of cellular signalling processes, including gene transcription, muscle contraction, and cell proliferation.[1] As a result, the ability to detect and quantify intracellular free Ca^{2+} is of great importance in understanding these processes. A number of different Ca^{2+} indicator molecules have been designed, synthesized and characterized. Some of the most widely used types of indicators are fluorescence-based, and these are often used for the measurement of cytosolic free Ca^{2+}. Their popularity stems from the ease with which they can be incorporated into the cells as well as the sensitivity and versatility that fluorescence measurements bring about. In this work, our objective was to perform a spectroscopic characterization of Calcium-Green 1 (CG-1), a fluorescence-based Ca^{2+} indicator, via a combination of ensemble and single-molecule (SM) fluorescence characterization, and to compare the mechanism of action of CG-1 with a closely related variant, Calcium-Green 2 (CG-2). The work is an extension of a previous study on the photophysical behaviour of CG-2, a dual-fluorophore variant of CG-1.[2]

The ensemble spectroscopy measurements revealed that the overall fluorescence intensity of CG-1 increases with increasing $[Ca^{2+}]_{free}$ in the solution before saturation. In addition, the SM measurements allow us to unveil the heterogeneity in the emission behaviour of each CG-1 molecule, which is obscured by the "ensemble average". Using SM measurements, we determined that the fluorescent species in the CG-1 sample both in the presence and absence of Ca^{2+} has identical fluorescent properties. The low fluorescence intensity of CG-1 in Calcium-free

condition could be attributed to fluorescence quenching caused by photoinduced electron transfer (PET).

The fluorescence intensity and on-time of individual molecules was obtained by measuring the brightness and the duration of individual fluorescence emission spots. In terms of data analysis, this chapter introduces the method of constructing frequency histograms (distributions) of fluorescence intensities and on-times, which was also used for other SM experiments described in subsequent chapters. The shape and other properties of these distributions could provide invaluable insight into the photophysical or photochemical processes that are involved in and influence the fluorescence emission.

For this current research paper[3], I prepared samples, performed all of the measurements, and played a major role in interpreting the results. My supervisor provided guidance throughout the entire experimental work and was greatly involved in result interpretation. For this work, the first published manuscript of my PhD degree, he played a significant role in organizing the results and wrote the final draft of the paper.

2. An Ensemble and Single-molecule Fluorescence Spectroscopy Investigation of Calcium Green 1, a Calcium-ion Sensor

*Yin Lu and Matthew F. Paige**

Department of Chemistry, University of Saskatchewan, 110 Science Place, Saskatoon, SK. Canada S7N 5C9

Received January 29, 2007. In Final form: July 20, 2007

2.1 Abstract

The calcium-ion indicator dye, Calcium-Green 1 (CG-1), has been characterized using a combination of ensemble and single-molecule optical spectroscopy measurements. In terms of ensemble measurements, CG-1 demonstrated a strong increase in fluorescence emission as a function of increasing [Ca^{2+}]. This was accompanied by a change in the relative proportions of two chemical forms of the dye, each with a different fluorescence lifetime, which were found to co-exist in solution. From single-molecule (SM) fluorescence measurements, it was found that the fluorescence intensity and photobleaching time (on-time) of each CG-1 molecule was invariant with [Ca^{2+}] and that changes in ensemble fluorescence intensity simply correlates with the number of fluorescent molecules in solution. These results are compared with that of the related system, Calcium-Green 2 (CG-2), and the mechanisms of operation of these two indicator dyes are discussed.

2.2 Introduction

Single-molecule (SM) spectroscopy is a young but rapidly-developing field of research in which the optical properties of individual, isolated molecules can be probed in the absence of ensemble averaging [4-7]. The SM approach to optical spectroscopy has now been applied to a host

of systems, ranging from single impurity atoms in crystals, to complex biological systems and beyond. Fluorescence emission of individual molecules can be an extremely sensitive probe of local environmental conditions, and has provided valuable insight into the heterogeneous nature of numerous systems. While interesting in and of themselves, one of the major practical benefits of spectroscopic measurements on individual molecules is that they can provide invaluable complementary information to more conventional ensemble spectroscopy measurements. While not yet routine, it is conceivable that SM measurements might soon become a standard tool when characterizing novel new fluorophores and photophysical processes.

Of recent interest to our research group has been the application of SM spectroscopy for characterizing luminescent ion-indicator molecules, chemical entities that undergo significant changes in fluorescence emission upon binding with inorganic ions. The design, synthesis and characterization of a huge number of different ion-indicators has been reported in the literature (for a number of important reviews, see [8-12]). Indicators have been developed to detect different types of ions, to emit over a wide range of emission wavelengths and to operate through a variety of signal transduction mechanisms. Ion-indicators have found numerous applications, including detection and quantification of harmful inorganic analytes in environmental analysis, as well as to visualize, through high-sensitivity fluorescence imaging, localized ion-dependent processes in live cells and tissues.

SM measurements have been applied to a number of important ion-sensor systems. For example, Adams et al. have reported the synthesis and characterization of a novel perylene-based sensor that can detect binding events at the single-molecule level via a photoinduced electron transfer (PET) mechanism [13]. Brasselet et al. have described the fluorescence behaviour of the seminaphtorhodafluor SNARF-1 for pH sensing in agarose matrices [14], as well as the use of a "cameleon" protein construct to detect Ca^{2+} binding [15]. While not directly attempting to produce an indicator-ion system, Ha et al. [16] demonstrated changes in energy transfer between fluorescently labeled components of an RNA assembly upon Mg^{2+} binding.

Fluorescence-based ion-indicators that can be used to detect Ca^{2+} are arguably the most important and widely used types of indicators because of the great importance of intracellular Ca^{2+} in biological signaling pathways [17,18]. These indicators are used routinely in fluorescence microscopy experiments, in which the indicator fluorescence is used to directly visualize the presence of Ca^{2+} in tissues or cells. Many varieties of these ion-indicators have been developed,

and indeed many are now commercially available. We have recently reported a combined ensemble and single-molecule investigation of Calcium-Green 2 (CG-2), a commercially available calcium-ion indicator that exhibits a large increase in fluorescence emission intensity upon binding Ca^{2+} [2]. The Calcium Green class of indicators are based upon the calcium-chelating ligand 1,2 bis(o-aminophenoxy) ethane-N,N,N′N′-tetracetic acid (BAPTA) [19]. The BAPTA moiety has excellent Ca^{2+} binding properties, including a low dissociation constant, high selectivity and rapid substrate binding. By coupling BAPTA to a xanthene (rhodamine-based) fluorophore, sensors that become highly fluorescent in the visible region of the spectrum have been developed [20-23]. The Calcium Green class of indicators consists of a single BAPTA moiety combined with either one (CG-1) or two (CG-2) rhodamine-based fluorophores. These indicators have low calcium dissociation constants (manufacturer lists K_d values of 0.19 μM and 0.55 μM, for CG-1 and CG-2, respectively) and high quantum yields (0.75 in high [Ca^{2+}]) at physiological pHs. Structures of CG-1 and CG-2 are shown in Figure 2-1 (a), (b).

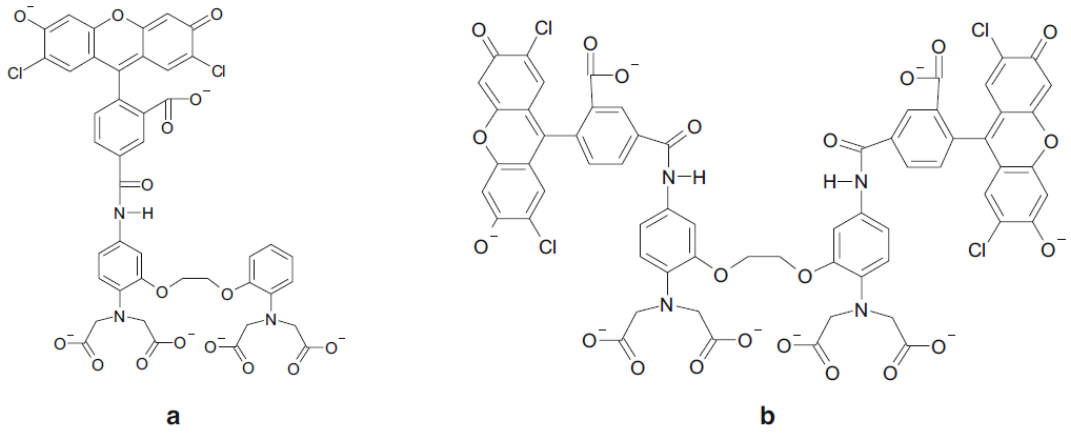

Figure 2-1. Chemical structures for (a) Calcium-Green 1 and (b) Calcium-Green 2

While the mechanism by which signal transduction occurs in some ion-indicators is well known, this was not the case for CG-2. In our previous work, a combination of optical spectroscopy measurements was used to determine why the molecule becomes strongly fluorescent on Ca^{2+} binding [2]. It was found that in the absence of Ca^{2+}, CG-2 adopts a conformation in which the transition dipoles for the two fluorophores are coplanar. This gives rise to intramolecular exciton formation and a corresponding "self-quenching" of fluorescence emission. When the molecule binds to Ca^{2+}, the relative separation and orientation of the constituent fluorophores are shifted, a large increase in fluorescence emission intensity is

observed and an accompanying shift in CG-2's absorption spectrum takes place. This suggests that upon binding of Ca^{2+}, the intermolecular exciton formation for this system is disrupted.

From complementary SM experiments, it was observed that the change in bulk fluorescence correlated with a simple statistical increase in the number of fluorescent molecules in solution, as anticipated from ensemble measurements. In addition, it was also found that the majority of CG-2 molecules photobleached in a single step (collective photobleaching), despite the presence of two fluorophores per molecule. This provided an excellent opportunity to investigate collective photobleaching, a well-known phenomenon in multi-fluorophore systems, in a comparatively simple and controllable test-system. It was postulated that for CG-2, collective photobleaching could be attributed to rapid dipole-dipole Förster coupling between the two fluorophores in conjunction with the formation of a photo-damaged induced trap site on one of the fluorophores.

The mechanism of action of CG-1 and a number of closely-related compounds has been shown by de Silva et al. [24] to be PET, in which rapid electron transfer from the Ca^{2+} binding domain donor to the photoexcited fluorophore acceptor takes place and renders it non-fluorescent. Upon Ca^{2+} binding, the PET process is retarded (the oxidation potential of the binding domain shifts significantly upon Ca^{2+} uptake) and fluorescence is re-activated. It is anticipated that while there will be some similarities between CG-1 and CG-2 in terms of basic spectroscopic properties, differences between the two will provide further useful insight into the mechanism of operation of both dyes. For example, the nature of the excitonic "quenched" state in CG-2 should be readily distinguishable through comparison of absorption spectra for the two molecules. One might also reasonably expect to distinguish between CG-1 and CG-2 at the single-molecule level by simply comparing mean fluorescence intensity levels. In this paper, we present a combined ensemble and SM spectroscopic characterization of CG-1 and compare these findings with those obtained previously for CG-2.

2.3 Materials and Methods

2.3.1 Ensemble spectroscopy measurements

CG-1, CG-1 conjugated dextran, CG-2 and calcium buffers that contain a well-defined concentration of free Ca^{2+} (not chelated, referred to as Ca^{2+} free) were obtained from Invitrogen Inc. (Burlington, ON, Canada) and used as received. For ensemble measurement, stock solutions

of indicators were prepared by dissolving the bulk solid in pH 7.2 Tris buffer. Immediately before taking spectroscopic measurements, aliquots of the stock solution were added to an appropriate Ca^{2+} free buffer. Absorption and emission spectra were collected in quartz cuvettes on a Varian Cary 500 UV-Vis spectrophotometer and a SPEX 212 spectrofluorimeter, respectively. Fluorescence lifetimes were measured using the method of time-correlated single-photon counting (TCSPC), on a system described in detail elsewhere [18]. Excitation was performed at 488 nm, with the emission collection wavelength of 536 nm. Fluorescence decay profiles were fit using a non-linear least squares reconvolution procedure based on the Marquardt algorithm. The quality of fit was assessed through the value of the reduced χ^2 and through the distribution of weighted residuals.(See detailed description in Appendix)

2.3.2 Single-molecule fluorescence spectroscopy measurements

Single-molecule fluorescence measurements were carried out using a home-built, wide-field epifluorescence microscope [25]. Samples were excited with circularly polarized, continuous wave light from a tunable argon-ion laser, with a wavelength of either 488 or 514 nm (see subsequent text for details). Excitation intensities were typically in the range of 0.5-2.0 kW/cm^2, as measured by dividing the incident power measured at the sample focal plane by the illumination area. Samples were prepared in either one of two ways. In the first approach, an aliquot of a dilute polymer (2% w/v poly(vinyl alcohol) in Millipore water) was spin-cast onto a clean microscope coverglass slide, followed by a dilute solution ($\sim 10^{-9}$ M) of indicator dye in an appropriate Ca^{2+} free buffer . In the second approach, a dilute solution of CG-1 conjugated dextran in Ca^{2+} buffer was mixed with melted, low-gelling temperature agarose (Sigma-Aldrich) which had been prepared using Ca^{2+} calibration buffers. The dye-doped agarose was then sandwiched between two clean pieces of coverglass and allowed to cool. Control samples with the absence of dye show no fluorescent impurities when examined under single-molecule imaging conditions. The use of dextran conjugated CG-1 prevented translational diffusion of the dye through the water-filled pores of the agarose matrix, a phenomenon that has been observed previously in other single-molecule investigations that made use of gels as a support medium [26,27]. We found that, other than slightly different background signal levels, the two sample preparation approaches gave comparable results in terms of single-molecule measurements.

2.4 Results and Discussion

2.4.1 Ensemble spectroscopy measurements

When fluorescence excitation was carried out at 488 nm, the emission spectrum of CG-1 consisted of a single peak with emission maximum at 534 nm. Addition of Ca^{2+} to CG-1 resulted in an increase in the overall emission intensity of the indicator dye solution. Figure 2-2 shows a series of fluorescence emission spectra in which the $[Ca^{2+}]_{free}$ was systematically varied over a concentration range of 0-1.35 μM. There was no substantial shift in peak positions observed with increasing $[Ca^{2+}]_{free}$, but rather a simple increase in the overall fluorescence intensity. Above $[Ca^{2+}]$ of 1.35 μM, there was no further increase in emission intensity with further addition of calcium, indicating saturation of CG-1 had occurred.

By assuming CG-1 binding can be modeled as a simple two-state equilibrium binding process in which the calcium free form of the indicator is non-fluorescent, one can derive Equation (2-1):

$$log\frac{(F_x - F_{min})}{(F_{max} - F_x)} = nlog[Ca^{2+}] - logK_d \qquad (2\text{-}1)$$

where F_x, F_{min} and F_{max} are the fluorescent intensities corresponding to the $[Ca^{2+}]_{free}$ of interest, the intensity at $[Ca^{2+}]_{free} = 0$ and the intensity measured at the maximum value of $[Ca^{2+}]_{free}$, K_d is the dissociation constant for the CG-1 {Ca^{2+}] complex and n is the binding stoichiometry. From the emission data, a K_d of 0.21 μM was calculated, which is in excellent agreement with the value of 0.19 μM reported by the manufacturer [19], along with a 1:1 binding stoichiometry between the indicator and Ca^{2+}.

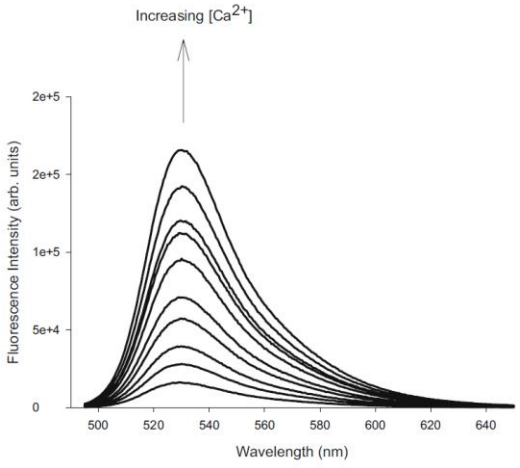

Figure 2-2. Fluorescence emission spectra showing the change in emission of CG-1 as a function of increasing $[Ca^{2+}]_{free}$ ($[Ca^{2+}]_{free}$ ranges from 0 to 1.35 μM, [CG-1] = 1.50 μM)

At saturating conditions of $[Ca^{2+}]_{free}$ (>1.35 μM), the total fluorescence emission intensity, as determined by measuring the integrated area under the emission spectra, increased 16-fold over that of the nominal calcium free buffer. For the calcium free buffer, the emission intensity was extremely low but not precisely zero. This is consistent with the previous measurements carried out on the CG-2 system. The likely sources of this residual fluorescence is trace amounts of unchelated Ca^{2+} in the system and weak fluorescence from uncomplexed CG-1. It is worth noting that the net change in fluorescence emission intensity for CG-1 is almost exactly half of the value that we have reported previously for the CG-2 system (38-fold over the calcium free buffer). This result is entirely consistent with the chemical structures of the two sensor dyes--one would anticipate an approximate doubling of the absorption cross-section of CG-2 over CG-1 simply because of the presence of the two fluorophores in the molecule, and hence a proportional increase in fluorescence output.

In addition to steady-state measurements, time-resolved (lifetime) fluorescence measurements have also been carried out on CG-1. Fluorescence lifetime decay curves, measured for samples ranging in $[Ca^{2+}]_{free}$ from zero to saturation, were well fit by a double-exponential decay (Equation (2-2)) in which none of the fitting parameters (lifetime or pre-exponential factors) were fixed.

$$I(t) = \alpha_1 e^{-t/\tau_1} + \alpha_2 e^{-t/\tau_2} \qquad (2\text{-}2)$$

Curve fitting indicated the presence of two different lifetime components, a long-lived component with a lifetime of 3.4 ± 0.1 ns and a short-lived component with lifetime of 0.2 ± 0.1 ns. A typical fluorescence lifetime decay curve taken at $[Ca^{2+}]_{free}$ = 0.605 μM is shown in Figure 2-3. The relative weighting of the two lifetime components, as determined by the pre-exponential factors (amplitudes), shifted as a function of $[Ca^{2+}]_{free}$. As the $[Ca^{2+}]_{free}$ increased, the pre-exponential factor of the long-lived component increased (0.05 at zero calcium levels, increasing to 0.62 at saturating levels of calcium) and the pre-exponential factor of the short-lived component correspondingly decreased.

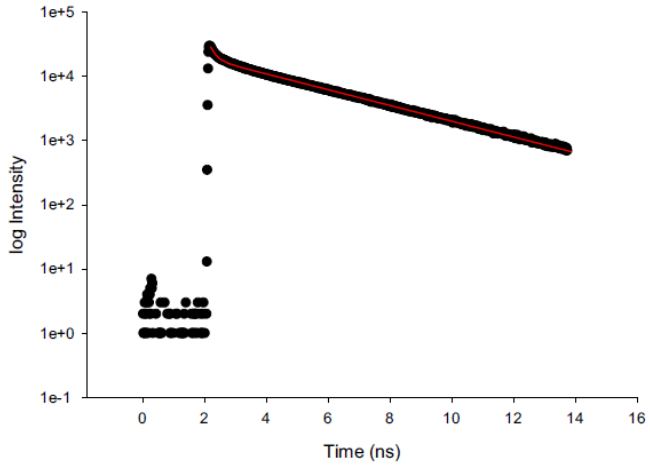

Figure 2-3. Typical fluorescence life-time measurement taken from $[Ca^{2+}]_{free}$ = 0.602 μM. The red line is a double-exponential fit, as described in the main text body.

For CG-1 we interpret this behaviour as being caused by the presence of two distinct chemical species in solution, with the long-lived component corresponding to the presence of the highly-fluorescent (Ca^{2+} bound) specie, and the short-lived component corresponding to the weakly-fluorescent Ca^{2+} free specie. Changes in the pre-exponential factors correspond to changes in the relative proportions of the two species in solution. Similar results for CG-1 lifetimes have been reported by Sanders et al. [28] during fluorescence lifetime imaging experiments on live cells, as well as by Tessier et al. in a fluorescence correlation spectroscopy characterization of conformational dynamics in the CG-1 system [29]. The behaviour and the values for fluorescence lifetimes that have been measured here for CG-1 are also comparable with those we have measured previously for the CG-2 system [2]. For CG-2, two different lifetime components (3.5 ± 0.1 and 0.3 ± 0.1 ns) were also observed, with the pre-exponential factors changing in response to the $[Ca^{2+}]_{free}$. Again, it is not particularly surprising that there is excellent agreement between the lifetimes observed for CG-1 and CG-2, since the fluorophores, while differing in number, are structurally identical. While the mechanism that gives rise to the onset of fluorescence may differ between the two indicators, in both cases the end result of calcium binding is that the fluorophore becomes uncoupled from the rest of the molecule and behaves as an independent fluorophore.

In addition to fluorescence spectroscopy characterization, absorption spectroscopy can also provide valuable insight into the nature of the CG-1 system. Figure 2-4 shows an absorption spectrum for CG-1 taken at zero $[Ca^{2+}]_{free}$. For comparison, this has been overlapped with the

absorption spectrum for CG-2 taken under the same solution conditions. For CG-1, the spectrum consists of a strong peak with absorption maximum at 508 nm and a small shoulder around 460-470 nm. The relative sizes and positions of these spectral features were unaffected by the $[Ca^{2+}]_{free}$ over the entire range of concentrations used in the fluorescence measurements. This is in direct contrast with the behaviour that was reported previously for CG-2, which, at zero $[Ca^{2+}]_{free}$ has two strong peaks located at 490 and 508 nm. Upon increasing $[Ca^{2+}]_{free}$ in CG-2, the relative peak heights were found to shift in favour of the 508 nm peak, to the point where, at saturating concentrations, the blue-shifted shoulder could no longer be distinguished from the dominant red-shifted peak. In combination with force-field based conformational search calculations and fluorescence measurements, the blue-shifted peak was attributed to the formation of a fluorescently quenched exciton state, while the red-shifted peak was tentatively attributed to the two constituent fluorophores on CG-2 behaving as independent monomers resulting from the elimination of exciton splitting. While the previous argument was entirely consistent with the experimental data, an alternative interpretation of the spectra is that the red-shifted peak may be attributed to the formation of an additional excitonic state.

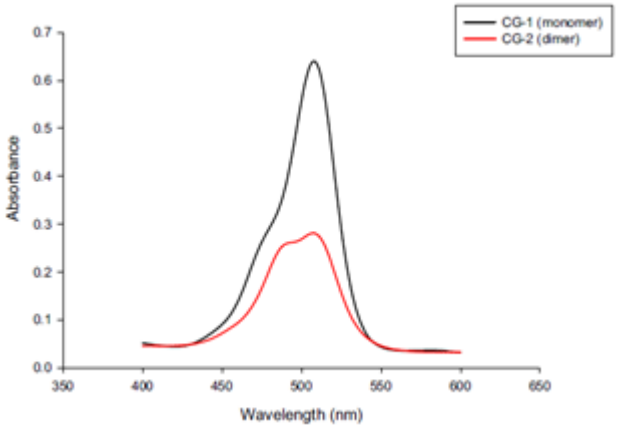

Figure 2-4. Comparison of absorbance spectra for CG-1 and CG-2 at nominal $[Ca^{2+}]_{free}$ = 0 μM

By comparing the absorption spectrum of CG-1 with CG-2, one can definitively identify the nature of the red-shifted peak. Since this peak overlaps exactly with the absorption peak of the "monomeric" CG-1, one can attribute the red-shifted peak of CG-2 to the pure monomer. This additional measurement clearly shows that once CG-2 has bound Ca^{2+}, the two fluorophores no longer quench one another and behave as independent monomers. In the case of CG-1 which operates via a PET mechanism, no significant alterations in the absorption spectrum of the

indicator as a function of $[Ca^{2+}]_{free}$ would be anticipated, which is in agreement with the experimental results obtained here.

2.4.2 Single-molecule fluorescence spectroscopy measurements

Preparation of samples as described in the "Materials and methods" gave rise to a series of bright, fluorescent spots when the samples were imaged in the fluorescence microscope. Under constant laser illumination, the fluorescent spots underwent single-step photobleaching which is taken here, in combination with the diffraction-limited fluorescent spot size and low fluorophore concentration levels, as the signature of individual molecules. A typical fluorescence microscope image of single CG-1 molecules and a fluorescence time trajectory (fluorescence intensity of an individual molecule as a function of time) is shown in Figure 2-5.

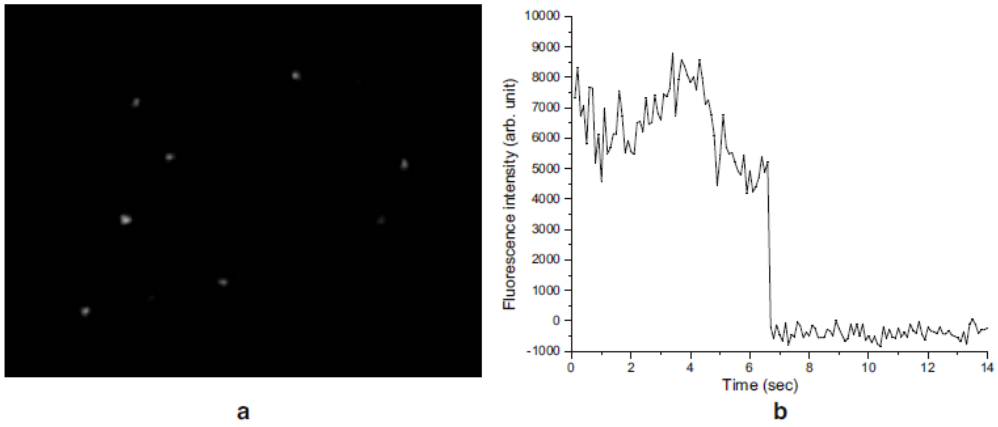

Figure 2-5. (a) Fluorescence image of single CG-1 molecules (~ 10 × 12 μm) and (b) a typical single-molecule fluorescence time trajectory ([CG-1] = 1×10^{-9} M, $[Ca^{2+}]_{free}$ = 5 μM , excitation intensity = 0.8 kW/cm^2)

The fluorescence intensity of individual molecules of CG-1 was measured over $[Ca^{2+}]_{free}$ ranging from the nominal zero concentration to past the saturation level. Consistent with the ensemble fluorescence spectroscopy, samples prepared at $[Ca^{2+}]_{free} = 0$ were not entirely free of fluorescent entities. At zero calcium concentration individual fluorescent molecules could still be detected, though at nanomolar dye concentrations, their number density was very low. To make counting and analysis of these molecules easier, samples were prepared at a higher indicator dye concentration. Increasing the $[Ca^{2+}]_{free}$ resulted in a significant increase in the number of fluorescent molecules that could be detected, but did not affect the average fluorescence intensity

of the molecules. Figure 2-6 shows two histograms of single-molecule fluorescence intensities (in CCD counts) taken at $[Ca^{2+}]_{free} = 0$ and at a $[Ca^{2+}]_{free}$ above saturation. The two histograms do not differ significantly from one another, and in view of this, we can attribute the general increase in fluorescence intensity of the dye solutions with a simple increase in the number of fluorescent molecules in solution which is as expected from the ensemble measurements. Indeed, samples prepared at saturating $[Ca^{2+}]_{free}$ can be prepared at lower indicator dye concentrations in order to achieve the same number density of molecules in the sample. We note that the fluorescent intensities of the individual CG-1 molecules are comparable with the emission intensities we have reported previously, under similar imaging conditions, for individual rhodamine 6G molecules [25], which is entirely reasonable given the nature of the fluorophore.

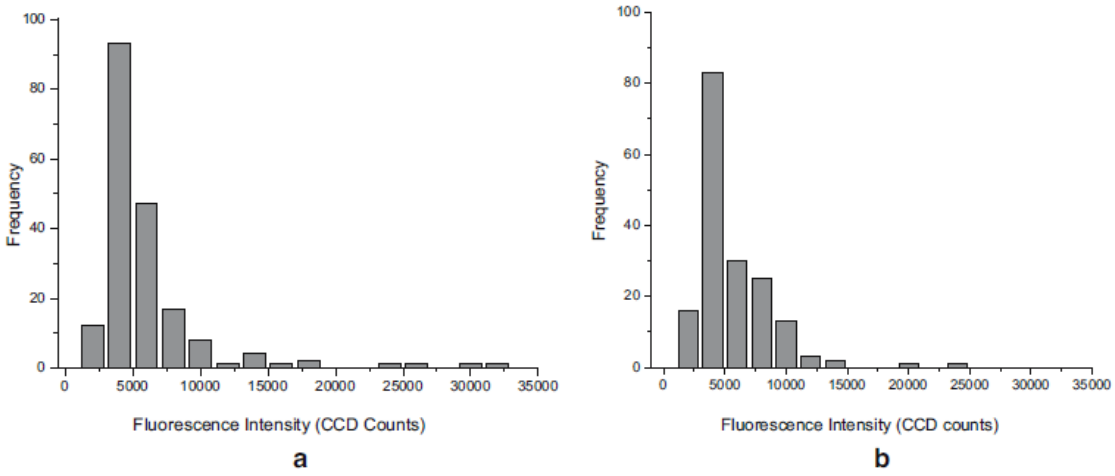

Figure 2-6. Histograms of single-molecule fluorescence intensities for (a) $[Ca^{2+}]_{free} = 0$ μM and (b) $[Ca^{2+}]_{free} = 5$ μM. In both cases, excitation intensity was 0.8 kW/cm^2

As an additional, simple verification that there were no significant changes in the spectroscopic nature of CG-1 molecules as a function of $[Ca^{2+}]_{free}$, histograms of photobleaching times (on-times) were measured for a number of different calcium concentrations. If the emission properties of CG-1 molecules are indeed independent of $[Ca^{2+}]_{free}$, then one would anticipate no significant differences in the mean photobleaching times measured as a function of concentration. Figure 2-7 shows on-time histograms for CG-1 taken at two extreme points of $[Ca^{2+}]_{free}$, one in the absence of calcium the other under saturating calcium concentrations. In both cases, the data was well fit by a single exponential function, as expected for a simple, random Poisson process [30]. Fitting constants were within one measure of standard error of each

other, indicating that within the time resolution of our system, there was no significant difference in photobleaching time for the two different set of conditions. While these simple photobleaching experiments will not probe more subtle differences between fluorophores, it is reasonable to assume from the combination of these measurements and the SM intensity characterization, that there is no substantial difference in the spectroscopic properties of CG-1 as a function of $[Ca^{2+}]_{free}$.

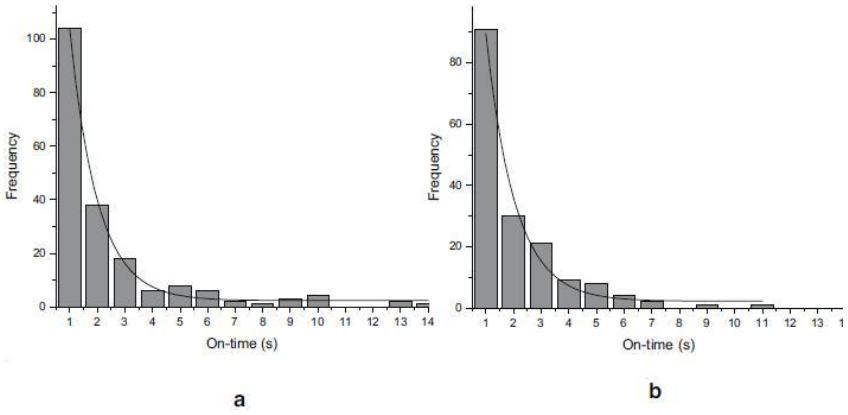

Figure 2-7. Histogram of fluorescence on-times along with single-exponential fits (fitting equation was $f(x) = A_1 \exp(-x/t_1) + y_0$) for individual CG-1 molecules measured at (a) $[Ca^{2+}]_{free}$ = 0 μM (t_1 = 1.00 ± 0.05 s^{-1}), (b) $[Ca^{2+}]_{free}$ = 5 μM (t_1 = 1.05 ± 0.11 s^{-1}). In both cases, the laser excitation intensity was 0.8 kW/cm^2.

During the course of their SM studies, both Ha et al. [16] and Brasselet et al. [14] noted statistically significant variations in the width of a variety of single-molecule measurement histograms as a function of target ion concentration. These width variations were tentatively attributed to a distribution of free energy changes for the deprotonation-protonation equilibrium related to local environmental effects. For Brasselet's pH sensor system, it was proposed that a possible source of variation in the local environment were interactions of the dextran chain (Brasselet et al. also made use of a dye-labeled dextran chain to minimize translational diffusion in agarose) with the wall of the agarose pores. For the CG-1 dextran system, these effects, if they exist, do not appear to significantly affect the observed SM histogram widths. However, since CG-1 binds its target ion much more strongly than the SNARF-1 pH sensor it is reasonable to expect that effects related to binding and unbinding of the target ion would be negligible. In general, there is much

information that could potentially be extracted from the shapes of histograms in SM experiments, and further efforts need to be devoted to this important aspect of data analysis in the future.

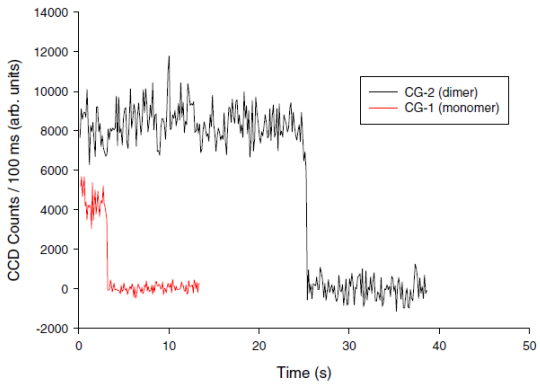

Figure 2-8. Single-molecule fluorescence time trajectories for a molecule of CG-2 and a molecule of CG-1 taken under comparable fluorescence imaging conditions

In addition to probing the nature of the CG-1 fluorophore and SM histogram widths, it is also informative to compare the relative intensities of individual CG-1 and CG-2 molecules. Figure 2-8 shows an overlay of two typical single-molecule fluorescence time trajectories for CG-1 and CG-2. It must be noted that in preliminary single-molecule measurements of CG-1, experiments were carried out under the same conditions as those used to characterize CG-2 (488 nm excitation, 0.9 kW/cm^2 excitation intensity, same emission filters and CCD multiplier gain) in order to allow direct comparison of experimental data. However, it was found that the CG-1 single-molecule emission intensity was significantly lower than that obtained for CG-2 with the same instrumental settings, and in order to produce acceptable signal-to-noise ratios, the excitation wavelength was adjusted to 514 nm (absorption maximum is 508 nm) and appropriate emission filters were selected. In general, it was observed that CG-2 molecules always had a significantly greater emission intensity than CG-1 molecules (typically~ 9,000 CCD counts/100 ms for CG-2 versus ~ 4,500 CCD counts/100 ms for CG-1). While comparing absolute intensities in single-molecule measurements is often problematic because of the influence of randomly oriented transition dipoles and minor inhomogeneities in illumination intensity across the diameter of the epifluorescence illumination spot, it was found that CG-2 molecules had approximately twice the intensity of CG-1 molecules. Of course, the relative difference in excitation efficiency that comes from using 514 nm over 488 nm must be accounted for in this comparison, though this should lead to relatively minor (order one) corrections in the overall

CG-1 intensity. It should also be noted that the emission filter sets used for 514 and 488 nm excitation had comparable transmission efficiencies over the emission range of CG-1, and will not substantially alter the overall signals.

Even accounting for the minor differences in excitation wavelength, the results of the single-molecule imaging experiments are consistent with those obtained from the bulk studies. That is, at the single-molecule level, CG-2 is approximately twice as bright as CG-1. Again, this is exactly the expected result. On a per molecule basis, the fluorescence signal of CG-2 should be approximately twice that of the monomeric CG-1, simply because the molecule will have an absorption cross-section that is approximately twice as large.

2.5 Summary

In this work, the spectroscopic properties of the Ca^{2+} indicator dye CG-1 has been characterized using a combination of ensemble and SM techniques. It was found that the overall increase in fluorescence intensity of this dye with $[Ca^{2+}]_{free}$ can simply be attributed to an increase in number of fluorescent molecules rather than a general increase in the emission intensity of a molecule. Comparison of the absorption spectra for CG-1 and it's dimeric variant, CG-2, allowed for the definitive assignment of a peak in the CG-2 spectrum, further reinforcing the previously proposed mechanism of action. Finally, in a comparison of the two indicator dyes, CG-1 was found to have one half of the emission intensity of CG-2, which is the simple, expected result for a molecule containing half as many fluorophores.

2.6 Acknowledgements

Funding for this work was provided by the Natural Sciences and Engineering Research Council of Canada and by the University of Saskatchewan. Professor Ron Steer, Dr. Sophie Brunet and the Saskatchewan Structural Sciences Centre are acknowledged for providing access and technical assistance with fluorescence lifetime measurements.

2.7 References

1. Bootman, M. D.; Collins, T. J.; Peppiatt, C. M.; Prothero, L. S.; MacKenzie, L.; De Smet, P.; Travers, M.; Tovey, S. C.; Seo, J. T.; Berridge, M. J.; Ciccolini, F.; Lipp, P. *Seminars in Cell & Developmental Biology* **2001**, *12*, 3-10.
2. Bagh, S.; Paige, M. F. *Journal of Physical Chemistry A* **2006**, *110*, 7057-7066.
3. Lu, Y.; Paige, M. F. *Journal of Fluorescence* **2007**, *17*, 739-748.
4. Weiss, S. *Science* **1999**, *283*, 1676-1683.
5. Moerner, W. E.; Orrit, M. *Science* **1999**, *283*, 1670-1676.
6. Moerner, W. E. *Journal of Physical Chemistry B* **2002**, *106*, 910-927.
7. Ambrose, W. P.; Goodwin, P. M.; Jett, J. H.; Van Orden, A.; Werner, J. H.; Keller, R. A. *Chemical Reviews* **1999**, *99*, 2929-2956.
8. Prodi, L. *New Journal of Chemistry* **2005**, *29*, 20-31.
9. Prodi, L.; Bolletta, F.; Montalti, M.; Zaccheroni, N. *Coordination Chemistry Reviews* **2000**, *205*, 59-83.
10. Czarnik, A. W. *Accounts of Chemical Research* **1994**, *27*, 302-308.
11. de Silva, A.; Gunnlaugsson, T.; Rice, T. *Analyst* **1996**, *121*, 1759-1762.
12. Callan, J. F.; de Silva, A. P.; Magri, D. C. *Tetrahedron* **2005**, *61*, 8551-8588.
13. Zang, L.; Liu, R. C.; Holman, M. W.; Nguyen, K. T.; Adams, D. M. *Journal of the American Chemical Society* **2002**, *124*, 10640-10641.
14. Brasselet, S.; Moerner, W. E. *Single Molecules* **2000**, *1*, 17-23.
15. Brasselet, S.; Peterman, E. J. G.; Miyawaki, A.; Moerner, W. E. *Journal of Physical Chemistry B* **2000**, *104*, 3676-3682.
16. Ha, T.; Zhuang, X. W.; Kim, H. D.; Orr, J. W.; Williamson, J. R.; Chu, S. *Proceedings of the National Academy of Sciences of the United States of America* **1999**, *96*, 9077-9082.
17. Cossart, R.; Lkegaya, Y.; Yuste, R. *Cell Calcium* **2005**, *37*, 451-457.
18. Knot, H. J.; Laher, I.; Sobie, E. A.; Guatimosim, S.; Gomez-Viquez, L.; Hartmann, H.; Song, L. S.; Lederer, W. J.; Graier, W. F.; Malli, R.; Frieden, M.; Petersen, O. H. *Molecular Interventions* **2005**, *5*, 112-127.
19. Haugland, R. P.; 9 ed.; Molecular Probes Inc.: 2002.
20. Tsien, R.; Pozzan, T. *Methods in Enzymology* **1989**, *172*, 230-262.

21. Tsien, R. Y. *Biochemistry* **1980**, *19*, 2396-2404.
22. Grynkiewicz, G.; Poenie, M.; Tsien, R. Y. *Journal of Biological Chemistry* **1985**, *260*, 3440-3450.
23. Minta, A.; Kao, J. P. Y.; Tsien, R. Y. *Journal of Biological Chemistry* **1989**, *264*, 8171-8178.
24. de Silva, A. P.; Gunaratne, H. Q. N. *Journal of the Chemical Society-Chemical Communications* **1990**, 186-188.
25. Bagh, S.; Paige, M. F. *Canadian Journal of Chemistry-Revue Canadienne De Chimie* **2005**, *83*, 435-442.
26. Dickson, R. M.; Norris, D. J.; Tzeng, Y. L.; Moerner, W. E. *Science* **1996**, *274*, 966-969.
27. Dickson, R. M.; Cubitt, A. B.; Tsien, R. Y.; Moerner, W. E. *Nature* **1997**, *388*, 355-358.
28. Sanders, R.; Gerritsen, H. C.; Draaijer, A.; Houpt, P. M.; Levine, Y. K. *Bioimaging* **1994**, *2*, 131-138.
29. Tessier, A.; Meallet-Renault, R.; Denjean, P.; Miller, D.; Pansu, R. B. *Physical Chemistry Chemical Physics* **1999**, *1*, 5767-5769.
30. Basche, T.; Ambrose, W. P.; Moerner, W. E. *Journal of the Optical Society of America B-Optical Physics* **1992**, *9*, 829-836.

APPENDIX

TIME-CORRELATED SINGLE PHOTON COUNTING

1. Introduction

Time-Correlated Single Photon Counting (TCSPC) is a technique to record the low light signals with picosecond time resolution. In this thesis, TCSPC was used to characterize the fluorescent lifetimes of our target fluorophores.

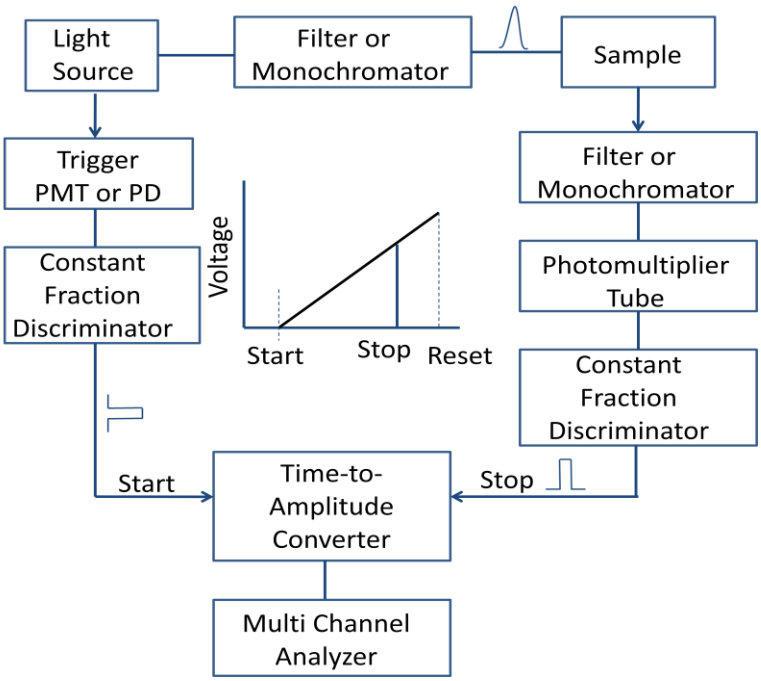

Figure 2-9. Schematic diagram illustrating the operational principles of TCSPC[1] (Reproduced with the permission from Review of Scientific Instruments **1999**, 70, 1837. Copyright 1999 American Institute of Physics)

In TCSPC measurements, the pulsed light source (usually pulsed laser) is utilized to repetitively excite the sample. The pulse will also be optically monitored by the photo multiplier tube (PMT) and then generate a start signal to trigger the voltage ramp of the time-to-amplitude converter (TAC). Analogous to an ultrafast stopwatch, TAC will stop the voltage ramp as soon

as the first fluorescence photon is detected. The voltage of the output pulse provided by TAC is always linearly proportional to the time interval between the start and stop signal. Such voltage is converted to a time channel by a multichannel analyzer (MCA) using an analog-to-digital converter (ADC). After a certain period of dead time, the measurement will start over again, and the experiment is continued until a suitable number of counts are collected in the peak channel. By summing over all the measurements, the MCA will build up a probability diagram of counts (number of arrival photons) as a function of time channels (shown in Figure 2-10.).

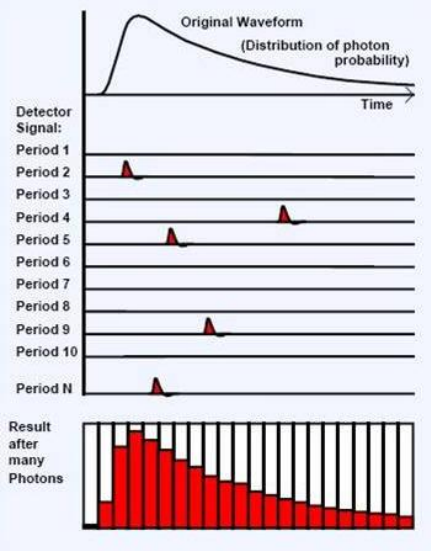

Figure 2-10. Schematic illustration showing the process by which a fluorescence decay profile is developed[2] (Reproduced with the permission from The BH TCSPC Handbook. Copyright 2010 http://www.becker-hickl.com)

2. Date Analysis

As shown in Figure 2-11., the instrument response function (IRF), known as the response of the instrument to a zero-lifetime sample (usually a Ludox solution), is also collected in the TCSPC measurements. The measured decay function is a convolution of the IRF and the true fluorescence decay. One needs to deconvolve the two functions to extract the true fluorescence decay. The true fluorescence decay can then be fit to an appropriate function and the fluorescence lifetime can be extracted.

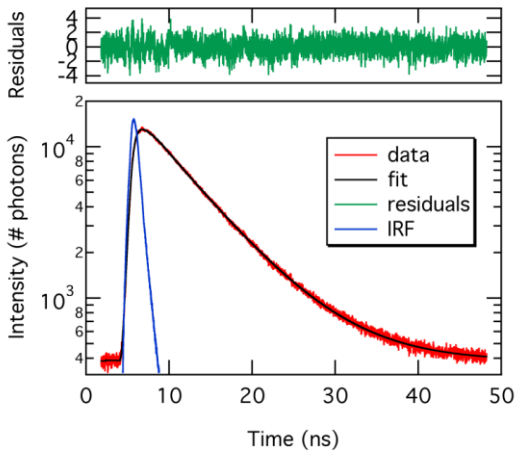

Figure 2-11. Sample fluorescence decay profile (in red), instrument response function (IRF), the convolved exponential fit (blank), and fit residuals (green)

In this thesis, the quality of the data fitting was evaluated by means of the reduced χ^2 and the distribution of the weighted residuals (see Figure 2-11.). The value of χ^2_{red} can be calculated from the following equation,

$$\chi^2_{red} = \frac{1}{\upsilon}\Sigma\frac{(O-E)^2}{\sigma^2} \qquad (2\text{-}3)$$

where υ is the degrees of freedom, O and E represents for the observed and estimated value respectively, and σ^2 is the variance of the observation. In general, a large χ^2_{red} value indicates a poor model fit. In principle, a value of $\chi^2_{red}=1$ indicates that the extent of the match between observation and estimates is in accord with the error variance.

3. References

1. Becker, W.; Hickl, H.; Zander, C.; Drexhage, K. H.; Sauer, M.; Siebert, S.; Wolfrum, J. *Review of Scientific Instruments* **1999**, *70*, 1835-1841.
2. Becker & Hickl GmbH, *The BH TCSPC Handbook*, http://www.becker-hickl.com/literature.htm (accessed Jan 2011).

CHAPTER 3

DUAL-POLARIZATION IMAGING OF A DUAL-FLUOROPHORE ION SENSOR: A SINGLE-MOLECULE STUDY

This chapter is a slightly modified copy of an article published in *ChemPhysChem* in September 2008. (Reproduced with permission from ChemPhysChem **2008**, 9, 1947-1953. Copyright 2008 WILEY-VCH Verlag GmbH & Co. KGaA, Weinheim)

From previous investigations in the Paige research group, it has been determined that the dual-fluorophore Ca^{2+} indicator, CG-2, will, in the absence of Ca^{2+}, adopt a self-quenching conformation in which the molecular planes of the two fluorophores are parallel to each other. When bound to Ca^{2+}, the molecule planes of the two fluorophores make an angle of ~ 120 ° with respect to each other, and CG-2 becomes strongly fluorescent.

In this chapter, experiments are described in which the single-molecule epifluorescence microscope was converted into a dual-polarization fluorescence microscope, allowing us to directly determine the relative orientation of the two fluorophores in the dual-fluorophoric system. The CG-2 samples were prepared following the same procedure as the conventional SM measurements, and the molecules are considered randomly-orientated on the surface of the glass coverslip. Frequency histograms of fluorescence polarization were constructed, and the results were compared with results simulated using a simple mathematical model. These measurements confirmed the molecular conformation of the two fluorophore subunits in CG-2 when bound to Ca^{2+}. The results were in good agreement with the results determined in earlier investigations.

For this research paper, I prepared samples, performed the measurements, played a major role in developing the mathematical model, interpreting the results, and the preparation of the paper. Dr. Richard Bowles provided guidance in the mathematical model construction. My supervisor provided guidance throughout the experimental work and was involved in result interpretation and in writing this paper.

3. Dual-Polarization Imaging of a Dual-Fluorophore Ion Sensor: A Single-Molecule Study

*Yin Lu, Richard K. Bowles, and Matthew F. Paige**

Department of Chemistry, University of Saskatchewan, 110 Science Place, Saskatoon, SK. Canada S7N 5C9

Published: September 15, 2008

3.1 Abstract

The fluorescence emission of the dual-fluorophore Ca^{2+} ion sensor molecule, Calcium-Green 2 (CG-2), has been characterized using dual-polarization imaging at the single-molecule level. By comparing the fluorescence intensity of individual CG-2 molecules in two mutually orthogonal polarization image channels, information about the relative orientation of the two constituent fluorophores in the molecule is obtained. Experimental results from polarization measurements are compared with those predicted from a geometric model based on coupled-fluorophores that are randomly distributed in space. The results confirm previous optical spectroscopy-based predictions of the orientation of CG-2's fluorophores, and the general applications of this dual-polarization imaging approach for characterizing the optical properties of molecules containing multiple fluorophores is discussed.

3.2 Introduction

Intramolecular energy transfer in multifluorophoric molecules is a topic of considerable importance shown by the recent interest in the scientific literature.[1-6] Significant advances have been made in understanding these energy-exchange processes through the application of single-molecule fluorescence measurements,[7-11] as these measurements provide information that is averaged in conventional ensemble spectroscopy measurements. Some of the particularly

important observations that have been made in this field of study include the observation of collective photobleaching and exciton dynamics, to name a few.

Of interest to our research group have been the combined ensemble and single-molecule investigations of commercial calcium-ion indicators know as the "calcium green" family, as these indicator dyes provide an opportunity to study energy exchange in multifluorophoric systems in a highly-controlled manner. In general, Ca^{2+}-indicators are chemical entities that undergo significant increases in fluorescence emission upon binding with Ca^{2+} ions.[12] The ability to detect and quantify intracellular free Ca^{2+} is of great importance in understanding a wide range of cellular processes, and fluorescence-based ion indicators that can be used to detect Ca^{2+} are one of the most widely used types of indicator for in vivo detection of free Ca^{2+}.

We have recently reported the spectroscopic characterization of calcium-green 2 (CG-2) using both ensemble and single-molecule (SM) measurements.[13] CG-2 is a dual-fluorophore molecule, and is based on a Ca^{2+} chelating group (1,2- bis(o-aminophenoxy) ethane-N,N,N',N'-tetracetic acid or BAPTA) tethered to two fluorescein-like fluorophores (Figure 3-1).[14] Ensemble-based optical spectroscopy in conjunction with molecular-mechanics calculations indicate that in the absence of Ca^{2+}, the molecule adopts a conformation in which the two fluorophores adopt an approximately coplanar arrangement, and the fluorescence is quenched by intramolecular exciton formation. Binding of Ca^{2+} gives rise to a structural change, which disrupts quenching and results in strongly emissive fluorophores. In effect, addition of Ca^{2+} provides a chemical "handle" to enable or disable energy transfer in this system. Single-molecule measurements indicate that for the Ca^{2+} bound form, Förster energy-transfer can take place between the two fluorophores at a rate that exceeds the rate of fluorescence, which gives rise to collective photobleaching of both fluorophores upon formation of a damaged (trap) state.

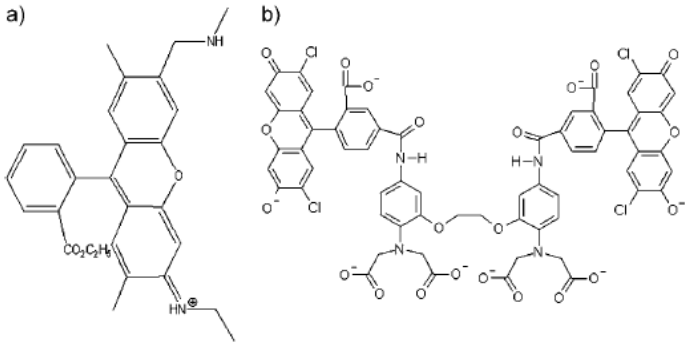

Figure 3-1. Chemical structures for a) rhodamine 6G (R6G) and b) calcium-green 2 (CG-2).

An important property that controls the extent of energy transfer between fluorophores in this system, and in many other multifluorophoric systems, is the relative orientation of the constituent emission transition dipoles in the molecule.[1,3,5,6,15] Determining the relative orientation of fluorophores in multifluorophoric systems at the single-molecule level can provide significant insight into how energy exchange takes place, but extracting this information from a conventional single-molecule fluorescence experiment can be problematic.

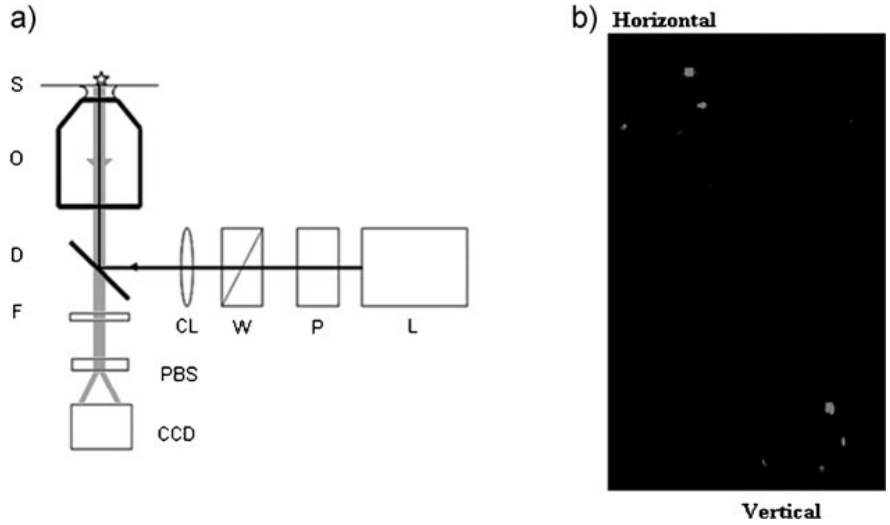

Figure 3-2. a) Schematic diagram of a dual-polarization fluorescence imaging microscope (L: illumination laser, P: polarizer, W: Berek waveplate, CL: convex lens, D: dichroic mirror, O: objective lens, S: sample, F: filter, PBS: polarizing beam splitter, CCD: CCD detector). b) Dual polarization image of FluoSpheres® (amine-modified microspheres, 1.0 μm).

Herein, we describe single-molecule fluorescence polarization imaging experiments that allow the determination of relative orientation of the two transition dipole moments in Ca^{2+}-bound CG-2. A number of methods for determining single-molecule orientations have been reported in the literature, including the use of near-field scanning microscopy,[16] defocused emission patterns[17] and others (for a recent review, see Moerner and Fromm).[9] The experimental approach used in this work is based on "dual-view" polarization microscopy that was first described by Kinosita.[18] In dual-view polarization measurements, a single-molecule fluorescence emission image is split into two orthogonal polarization images, and the intensity ratio between the images provides information on the orientation of the constituent fluorophore (Figure 3-2). Our working approach in these experiments is to assume a particular orientation of fluorophores for CG-2 based on our

previous measurements,[13] calculate a theoretical intensity ratio distribution based on this assumed orientation, and then compare the experimentally measured data to that predicted by the theoretical model. As a control sample, individual molecules of the single-fluorophore molecule rhodamine 6G (R6G) were also measured in a similar way and compared to the results obtained for CG-2. In the following sections, we describe details of the experimental measurements and calculations necessary to accomplish this study.

3.3 Results and Discussion

3.3.1 Derivation of mathematical models

(A) Single Transition Dipole (R6G)

Fluorescence emission of individual molecules that have been immobilized in a polymer matrix can be modeled as randomly oriented, stationary1D transition dipoles. The mathematics underlying this situation have been reviewed in detail by Goldman et al.,[19] and the calculations described herein are based on this work. In dual-polarization imaging, the fluorescence emission from a single molecule is split into two orthogonal polarization components. The ratio of the two emission polarization components (referred to as the polarization ratio) provides information about the orientation of the emission transition dipole, and hence the molecule, with respect to the measurement system.

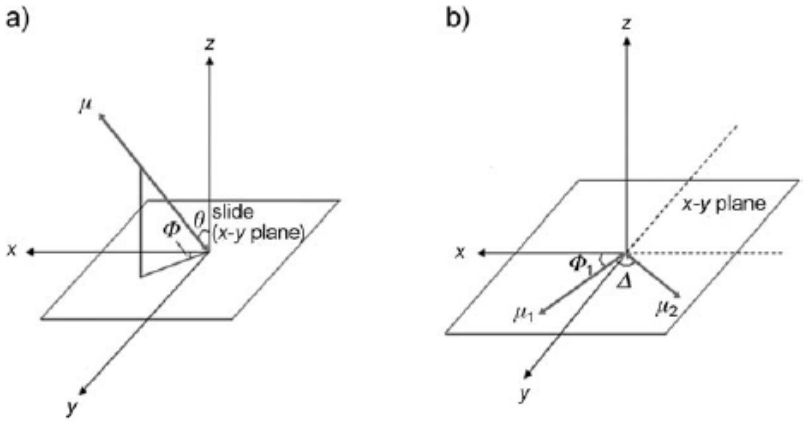

Figure 3-3. Schematic illustration of co-ordinate system used to calculate polarization ratios for a) 1D transition dipole (R6G) and b) dual transition dipoles (CG-2).

Geometrically, both the absorption and emission transition dipole orientations for a fluorophore can be defined through the polar angles, θ and ϕ, as shown in Figure 3-3. For these calculations, it is assumed that the absorption and emission transition dipoles are collinear (θ_a, ϕ_a) = (θ_e, ϕ_e) = (θ, ϕ) which is a reasonable assumption for fluorescein-like fluorophores.[20] During far-field excitation with laser illumination that is circularly polarized in the x-y plane, the absorption probability (f_a) depends on the transition dipole orientation according to Equation (3-1):

$$f_a = \frac{1}{2} sin^2\theta \tag{3-1}$$

The intensity of the detected fluorescence with polarization along the x- (referred to as I_x) and y- (referred to as I_y) directions are represented by Equations (3-2) and (3-3):

$$I_x \propto C_1 sin^2\theta cos^2\phi + C_2 sin^2\theta sin^2\phi + C_3 cos^2\theta \tag{3-2}$$

$$I_y \propto C_2 sin^2\theta cos^2\phi + C_1 sin^2\theta sin^2\phi + C_3 cos^2\theta \tag{3-3}$$

The coefficients C_1, C_2 and C_3 are closely related to the numerical aperture (NA) of the microscope objective. For the oil immersion objective with NA = 1.4 used in these experiments, the calculated values for these constants are C_1 = 0.742, C_2 = 0.016, C_3 = 0.243.

The dependence of fluorescence intensity on transition dipole orientation can be determined by combining the expressions for absorption and detection probabilities of the fluorophores. The general equations for the expected fluorescence intensities from a single, stationary molecule are shown in Equations (3-4) and (3-5):

$$I_x = \frac{1}{2} K sin^2\theta \, (C_1 sin^2\theta cos^2\phi + C_2 sin^2\theta sin^2\phi + C_3 cos^2\theta) \tag{3-4}$$

$$I_y = \frac{1}{2} K sin^2\theta \, (C_2 sin^2\theta cos^2\phi + C_1 sin^2\theta sin^2\phi + C_3 cos^2\theta) \tag{3-5}$$

where K is a constant that depends on the photophysical properties of the fluorophore (i.e. absorption cross-section) plus instrumental factors, and is independent of the orientation of the molecules.

As a result, the overall fluorescence polarization ratio, P, can be calculated from the intensities in Equations (3-4) and (3-5) and is represented by Equation (3-6):

$$P = \frac{I_x - I_y}{I_x + I_y} = \frac{(C_1 - C_2)(sin^2\phi - cos^2\phi)}{(C_1 + C_2) + 2C_3 cot^2\theta} \tag{3-6}$$

By calculating P for all possible values of ϕ and θ, a simulated histogram of P for randomly oriented 1D transition dipoles (individual molecules) can be generated, and compared with an experimentally measured histogram.

An additional complication that must be considered when comparing histograms calculated using Equation (3-6) with their experimental counterparts is that the need to attain acceptable signal-to-noise ratios will bias which transition dipole orientations can be experimentally observed. When illuminating the sample with light that is circularly polarized in the sample plane, transition dipoles that are z-oriented ($\theta = 0°$) will not absorb. In general, transition dipoles that have a significant degree of z-orientation will have a low probability of absorbing, which results in a low signal-to-noise ratio (SNR) in the fluorescence image. If the SNR is too low, then the molecule will not be observed. We accounted for this effect in the calculated histogram by including only transition dipoles that lie within the x–y plane ($\theta = 90°$). Calculations indicate that the overall shape of the polarization histogram does not change substantially even when θ deviates significantly from 90°, but for the sake of simplicity, we will restrict our calculations to orientations that fall within the x-y plane. For the experimental data, any molecule for which the total detector photocounts (the sum of I_x and I_y) was less than three times of the size of background fluctuation was deemed to be strongly aligned in the z-orientation, and this molecule's signal was discarded from the statistical results.

(B) Dual Transition Dipoles (CG-2)

As stated in the Introduction, CG-2 is a dual-fluorophore (dimer) molecule in which the relative orientation of the fluorophores controls the overall fluorescence emission intensity of the molecule. According to molecular-mechanics calculations carried out in previous studies, binding of Ca^{2+} causes the two transition dipoles to adopt an angle of ~ 120° with respect to one another. Generating a histogram of polarization values for randomly distributed, Ca^{2+}-bound CG-2 molecules is significantly more complicated than for the 1D transition dipole. The overall fluorescence polarization intensities can be calculated using the same approach as for the monomer system, but with summing the contributions from both transition dipoles as shown in Equations (3-7), (3-8) and (3-9):

$$I_x = I_{x(1)} + I_{x(2)} \tag{3-7}$$

$$I_y = I_{y(1)} + I_{y(2)} \tag{3-8}$$

$$P = \frac{I_x - I_y}{I_x + I_y} = \frac{I_{x(1)} + I_{x(2)} - I_{y(1)} - I_{y(2)}}{I_{x(1)} + I_{x(2)} + I_{y(1)} + I_{y(2)}}$$

$$= \frac{(C_1 - C_2)[\cos(2\phi_1) sin^4\theta_1 + \cos(2\phi_2) sin^4\theta_2]}{(C_1 + C_2)[sin^4\theta_1 + sin^4\theta_2] + 2C_3[cos\theta_1 sin^2\theta_1 + cos\theta_2 sin^2\theta_2]} \tag{3-9}$$

However, assuming that the two transition dipoles remain at a fixed angle with respect to each other during the experiment, and making the approximation that all molecules are oriented in the x-y plane simplifies the situation considerably. Referring to Figure 3-3 b), one can define ϕ_1 and ϕ_2 as the angle between each transition dipole and the x-axis, and Δ as the angle between the two transition dipoles. One can now derive a general expression in terms of these variables. Converting to radians and assuming the previously noted angle between dipoles yields Equations (3-10) and (3-11):

$$\Delta = \pi - \phi_2 - \phi_1 = \frac{2}{3}\pi \tag{3-10}$$

$$P = \frac{(C_1 - C_2)cos\Delta\cos(2\phi_1 + \Delta)}{C_1 + C_2} \tag{3-11}$$

Again, by simply calculating P for all possible values of ϕ_1 in the x-y plane, a polarization histogram can be developed. A further benefit of this expression is that one can explore the influence that fluctuations in the angle between transition dipoles (Δ) have on the overall polarization distribution.

3.3.2 Fluorescence polarization

Dual-polarization images of individual CG-2 and R6G molecules were collected and analyzed. Figures 3-4 a) and b) show typical results from a single-molecule measurement for CG-2, both in terms of a dual-polarization image and in fluorescence-intensity time trajectories. Fluorescent spots were ~ 300 nm in diameter (as determined by calibrating the detector pixel size against a standard USAF test target), which is consistent with the diffraction limited size expected for an individual molecule. Upon continuous laser illumination at an excitation intensity of 1.5 kW/cm^2, the majority of the fluorescence spots photobleach in a single step (typical time-trace shown in Figure 3-4 b), which we take as the signature of an individual molecule. Typical single-molecule signal intensities (taken as the sum of signals from the x- and y- directions) were ~ 8900 detector photocounts, which is comparable with the signal intensities measured in our previous single-molecule imaging measurements taken under similar experimental conditions (same optical filters, illumination intensity and on-chip multiplier gain). Samples prepared from R6G showed similar properties, though the single-molecule intensities were lower than that for CG-2 (typically ~ 4500 detector photocounts).

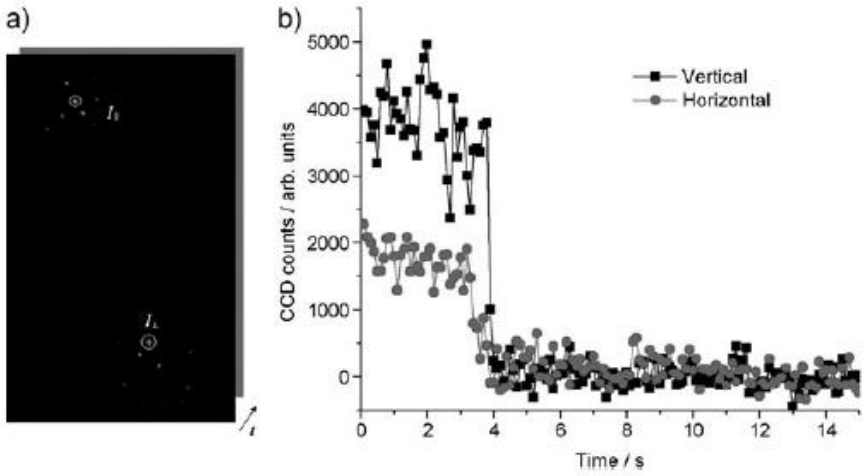

Figure 3-4. a) Dual-polarization fluorescence image of single CG-2 molecules (~ 10 μm × 12 μm). Collecting a sequential time series of these images allows the generation of fluorescence time trajectories. b) Dual-polarization single-molecule fluorescence time trajectory of a CG-2 molecule. The two traces represent the signal intensity in each polarization channel.

By measuring fluorescence-time trajectories for many (~ 200) different R6G molecules and calculating experimentally measured polarization ratios, histograms of polarization ratios were generated. Figures 3-5 a) and b) show the histograms of polarization ratios calculated for the 1D transition dipole (Equation (3-6)) and the experimentally measured histogram for R6G. The calculated histogram consists of two maxima at polarization values 1.0 to 0.8 and -1.0 to -0.8, and a range of values in between that slowly decrease to a central minimum. This result is the same as that calculated by Bawendi et al.[21] as well as a number of others who have modelled 1D transition dipoles. It should be noted that the maxima in this distribution do not indicate a preferred orientation of the molecules along the x- or y-axis, but rather reflects the fact that Equation (3-6) changes very slowly at extreme angles of the in-plane angle, ϕ. The experimental polarization ratio histogram measured for R6G is in good agreement with the calculated distribution, as shown in Figure 3-5 b) and verified by a χ^2 test. We note that while the measurements were able to reproduce the two maxima at the extreme ends of the histogram, the subtle decrease in probability as the polarization ratio approaches zero is lost, simply because of statistical noise. Nonetheless, the main features of the calculated distribution are observed in the experimental data and we take this result to mean that the dual-polarization imaging approach works well, and can be reliably applied to the dimeric transition dipole system.

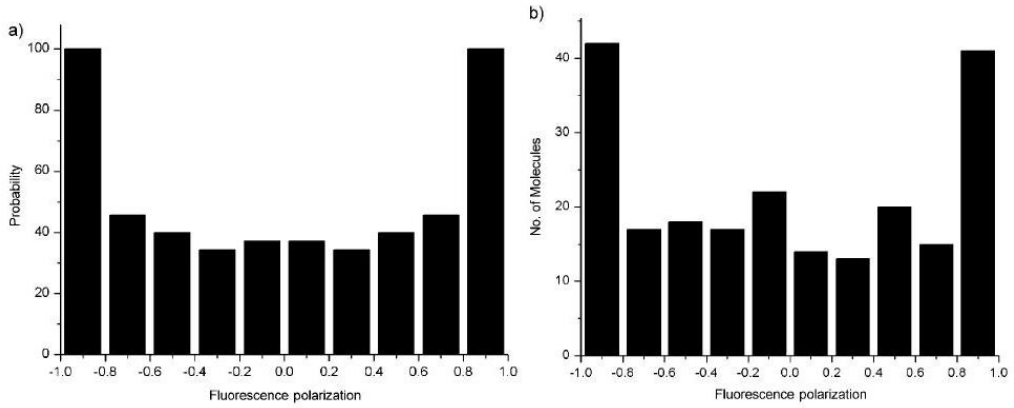

Figure 3-5. a) Fluorescence-polarization histogram for randomly oriented 1D transition dipole moments. Histogram was calculated using Equation (3-6). b) Experimentally determined fluorescence-polarization histogram for individual R6G molecules on poly(vinyl alcohol).

It is worth noting that the rate of energy transfer between fluorophores plays an important role in the polarization ratio histograms that are measured for CG-2. In a related study, Schroeyers et al. have reported time-dependent changes in single-molecule emission polarization patterns when measured using de-focused epifluorescence imaging for perylene imide-based dendrimers.[22] In Schroeyers' dendrimer system, there are four fluorophores per molecule and only one will emit at a time because of intramolecular energy transfer. Long-term observation (several hundreds of seconds) of these molecules shows that the emission pattern changes because different emitters will turn on during the course of the measurement. This effect has been attributed, in part, to dynamics of the polymer matrix in which the dendrimer was embedded. However, this effect will not be observed in the CG-2 system simply because of the high rate of intra-molecular energy transfer between the two fluorophores. We have previously calculated that the rate of energy transfer between the two fluorophores is ~ 1000 times faster than the rate of fluorescence emission.[13] This means that during the time course of the experiments described here (our CCD camera has the acquisition rates of ~ 30 ms/frame) we observe the time-averaged emission of both fluorophores. That is, the different emission patterns of the two emitters will be blended together because of the rate of energy transfer in comparison with our data collection rate. Our

model calculations also assume that both emitters contribute to the polarization pattern, which is correct given the rate of energy transfer between them.

For CG-2, samples that had been prepared under both Ca^{2+} free and Ca^{2+} saturated conditions were measured and polarization ratio histograms were compared with those calculated using Equation (3-11). Results from these calculations and measurements are shown in Figures 3-6 a)-c). In terms of calculations, the net result of adding a second transition dipole moment at fixed angle Δ to the original 1D transition dipole is to simply compress the polarization ratio histogram into a more narrow range of polarization ratios. That is, the histogram for the dimeric system oriented in the x-y plane consists of a pair of maxima located at polarization ratios of 0.6 to 0.4 and -0.6 to -0.4. This is an entirely reasonable result, because for a CG-2 molecule in which both transition dipoles lie entirely in the x-y plane, one will never observe a polarization ratio value equal to 1.0. If one transition dipole is perfectly aligned along one axis, the second will always have a significant component along the orthogonal axis. Hence, one would anticipate seeing maxima in the histogram of polarization ratio at values that are less than +1.0 and more positive than -1.0.

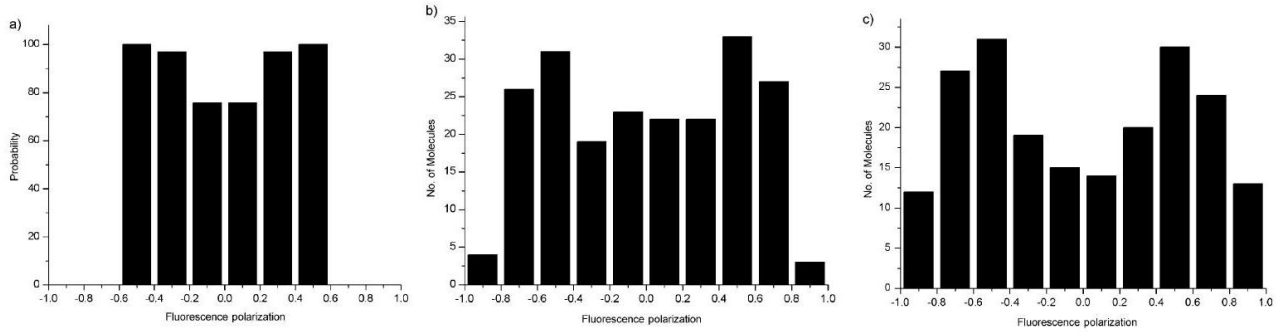

Figure 3-6. a) Calculated fluorescence-polarization histograms for randomly orientated dual-chromophore molecule within the x-y plane, b) Experimentally determined fluorescence-polarization histogram for individual CG-2 molecules on poly(vinyl alcohol) under saturated [Ca^{2+}] conditions. c) Experimentally determined fluorescence-polarization histogram for individual CG-2 molecules on poly (vinyl alcohol) under zero [Ca^{2+}] condition.

The experimentally measured polarization histograms for the Ca^{2+} free and Ca^{2+} saturated measurements are shown in Figures 3-6 b) and c), respectively. We note some key similarities and differences between the experimental histograms and those determined via calculation. While the experimental histograms do have peak maxima in the appropriate regions, they also display significant probabilities at larger polarization ratios (>0.8 and <-0.8) that are not reproduced in the calculated distributions. These "tails" in the histograms are genuine experimental results and may indicate a limitation of the simplified calculations carried out here. While it is correct to state that the most strongly-emissive species will lie in the x-y plane, there are still some molecular orientations for CG-2 (and for R6G) that will be observable in the SM measurements that fall outside of this plane. A more detailed mathematical treatment of the dimeric system, in which out-of-plane contributions are included, reproduces these tails on the histogram, but for the sake of clarity and simplicity, this result will not be stated explicitly here. The plane, in which both transition dipoles lie, is defined as a reference plane in calculations for out-of plane distributions. In general, however, when the reference plane makes an angle of $\geq 40°$ to the x-y plane, calculations yield a polarization ratio of greater than 0.6 and the dipoles will still have a significant projection onto the x-y plane, yielding a significant SM signal. Accounting for the limitations of the simplified mathematical model used here, however, the experimental results from the CG-2 measurements are in reasonable agreement with the anticipated results for dimeric transition dipoles that are oriented at a $\Delta \approx 120°$ angle with respect to each other.

As well as providing basic confirmation of the relative orientation of the constituent transition-dipole geometry predicted by our previous studies, further information about average molecular orientations of CG-2 can be extracted from the SM polarization histograms. As an aside, we note that the approach developed here does not provide information about the relative orientation of transition dipoles for each individual molecule, but rather indicates a range of possible angles for the entire ensemble of molecules studied in the sample. The calculations carried out here make the assumption that the molecules remained "frozen" in the polymer matrix and that the transition dipoles remain in a fixed relative orientation throughout the measurement. However, one can probe the effect that altering the relative orientation between transition dipoles has on the polarization ratio by varying the angle Δ in Equation (3-11). Figure 3-7 shows a series of calculated histograms as a function of Δ. As seen in the plot, the polarization ratio histogram is

reasonably sensitive to variations in the relative transition dipole orientation. For example, changing Δ from 120 ° to 100 ° causes the histogram peak maximum to shift to the centre (from -0.1 to 0.1), and changing Δ to 140 ° changes the distribution into one that closely resembles that for the simple 1D transition dipole. While our ability to assign a precise range of possible angles to Δ is limited by experimental noise in the data, we can reasonably estimate that the average angle between transition dipoles in CG-2 is in the range Δ = 120 ° ± 10 °. It is also worth noting that changing the angle to Δ = 130 ° also gives rise to peaks in the histogram at polarization values of 0.8 to 0.6 and -0.8 to -0.6, as well as producing the previously noted "tails", which more closely reflects the experimental data. This suggests additional possible explanations for these "tails" in the histogram: the first is that the calculations for the x-y plane are overly simplified, whereas the second is that the true angle between transition dipoles is actually closer to Δ = 130 ° than Δ = 120 °. Unfortunately, the experimental data is not of sufficient quality to distinguish between these effects at this time.

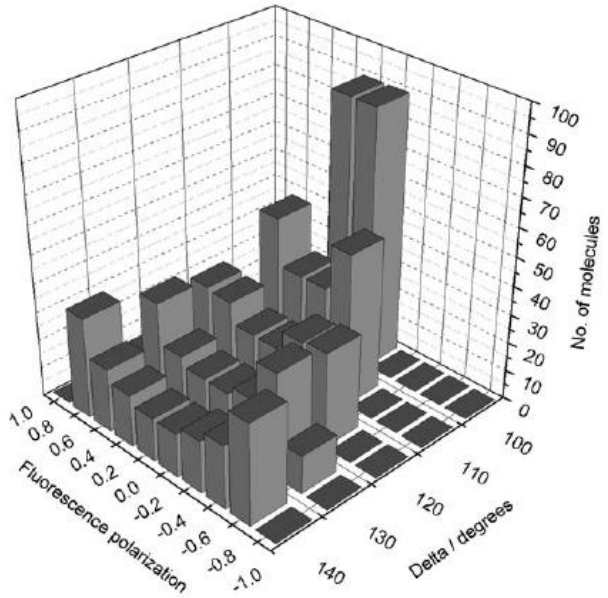

Figure 3-7. Calculated fluorescence-polarization histograms as a function of relative transition dipole orientation, Δ, as defined in Equation (3-11).

Additional information concerning the nature of the emissive specie at low [Ca^{2+}] can also be obtained through inspection of the SM histograms. In our previous studies, it has been observed that even in the nominal absence of Ca^{2+}, a small number of CG-2 molecules are highly fluorescent and that the general increase in the fluorescence intensity of bulk CG-2 solutions can

be attributed to a simple increase in the number of emissive CG-2 molecules. The typical fluorescence intensities of CG-2 molecules at zero [Ca^{2+}] is the same as that observed at higher ion concentrations, suggesting the spots observed in the SM measurements are not caused by dissociated CG-2 molecules. This suggests that the visible molecules are caused by either trace amounts of Ca^{2+} in the nominally Ca^{2+} free solution, or by an occasional CG-2 molecule that happens to take on a conformation where fluorescence quenching is negligible. While the polarization ratio measurements cannot definitively rule out either of these scenarios, it can provide some further insights into the situation. The polarization histogram for CG-2 at zero [Ca^{2+}] is shown in Figure 3-6 c). Again, this histogram compares well with the anticipated result for the dimeric transition dipoles and the differences between this histogram and that for CG-2 in saturated Ca^{2+} solution is statistically negligible (verified by a χ^2 test). This indicates that the relative orientations of the transition dipoles in the zero [Ca^{2+}] samples are essentially the same as the saturated [Ca^{2+}]. It seems unlikely, but not impossible, that randomly oriented CG-2 molecules would, on average, take on an identical conformation as the Ca^{2+} bound form of the molecule and we hypothesize that the root cause of this residual fluorescence is extremely low levels of Ca^{2+} in the buffer materials. Further measurements, perhaps ultra-sensitive inductively-coupled-plasma mass-spectrometry (ICP-MS) measurements, may finally help resolve this question.

3.4 Conclusions

Single-molecule dual-polarization fluorescence imaging has been used to characterize the relative orientation of fluorophores in the dual fluorophore molecule CG-2. A simplified geometric model was developed to calculate a theoretical polarization ratio histogram for CG-2 molecules that are randomly distributed in space, and this was compared with its experimentally measured counterpart. The experimental histograms of polarization ratios agree well with those predicted by theory, allowing for an approximate determination of relative orientation of the two constituent fluorophores. This method of SM analysis has significant potential as a general tool for studying transition dipole orientations in multifluorophoric molecules, and may prove invaluable in probing and understanding intramolecular energy transfer in these important systems.

3.5 Experimental Section

Single-molecule fluorescence measurements were carried out using a home-built, wide-field epifluorescence microscope.[23] Samples were excited with circularly polarized, 514 nm continuous wave light from a tunable argon-ion laser. The incident beam was converted into circularly polarized light from its original linear polarization at the laser output by directing it through a Berek variable waveplate (New Focus, San Jose, CA.). Samples were illuminated with an excitation intensity of ~ 1.5 kW/cm^2, as measured by dividing the incident power measured at the sample focal plane by the illumination area. Fluorescence emission from the sample was collected with an oil-immersion microscope objective (60×, 1.4 NA), passed through two band-pass filters (530-590 3RD, Omega Optical, Brattleboro, VT.) to attenuate residual excitation light and directed onto a front illuminated CCD photodetector (Cascade 512F, Photometrics, Tucson, AZ.). A Wollaston prism (ThorLabs, Newton, NJ.) was mounted between the microscope output port and the CCD detector, in order to split the fluorescence image into constituent vertical and horizontal polarization images (external configuration, as described by Kinosita [18]).

Samples for SM fluorescence experiments were prepared by first spin-casting an aliquot of dilute polymer [2% w/v poly(vinyl alcohol) in Millipore water] onto a clean microscope coverglass slide, followed by depositing an aliquot of dilute aqueous or ethanolic solution (~ 10^{-9} -10^{-10} M) of the appropriate dye onto the coverglass. CG-2 (Invitrogen, Burlington, ON) was prepared in Ca^{2+} buffers purchased from the dye manufacturer ([Ca^{2+}] = 0 μM and 1000 μM for calcium free and saturated conditions, respectively). The dye solutions were allowed to evaporate under ambient conditions prior to imaging in the single-molecule microscope. Control samples prepared in absence of dye show no fluorescence impurities when examined under single-molecule imaging conditions. Experimental polarization ratios for individual molecules (see the Results and Discussion Section) were determined by calculating the ratio of the intensity of the x-polarization channel to the y-polarization channel. A separate background signal was determined for each polarization channel, and the data from each channel was corrected for its own unique background.

3.6 Acknowledgments

Funding for this work was provided by the National Sciences and Engineering Research Council of Canada and by the University of Saskatchewan.

3.7 References

1. Gensch, T.; Hofkens, J.; Heirmann, A.; Tsuda, K.; Verheijen, W.; Vosch, T.; Christ, T.; Basche, T.; Mullen, K.; De Schryver, F. C. *Angewandte Chemie-International Edition* 1999, *38*, 3752-3756.
2. Hofkens, J.; Maus, M.; Gensch, T.; Vosch, T.; Cotlet, M.; Kohn, F.; Herrmann, A.; Mullen, K.; De Schryver, F. *Journal of the American Chemical Society* 2000, *122*, 9278-9288.
3. Lounis, B.; Deich, J.; Rosell, F. I.; Boxer, S. G.; Moerner, W. E. *Journal of Physical Chemistry B* 2001, *105*, 5048-5054.
4. Packard, B. Z.; Toptygin, D. D.; Komoriya, A.; Brand, L. *Proceedings of the National Academy of Sciences of the United States of America* 1996, *93*, 11640-11645.
5. VandenBout, D. A.; Yip, W. T.; Hu, D. H.; Fu, D. K.; Swager, T. M.; Barbara, P. F. *Science* 1997, *277*, 1074-1077.
6. Ying, L. M.; Xie, X. S. *Journal of Physical Chemistry B* 1998, *102*, 10399-10409.
7. Ambrose, W. P.; Goodwin, P. M.; Jett, J. H.; Van Orden, A.; Werner, J. H.; Keller, R. A. *Chemical Reviews* 1999, *99*, 2929-2956.
8. Moerner, W. E. *Journal of Physical Chemistry B* 2002, *106*, 910-927.
9. Moerner, W. E.; Fromm, D. P. *Review of Scientific Instruments* 2003, *74*, 3597-3619.
10. Moerner, W. E.; Orrit, M. *Science* 1999, *283*, 1670-1676.
11. Weiss, S. *Science* 1999, *283*, 1676-1683.
12. Grynkiewicz, G.; Poenie, M.; Tsien, R. Y. *Journal of Biological Chemistry* 1985, *260*, 3440-3450.
13. Bagh, S.; Paige, M. F. *Journal of Physical Chemistry A* 2006, *110*, 7057-7066.
14. *Handbook of fluorescent probes and research products*; 9 ed.; Haugland, R. P., Ed.; Molecular Probes Inc., 2002.

15. Yip, W. T.; Hu, D. H.; Yu, J.; Vanden Bout, D. A.; Barbara, P. F. *Journal of Physical Chemistry A* 1998, *102*, 7564-7575.
16. Betzig, E.; Chichester, R. J. *Science* 1993, *262*, 1422-1425.
17. Dickson, R. M.; Norris, D. J.; Moerner, W. E. *Physical Review Letters* 1998, *81*, 5322-5325.
18. Kinosita, K.; Itoh, H.; Ishiwata, S.; Hirano, K.; Nishizaka, T.; Hayakawa, T. *Journal of Cell Biology* 1991, *115*, 67-73.
19. Forkey, J. N.; Quinlan, M. E.; Goldman, Y. E. *Progress in Biophysics & Molecular Biology* 2000, *74*, 1-35.
20. Hopkins, S. C.; Sabido-David, C.; Corrie, J. E. T.; Irving, M.; Goldman, Y. E. *Biophysical Journal* 1998, *74*, 3093-3110.
21. Chung, I. H.; Shimizu, K. T.; Bawendi, M. G. *Proceedings of the National Academy of Sciences of the United States of America* 2003, *100*, 405-408.
22. Schroeyers, W.; Vallee, R.; Patra, D.; Hofkens, J.; Habuchi, S.; Vosch, T.; Cotlet, M.; Mullen, K.; Enderlein, J.; De Schryver, F. C. *Journal of the American Chemical Society* 2004, *126*, 14310-14311.
23. Bagh, S.; Paige, M. F. *Canadian Journal of Chemistry-Revue Canadienne De Chimie* 2005, *83*, 435-442.

CHAPTER 4

AN ENSEMBLE AND SINGLE-MOLECULE FLUORESCENCE MICROSCOPY INVESTIGATION OF PHASE-SEPARATED MONOLAYER FILMS STAINED WITH NILE RED

This chapter is a slightly modified copy of a manuscript accepted by *Spectrochimica Acta Part A: Molecular and Biomolecular Spectroscopy* in October 2010. (Reproduced with the permission from Spectrochimica Acta Part A: Molecular and Biomolecular Sepctroscop*y* **2010** (doi: 10.1016/j.saa.2010.09.024).

In this research paper, the spectroscopic properties of a lipid stain, Nile Red (NR), that was incorporated into a phase-separated monolayer system composed of arachidic acid ($C_{19}H_{39}COOH$, AA) and perfluorotetradecanoic acid ($C_{13}F_{27}COOH$, PA) were investigated at the ensemble and single-molecule level. According to previous structural and compositional mapping experiments by atomic force microscopy (AFM), AA phase-separates from PA to form elevated micron-sized hexagonal domains (referred to as discontinuous domains). The surrounding continuous domain is enriched in PA, though it does contain occasional small deposits of residual hydrocarbon.[1] The compositional difference in the separated domains could create two physically and chemically distinct environments, which allows us to study environmental effects on NR fluorescence at both bulk and single-molecule scale. For the solvatochromic dye NR, the local environment was found to play two roles: it influenced spectroscopic properties of NR (though to a small degree) and it gave rise to preferential adsorption of the dye to one region (the hydrocarbon) of the sample.

As described in Chapter 2, a combination of ensemble and single-molecule fluorescence spectroscopy methods was used in this study. In addition, fluorescence confocal spectromicroscopy was specifically chosen to study the solvatochromism effect of NR in different regions. This required a major modification of the fluorescence microscopy instrumentation used in the preceding parts of this thesis.

For this research paper, the sample preparation and the single-molecule fluorescence microscopy measurements were performed jointly by me, Terri Thunder and Robyn Porterfield (University of Concordia, Montreal), with me acting as main coordinator for the project. In addition to this work, I was responsible for the major modification of the fluorescence microscope by setting up the fluorescence confocal spectromicroscopy system. I played the lead role in interpreting the results and preparing the paper. My supervisor provided guidance throughout the experimental work, result interpretation and editing of the manuscript.

4. An ensemble and single-molecule fluorescence microscopy investigation of phase-separated monolayer films stained with Nile Red

Yin Lu[a], *Robyn Porterfield*[b], *Terri Thunder*[a], *Matthew F. Paige*[a,*]

[a] Department of Chemistry, University of Saskatchewan 110 Science Place, Saskatoon, SK S7N 5C9, Canada

[b] Department of Chemistry and Biochemistry, Concordia University, 7141 Sherbrooke Street West, Montreal, QC H4B 1R6, Canada

Accepted 29 September, 2010

4.1 Abstract

Phase-separated Langmuir–Blodgett monolayer films prepared from mixtures of arachidic acid ($C_{19}H_{39}COOH$) and perfluorotetradecanoic acid ($C_{13}F_{27}COOH$) were stained via spin-casting with the polarity sensitive phenoxazine dye Nile Red, and characterized using a combination of ensemble and single-molecule fluorescence microscopy measurements. Ensemble fluorescence microscopy and spectromicroscopy showed that Nile Red preferentially associated with the hydrogenated domains of the phase-separated films, and was strongly fluorescent in these areas of the film. These measurements, in conjunction with single-molecule fluorescence imaging experiments, also indicated that a small sub-population of dye molecules localizes on the perfluorinated regions of the sample, but that this subpopulation is spectroscopically indistinguishable from that associated with the hydrogenated domains. The relative importance of selective dye adsorption and local polarity sensitivity of Nile Red for staining applications in phase-separated LB films as well as in cellular environments is discussed in context of the experimental results.

4.2 Introduction

The fluorescent dye Nile Red (9-diethylamino-5H-benzo [α] phenoxazine-5-one, chemical structure shown in Figure 4-1 (A) has found widespread use as a neutral lipid stain for cellular imaging applications[2,3]. Much of the utility of Nile Red (NR) as a stain has been attributed to fluorescence emission that is strongly dependent upon the polarity of its local environment (solvatochromism); in polar solvents such as water, NR emission is strongly quenched but in non-polar solvents the fluorophore becomes strongly emissive, with both excitation and emission maxima shifting to shorter wavelengths. Fluorescence emission of NR has been used to probe environmental polarity in a wide variety of systems, including cell membranes and cytoplasmic lipid deposits[2,3], lipid vesicles[4], protein surfaces[5], LB films[6] and others. Of additional recent interest for fluorescence applications is that since NR is an excellent fluorophore (e.g. high absorption cross-section, quantum yield and comparatively low photobleaching quantum yield), it can be detected at the single-molecule level, enabling measurements of molecular-scale local environments and other nanoscale effects with remarkable sensitivity and spatial resolution. Measurements of particular note in this field include detection of both static and dynamic environmental effects in polymer systems and molecular diffusion dynamics in mesoporous sol-gel films[7-9].

While solvatochromic effects are an important feature of NR's efficacy as a neutral lipid stain, another key issue that must also be considered when generating contrast in fluorescence images is the general affinity of the dye for the target molecules. For a solvatochromic dye like NR, fluorescence image contrast through staining must come from a combination of the dye's environmentally sensitive spectroscopic properties as well as the amount of dye that has accumulated in the sample region of interest. For NR-stained samples, it is not always clear whether a strong fluorescence signal can be attributed to a highly emissive form of the dye, accumulation of dye in the area of interest or a combination of both.

To explore the relative importance of these factors in generating fluorescence contrast in NR stained samples, we have investigated the spectroscopic properties of a simple lipid system consisting of a phase-separated Langmuir-Blodgett (LB) monolayer film prepared from a binary mixture of hydrogenated and perfluorinated fatty-acids. The LB films consist of a 2:1 mole ratio mixture of arachidic acid ($C_{19}H_{39}COOH$) (AA – Figure 4-1 (B)) and perfluorotetradecanoic acid

($C_{13}F_{27}COOH$) (PA – Figure 4-1 (C)) deposited onto solid glass substrates. It has been shown previously [1,10-12] that mixtures of these two components undergo phase-separation at the air-water interface and when deposited onto solid substrates, the monolayer films consist of discrete, micron-sized hexagonal domains (referred herein as "discontinuous domains") that are almost exclusively comprised of arachidic acid. The surrounding continuous domain is enriched in perfluorotetradecanoic acid, though it does contain occasional small deposits of residual hydrocarbon[1]. Further details pertaining to the formation mechanism and domain growth kinetics in these films can be found elsewhere[10,12].

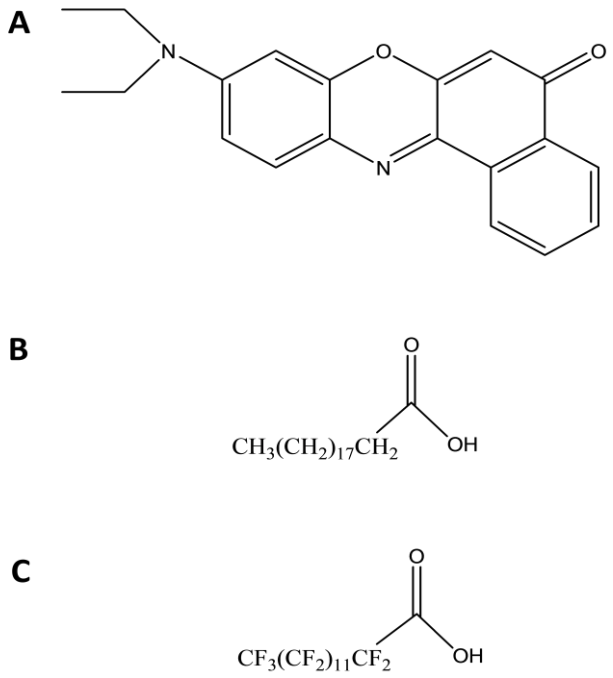

Figure 4-1. Chemical structures for (A) Nile Red, (B) arachidic acid ($C_{19}H_{39}COOH$), and (C) perfluorotetradecanoic acid ($C_{13}F_{27}COOH$).

By preparing samples that contain two physically and chemically distinct (hydrogenated and perfluorinated) regions and staining the sample with NR, we can simultaneously explore the relative importance and effect of dye localization and NR spectroscopic properties on fluorescence image contrast. In order to ensure that the two different regions of the film would be exposed to dye, samples were stained by spin-casting; incorporating a fluorescently labeled probe into the film would likely lead to exclusive accumulation of the probe into the discontinuous domains. The emission spectra of NR in n-alkane perfluorocarbons and their

hydrogenated counterparts differ significantly (vide infra), suggesting that this model-system is well-suited to distinguish between these two contributors to image contrast. A combination of fluorescence measurements, including traditional "ensemble" epifluorescence microscopy, as well as spectromicroscopy and single-molecule fluorescence microscopy have been employed to explore the relative contribution of these two effects on image contrast.

4.3 Materials and Methods

4.3.1 Ensemble spectroscopy measurements in solution

For ensemble measurement, stock solutions of NR were prepared by dissolving the bulk solid in various solvents with different polarities, including hexadecane, perfluorooctane, and chloroform. Emission spectra were collected in quartz cuvettes on a PTI QuantaMaster Luminescence Fluorometer (Photon Technology International).

4.3.2 LB film preparation and staining

LB films were prepared using a KSV 2000 Langmuir trough system (KSV Instruments), with ultrapure water (Millipore, resistivity 18.2 MΩ cm) as a subphase. Depositions were carried out at a subphase temperature of 30.0 ± 0.5 ℃. Stock solutions of 8.4×10^{-3} M AA and 5.1×10^{-3} M PA were prepared in a 9:1 volume ratio of hexanes/THF. The solutions were mixed in appropriate volumes to give a 2:1 mole ratio mixture of AA:PA, or used neat to prepare AA and PA control sample films. Before each measurement, the subphase surface was cleaned by vacuum suction, and the platinum Wilhelmy plate was cleaned with a propane torch. A 30 μL aliquot of surfactant solution was spread on the subphase and the solvent was allowed to evaporate for ~ 10 min prior to film compression.

For deposition experiments, the trough barriers were compressed at a rate of 10 mm min^{-1} until reaching a deposition pressure of 20 mN m^{-1}. Upon reaching the deposition pressure, films were allowed to stabilize for ~ 10 min, then a glass substrate that had previously been immersed under the subphase was withdrawn through the liquid-air interface at a rate of 5 mm min^{-1}. Samples were allowed to dry in a dust-free enclosure before further analysis. Film morphologies were measured with Atomic Force Microscope (AFM) imaging performed on a Dimension Hybrid Nanoscope system (Veeco Metrology Group) operating in contact mode, and the film morphologies were found to be consistent with those reported previously[1,10].

Samples for ensemble fluorescence microscopy measurements were prepared by first spin-casting 120 μL (~ 10^{-3} M) of NR in chloroform onto the LB film (spin-casting performed at 1000 rpm for 1 min), followed by a layer of dilute polymer (2% (w/v) poly (vinyl alcohol) in Millipore water) to minimize the effect of oxygen-induced photobleaching of fluorescence. Samples for single-molecule measurements were prepared using the same procedure but a more dilute solution of NR (~ 10^{-9} M) was used. Control samples that had not been stained with dye showed no significant fluorescent impurities when examined under single-molecule imaging conditions. The staining procedure was found to have no noticeable effect on the film structure, as determined by AFM imaging of the samples before and after staining.

4.3.3 Fluorescence microscopy

For ensemble and single-molecule fluorescence imaging experiments, a home-built, wide-field epifluorescence microscope was used[13]. A schematic diagram of the instrument is shown in Figure 4-2 (A). Briefly, a frequency-doubled cw Nd-YAG laser (emission wavelength of 532 nm, vertical polarization) was passed through a spatial filter, collimated, then focused by means of a 500 mm focal length lens onto the back focal plane of a 60×, 1.4 NA oil-immersion objective lens (PlanApo, Nikon). Fluorescence emission from the sample was collected through two long-pass filters (550LP, Omega Optical, Brattleboro, Vermont, USA) to remove residual excitation light and directed onto a wide-area, front-illuminated electron multiplying CCD camera (Cascade 512F, Photometrics).

For spectromicroscopy measurements, the microscope was converted into a confocal configuration, as shown in Figure 4-2 (B). The 500 mm focal length lens was removed from the beam path, and the microscope objective lens was used to focus the excitation light down to small (estimated ~ 600 nm diameter) spot. Fluorescence emission was passed through a pinhole (0.75 μm diameter), and focused into an imaging spectrograph (MS125 Spectrograph, Newport (Oriel) Instruments). Output from the spectrograph was imaged onto an electron multiplying CCD camera (iXon, Andor Technology) and converted into a 2D spectrum of the region of interest. The instrument was calibrated with the spectral emission of an Hg pen lamp. We note that the quantum yield of the iXon detector is reasonably invariant over the visible spectrum, and as such, there was no need to correct spectral data for the wavelength-dependent response of the detector. For collection of emission spectra, a frame exposure time of 100 ms was used for all

measurements. CCD pixels were binned to ensure maximum possible signal-to-noise ratio in the collected emission spectra.

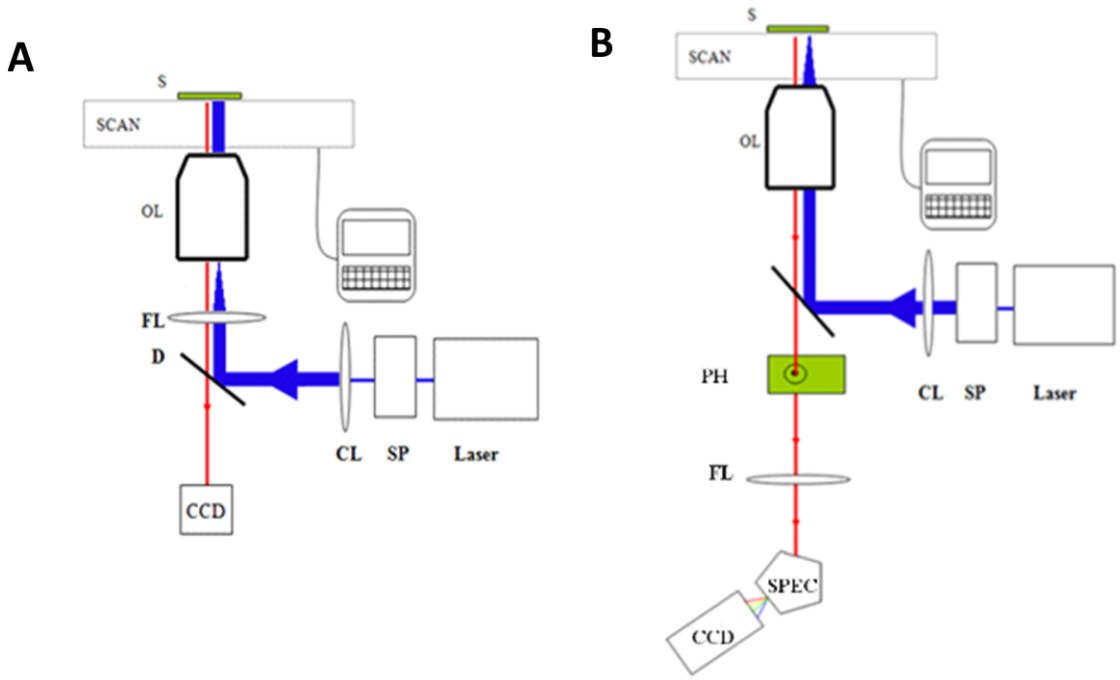

Figure 4-2. Schematic diagram of (A) epifluorescence microscope system and (B) fluorescence confocal spectromicroscopy system. SP: spatial filter, CL: collimating lens, D: dichroic beam splitter, PH: pinhole, FL: focusing lens, SPEC: spectrograph, CCD: CCD camera, OL: objective lens, SCAN: sample scan stage, S: sample.

4.4 Results and Discussion

4.4.1 Ensemble fluorescence measurements

As a simple model of the spectroscopic behavior of NR in the different chemical environments found in the phase-separated LB films, solution-based fluorescence spectra of NR in different solvents were collected. The solvents perfluorooctane and n-hexadecane were selected to simulate the chemical environments of the perfluorinated and hydrogenated sample regions, respectively. The solvatochromic effects of NR can be attributed to its appreciable induced dipole upon photoexcitation (differences between excited and ground state dipole moments as high as 11D have been reported in some solvents[14-17]) but has also been associated with the formation of twisted intramolecular charge transfer (TICT) excited states[14,18,19]. In NR TICT

states, it is believed that the diethylamino group donates charge into the rigid NR backbone, which is accompanied by rotation of the diethylamino group. This twist results in the spectral red-shift of emission relative to ICT states in which there is no bond rotation. More polar environments favour the formation of TICT states and as a result, NR exhibits a significant spectral shift towards longer wavelengths in solvents of larger polarity. In addition, a low fluorescence quantum yield has been associated with the formation of TICT states[8,14,17].

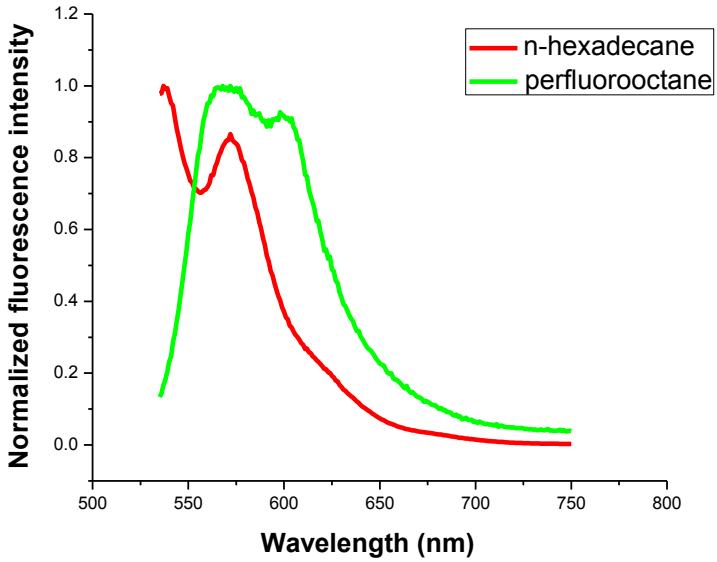

Figure 4-3. Fluorescence emission spectra of Nile Red in n-hexadecane, perfluorooctane excited at the wavelength of 532 nm.

During the fluorescence spectroscopy measurement, all samples were excited at the wavelength of 532 nm in order to reproduce the imaging conditions used in spectromicroscopy and the epifluorescence microscopy experiments. Normalized emission spectra are shown in Figure 4-3. In both solvents, NR exhibits two well-defined peaks, with the hypsochromic peak somewhat stronger in intensity, which is in good agreement with emission spectra reported in other hydrogenated solvents[2,6,14]. We note that the solubility of NR in the pure perfluorocarbon is low, resulting in a relatively poor signal-to-noise ratio for this spectrum. The presence of two band maxima in the emission spectra has been shown to originate from different vibronic levels of the same electronic state based on the excitation spectra and lifetime measurement excited at both band maxima[14]. The peak shape of the emission spectra of NR in n-hexadecane is truncated

because of its relatively small Stokes shift. A significant bathochromic shift (30 nm) in the fluorescence emission maxima was observed in perfluorooctane in comparison with n-hexadecane. Solvent polarities can be estimated through the use of the orientation polarizability solvent parameter Δf [20], which is given by Eq. (1):

$$\Delta f = \left(\frac{\varepsilon-1}{2\varepsilon+1}\right) - \left(\frac{n^2-1}{2n^2+1}\right) \quad (4\text{-}1)$$

where ε is the static dielectric constant and n is the refractive index for the solvent, respectively. Calculated values of Δf for perfluorooctane and hexadecane were 2.9×10^{-2} and 2.6×10^{-3}, respectively, with ε and n taken from Refs.[21,22]. While the differences in Δf values for the two solvents are small, the perfluorocarbon solvent should be slightly more polar than the hydrocarbon, and the red shift observed for the perfluorinated solvent is consistent with this behavior.

It is useful to consider the effect that the solvent-dependent spectral shifts might have upon the measured fluorescence intensity in a microscopy imaging experiment. Analysis of the emission spectra shows that the emission filters used in the imaging experiments (long-pass filters, with a strong spectral cutoff for wavelengths below 550 nm) should result in a significantly larger signal for NR in a perfluorocarbon environment than in a hydrocarbon environment. That is, approximately 22% of the NR's fluorescence emission in a hydrocarbon environment should be cut off by the emission filters in the optical beampath, versus ~ 5% for NR in a perfluorocarbon environment (values determined by integrating appropriate areas under the spectral curves). Based on these simple model systems, one might reasonably expect a substantial difference in fluorescence image intensity to arise from this effect alone.

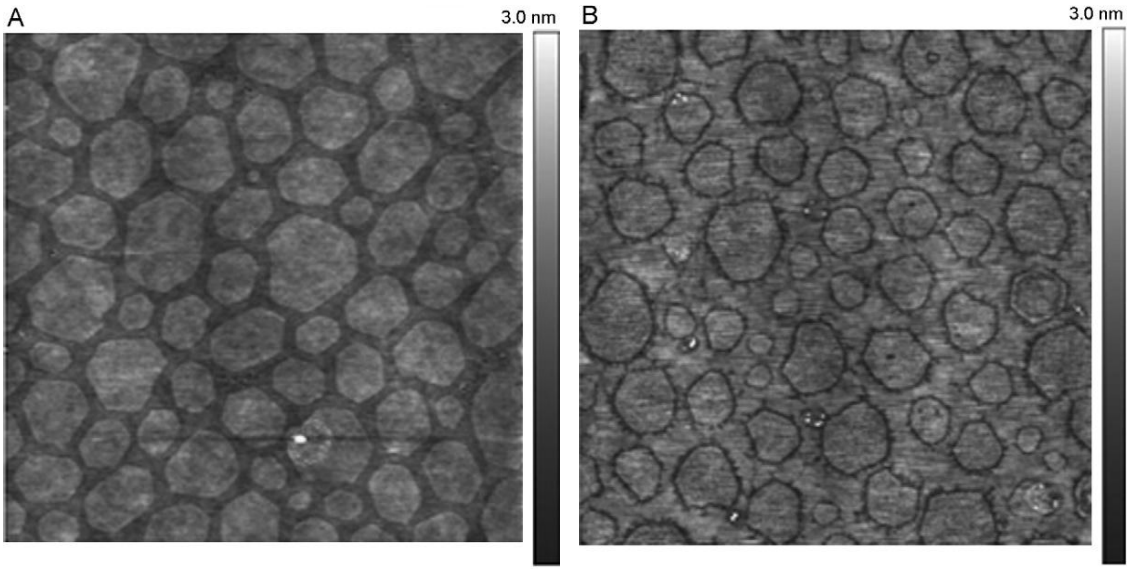

Figure 4-4. Atomic force microscope topography images of a 2:1 AA-PA film deposited onto glass microscope slide: (A) before spin-casting of Nile Red solution and (B) after spin-casting of Nile Red solution (Image size: 20 μm × 20 μm).

Following the procedure described in the experimental section, LB films composed of mixtures of AA and PA were deposited onto glass coverslides. Figure 4-4 (A) and (B) show typical AFM topography (height mode) images for an LB film deposited from a 2:1 mixture of AA and PA both before and after spin-casting with NR solution. The film components phase-separate into numerous micron-sized, discontinuous domains with well-defined hexagonal shapes, surrounded by a continuous domain that is lower in height. Before staining, the height differences measured here (~ 0.7 nm) were comparable with those described in previous reports[1]. As stated previously, it has been shown that the discontinuous domains are comprised almost exclusively of AA, and that the surrounding continuous domain contains primarily PA though with occasional small hydrocarbon deposit. In an attempt to measure the photophysical properties and staining preference of NR for the two domains with difference micropolarities, NR was spin-cast onto the LB films and characterized by both epifluorescence microscopy and spectromicroscopy. The height difference between the continuous and discontinuous domains was negligible after spin-casting (heights of the two regions were the same to within our ability to resolve), presumably because of the dye depositing onto the solid surface. However, the domain edges were still readily detected, indicating that the gross film morphology was not substantially altered by the deposition process.

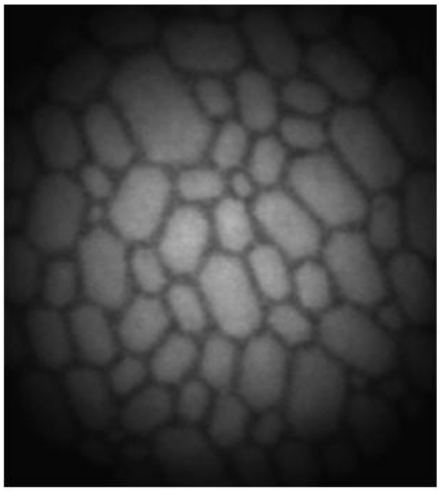

Figure 4-5. Epifluorescence microscopy image of the 2AA:1PA mixed film stained with Nile Red (Image size: ~ 17 μm × 17 μm, stain concentration = 1.5 mM, excitation intensity = 0.7 kW/cm^2).

Samples stained with concentrated solutions of NR were imaged in the epifluorescence microscope. A typical fluorescence image from these measurements is shown in Figure 4-5. In general, the stained samples gave a significant amount of image contrast when measured in the microscope, with fluorescence images exhibiting the same gross morphological features as those observed in AFM imaging. The hexagonal domains exhibited a significantly higher fluorescence signal than the surrounding continuous domain. Data was collected from numerous different samples, including images collected from mixed AA-PA films and control samples of pure AA, PA and bare glass alone. The average fluorescence intensity of NR for these various samples (in fluorescence counts per image pixel) is summarized in Table 1. For the one-component control samples, it was found that NR was not homogeneously distributed, and one often observed regions of the sample that contained large dye deposits (images consisted of a uniform bright region, with occasional bright deposits). The source of this heterogeneity is currently unclear, though it might be caused by accumulation of dye in defects in the LB film. We have observed in a closely related system[23] that the pure component films often contain occasional defects (pinholes, elevated regions) that are detectable in the AFM, and this likely also occurs in the systems measured here. It is also possible that the staining process, while having no affect on the gross film morphology, can induce some small number of defects in the film structure. To

minimize the influence these deposits had on image statistics, data was collected from homogenously stained regions of the sample, and sample regions with extremely high fluorescence counts were not included. As shown in the table, spin-casting NR onto bare glass substrates gave rise to the highest average fluorescence intensity among all the control samples, which lends support to the idea that the extremely high count regions in the pure AA films might be caused by defects in the LB film that allow NR to meet bare glass. More importantly, the fluorescence intensity measured in the pure AA control film was found to be higher than that in the PA control film, which is consistent with the hexagonal domains appearing brighter than the surrounding continuous domain.

Sample Name		Total Area (μm^2)	Average intensity (counts/pixel)	Relative deviation (%)
2AA:1PA mixture	Discontinuous domain	3.3×10^2	3960	14.2
	Continuous domain	2.4×10^2	2745	16.4
Control Samples	AA control	7.3×10^2	2232	9.5
	PA control	1.1×10^3	1984	4.8
	Clean slide	1.5×10^3	3502	0.6

Table 4-1. Average fluorescence intensity of NR as determined by epifluorescence microscopy in the 2AA:1PA mixture, pure PA and AA control samples

As noted in the Introduction, one need consider two possible contributors to fluorescence contrast in these systems: the variation in fluorescence intensity of NR due to polarity sensitivity of the dye, and preferential accumulation of the dye in specific regions of the sample. While the control samples for the pure films and the solution-based model systems suggest that NR is slightly more emissive in the hydrogenated regions of the sample, we actually believe that this effect plays a negligible role in the image contrast for this system. A series of additional experiments which provide support for this conclusion are outlined in the remainder of this paper.

Let us first consider the epifluorescence microscopy results in the context of the model solution calculations. If one assumes that the model solution measurements, corrected for the cutoff effects of the emission filters, are a reasonable representation of the properties of NR in films,

the hexagonal discontinuous domains should be at most ~ 17% brighter than the surrounding domains (spectromicroscopy measurements, described later in this paper, indicate that the difference in brightness is significantly less). The actual difference is closer to ~40%, suggesting the density of NR must be significantly higher in the hexagonal discontinuous domains than in the surrounding continuous domain. The brightness difference in the single-component control samples might be caused by a similar effect, with the NR simply adhering less well to the perfluorinated film surface than to the hydrogenated film.

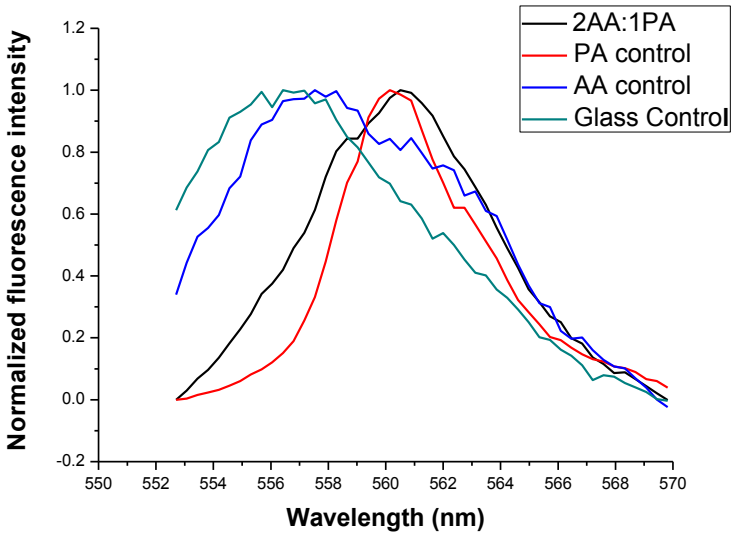

Figure 4-6. Comparison of emission spectra of NR in AA, PA control sample and the 2AA:1PA mixture by spectromicroscopy

While the model solution fluorescence measurements of NR's polarity dependence are useful, spectromicroscopic measurements of the LB films can provide more direct, useful information for understanding fluorescence contrast in the system. Emission spectra of NR doped LB films composed of AA, PA, and the AA-PA mixture were collected via spectromicroscopy and the normalized curves are shown in Figure 4-6. As an additional control sample, an emission spectrum for NR directly spin-cast on the glass surface alone was also measured. For spectromicroscopy experiments, the diameter of the confocal excitation spot was larger than the typical distance between adjacent discontinuous domains (spot diameter ~ 600 nm, space between domains was generally ~ 200 nm). This did not allow for selective illumination and excitation of NR in the "narrow" continuous domain. Consequently, the fluorescence counts

collected for the mixed AA-PA sample contain contributions from both the discontinuous and continuous domains. We also note, however, that because the continuous domains always contain a small portion of hydrocarbon, there will necessarily be a "mixed" signal from both of these chemical regions, even if the confocal spot were focused down to the diffraction limit. As such, an emission spectrum of NR on the continuous domain would be expected to display a combination of spectral features from both the PA and AA matrixes. Emission spectra of NR spin-cast onto LB films generally consisted of a broad peaks, with the emission maxima located between 550 and 560 nm. Compared with the corresponding solution models, the polarity dependence of spectral shift is more moderate in the solid matrix. However, a small but detectable (3 nm) red shift in the emission maximum for the pure PA control sample relative to pure AA was observed; the NR-stained AA film spectrum consisted of an emission band centered at 557 nm, with a strongly overlapping shoulder band centered at 561 nm, and the NR-stained PA sample consisted of a single peak, centered at 560 nm. For glass alone, a single broad peak that was slightly blue-shifted (~ 1 nm) relative to the spectrum for the NR-stained AA sample was measured, though the shoulder band that was present with the AA sample was not observed. As expected, the emission spectrum for the phase-separated AA-PA film had spectral features that were a combination of the two pure control samples, that is, a central peak maximum at 560 nm and a blue-shifted shoulder at 557 nm.

The small difference in the emission spectra for the control samples is somewhat surprising, given the results from the model solution measurements. If one assumes that NR can penetrate into the LB film and effectively be surrounded by perfluorinated (or hydrogenated) functional groups then results similar to model solution measurements are expected. For these samples, it appears that NR simply lies on the film surface rather than penetrating into the film interior, and the local environment each molecule encounters does not differ substantially for different film compositions. Regardless of the precise mechanism, the key information that can be extracted from these measurements is that after depositing NR onto the LB films, the effect of local environmental polarity on the fluorophore's emission spectra are negligible, particularly when taken in context of the spectral cutoff of the emission filters used in these experiments. That is, while there are some small spectral shifts that can be attributed to environmental polarity, the full emission spectrum of NR, regardless of local environment, will be passed by the long-pass filters in the microscope and will contribute to the total fluorescence signal in the microscope image.

A point worth considering is that, as stated previously, NR in TICT states have been reported to have lower fluorescent quantum yields than those in non-TICT states. While the small differences in emission spectra for the different control samples suggest that this effect is of minimal importance in these systems, a direct measure of the brightness of the fluorophores in the different films, as well as in the mixed film, would be of significant value. During the epifluorescence microscopy measurements, it was observed that after photobleaching the phase-separated samples for a brief period, individual molecules of NR could be detected in both the continuous and the discontinuous domains. These observations indicate that a small sub-population of NR does localize in the continuous regions of the film, and since they are observable at the single-molecule level, any quenching of the fluorophores is minimal. A more rigorous set of measurements aimed at characterizing the spectroscopic properties of individual molecules of NR in the films was carried out to explore this effect in more detail.

4.4.2 Single-molecule fluorescence measurements

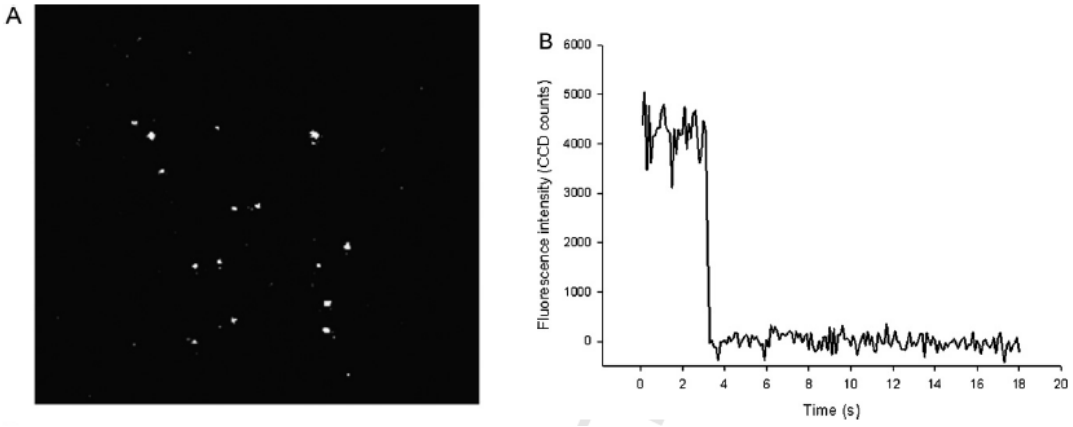

Figure 4-7. (A) Fluorescence image of single Nile Red molecules (image size ~ 21 μm × 19 μm) and (B) a typical single-molecule fluorescence time trajectory (stain concentration = 1×10^{-9} M, excitation intensity = 0.7 kW/cm^2).

To explore these effects, single-molecule measurements of NR were carried out by epifluorescence imaging of LB films that had been stained with nanomolar concentrations of dye. At nanomolar staining concentrations, one can no longer distinguish between molecules that are in the discontinuous and the continuous domains based on the image alone; the hexagonal domain structures can no longer be discerned. Hence, data obtained from these samples will contain information on molecules in both regions of the samples, and if there are two populations

of molecules with significantly different spectral properties, this should be detected in the statistical analysis of the single-molecule data. Images of individual NR molecules in LB films (including both the mixed film and control samples prepared from LB films of the pure, individual components) were collected and analyzed. Figure 4-7 shows a typical result in terms of an image of individual NR molecules collected from a phase-separated sample, along with a single-molecule fluorescence time trajectory (fluorescence intensity of an individual molecule as a function of time). Upon constant laser illumination, majority of fluorophores underwent single-step photobleaching (characteristic time trace shown in Figure 4-7 (B), which is taken as the signature of a single molecule. In addition, the fluorescence spots were ~ 300 nm in diameter, which is in consistent with the diffraction-limited fluorescence spot size expected for an individual molecule.

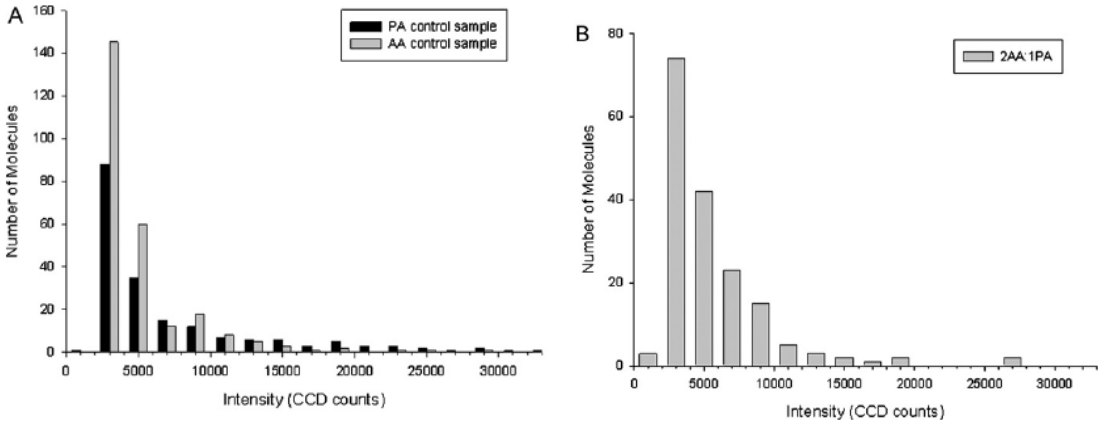

Figure 4-8. Histogram of single-molecule fluorescence intensities for (A) AA and PA control samples and (B) 2AA:1PA mixture. In both cases, excitation intensity was 0.9 kW/cm^2

Fluorescence intensities of individual NR molecule doped in the AA, PA, and AA-PA mixture system were measured independently. Figure 4-8 shows two histograms of single-molecule intensities (in CCD counts, taken under the same illumination and image collection conditions) measured for AA and PA control samples, as well as on the AA-PA mixture films. The single-molecule intensity histograms for the AA and PA films do not differ significantly from one another, as verified by the χ^2 test. Furthermore, the intensity distributions for the 2AA:1PA mixture show no significant difference with the control samples. In addition to these measurements, single-molecule photobleaching times were also measured for the pure and mixed LB films, and no substantial difference between the different systems was observed (data not

shown). We take these results in combination to mean that the local chemical environment does not play a significant role in terms of brightness or other important photophysical properties of NR for these systems. Certainly there may be more subtle variations in single-molecule fluorescence properties for these systems, but in terms of the primary contributions to image intensity in epifluorescence images, there are no major differences. In view of this, one can simply attribute the stronger fluorescence emission in the discontinuous domains to the preferential accumulation of NR on the hydrogenated hexagonal domains.

While the general applicability of these results for NR-based staining in other systems is currently unknown, they do bear further consideration. The true benefit of NR as a neutral lipid stain may not be its solvatochromism, the effect of which appears to be negligibly small for the simple systems studied here, but rather its tendency to localize and accumulate in nonpolar, lipophilic regions of a sample. The majority of standard fluorescence microscope systems make use of simple long-pass or band-pass emission filters to achieve spectral sensitivity and as such, the imaging experiments will not be sensitive to minor spectroscopic shifts in the emission spectra of dyes.

4.5 Summary

In this work, the spectroscopic properties of Nile Red, a solvatochromic stain, in chemically different regions of a phase-separated LB film has been characterized using a combination of ensemble and SM techniques. It was found that the overall difference in fluorescence intensity of Nile Red in different domains can be attributed to a preferential accumulation of NR on the discontinuous (hydrogenated) domains. While the emission spectra of NR in both solution phase and in solid LB films displayed solvatochromism, the effect was minor for the LB films, and the net effect on overall image contrast would be negligible. Individual Nile Red molecules were found to be equally bright in both hydrogenated and perfluorinated regions of the samples, further reinforcing the concept that image contrast for this system arises simply because the stain accumulates in one part of the sample.

4.6 Acknowledgements

Funding for this work was provided by the Natural Science and Engineering Research Council of Canada and by the University of Saskatchewan. Professor Ron Steer, Dr. Sophie Brunet and the Saskatchewan Structure Sciences Center are acknowledged for providing access to spectroscopy equipment and for technical assistance. Ala' Eftaiha is acknowledged for providing assistance with AFM imaging and sample preparation.

4.7 References

1. Qaqish, S. E.; Paige, M. F. *Langmuir* **2007**, *23*, 2582-2587.
2. Greenspan, P.; Fowler, S. D. *Journal of Lipid Research* **1985**, *26*, 781-789.
3. Greenspan, P.; Mayer, E. P.; Fowler, S. D. *Journal of Cell Biology* **1985**, *100*, 965-973.
4. Gao, F.; Mei, E. W.; Lim, M.; Hochstrasser, R. M. *Journal of the American Chemical Society* **2006**, *128*, 4814-4822.
5. Sackett, D. L.; Knutson, J. R.; Wolff, J. *Journal of Biological Chemistry* **1990**, *265*, 14899-14906.
6. Dutta, A. K.; Kamada, K.; Ohta, K. *Chemical Physics Letters* **1996**, *258*, 369-375.
7. Bardo, A. M.; Collinson, M. M.; Higgins, D. A. *Chemistry of Materials* **2001**, *13*, 3058-3058.
8. Hou, Y. W.; Bardo, A. M.; Martinez, C.; Higgins, D. A. *Journal of Physical Chemistry B* **2000**, *104*, 212-219.
9. Hou, Y. W.; Higgins, D. A. *Journal of Physical Chemistry B* **2002**, *106*, 10306-10315.
10. Qaqish, S. E.; Paige, M. F. *Langmuir* **2007**, *23*, 10088-10094.
11. Christensen, S.; Lanke, U. D.; Haines, B.; Qaqish, S. E.; Paige, M. F.; Urquhart, S. G. *Journal of Electron Spectroscopy and Related Phenomena* **2008**, *162*, 107-114.
12. Qaqish, S. E.; Paige, M. F. *Journal of Colloid and Interface Science* **2008**, *325*, 290-293.
13. Bagh, S.; Paige, M. F. *Canadian Journal of Chemistry-Revue Canadienne De Chimie* **2005**, *83*, 435-442.
14. Dutta, A. K.; Kamada, K.; Ohta, K. *Journal of Photochemistry and Photobiology A-Chemistry* **1996**, *93*, 57-64.

15. Ghoneim, N. *Spectrochimica Acta Part a-Molecular and Biomolecular Spectroscopy* **2000**, *56*, 1003-1010.
16. Kawski, A.; Kuklinski, B.; Bojarski, P. *Chemical Physics* **2009**, *359*, 58-64.
17. Sarkar, N.; Das, K.; Nath, D. N.; Bhattacharyya, K. *Langmuir* **1994**, *10*, 326-329.
18. Golini, C. M.; Williams, B. W.; Foresman, J. B. *Journal of Fluorescence* **1998**, *8*, 395-404.
19. Datta, A.; Mandal, D.; Pal, S. K.; Bhattacharyya, K. *Journal of Physical Chemistry B* **1997**, *101*, 10221-10225.
20. Lakowicz, J. *Principles of fluorescence spectrosopy*; 2nd ed.; Kluwer Academic: New York, 1999.
21. Wohlfarth, C.; Landolt-Bornstein *Group III Condensed Matter*; Springer-Verlag: Heidelberg, 2008.
22. Wohlfarth, C.; Landolt-Bornstein *Group IV Physical Chemistry Numerical Data and Functional Relationships in Science and Technology*; Spinger-Verlag: Heidelberg, 2008.
23. Qaqish, S. E.; Urquhart, S. G.; Lanke, U.; Brunet, S. M. K.; Paige, M. F. *Langmuir* **2009**, *25*, 7401-7409.

CHAPTER 5

FLUORESCENTLY LABELED GOLD NANOPARTICLES WITH MINIMAL FLUORESCENCE QUENCHING

This chapter is a slightly modified copy of an article published in *the Journal of Physical Chemistry C* in October 2010. (Reproduced with permission from the Journal of Physical Chemistry C **2010**, 14, 17446-17454.

The work in this chapter describes an investigation of fluorescence quenching of a fluorescent probe, AlexaFluor 514 (AF514), when it is covalently bound to water-soluble Au nanoparticles (NPs) with negligible plasmon bands (rapid oscillations of electron density on the surface of conducting metal). The purpose of investigating this system was to characterize the photophysical behaviour of AF514 before and after conjugating with Au NPs. In closely-related systems described in the literature, coupled fluorophores have shown strong quenching of fluorescence when coupled with plasmonic gold particles, and we reasonably expected that quenching in this (non-plasmonic) system would be minimal. One of the goals of this work is to explore the underlying quenching mechanisms for these systems.

The experiments were performed using a combination of steady-state and time-resolved ensemble spectroscopic measurements in conjunction with single molecule fluorescence microscopy. The ensemble measurements were used to quantify the extent of quenching of AF514 as a function of the concentration of the Au NPs in the system. These measurements were carried out in conjunction with fluorescence lifetime measurements of AF514 at different dye/Au NP loading ratios. In the SM fluorescence measurements, the conjugates exhibited either

single or multi-step photobleaching behavior, though the fluorescence emission of each step was comparable with the fluorescence emission of individual, unconjugated AF514 molecules.

For this research paper, the gold nanoparticle samples were prepared by Adam Leontowich and Mita Dasog. I carried out the conjugation reaction as well as the final purification process, performed all spectroscopy measurements, and played a major role in interpreting the results and the preparation of the manuscript. My supervisor provided guidance throughout the experimental work and was involved in result interpretation and in editing this paper. Dr. Robert Scott provided guidance throughout the synthesis of gold NPs.

5. Fluorescently Labeled Gold Nanoparticles with Minimal Fluorescence Quenching

Yin Lu, Mita Dasog, Adam F. G. Leontowich, Robert W. J. Scott, and Matthew F. Paige**

Department of Chemistry, 110 Science Place, University of Saskatchewan, Saskatoon, SK. S7N 5C9, Canada

Received June 15, 2010. In final Form: September 2, 2010

5.1 Abstract

Minimal quenching of fluorescence emission was observed when the fluorescent dye AlexaFluor 514 (AF514) was covalently bound to gold monolayer protected clusters (AuMPCs) that have negligible plasmon bands (diameters <2 nm). The fluorescence emission of the conjugated dye was measured as a function of dye-AuMPC mixing ratio with a combination of steady-state and time-resolved ensemble spectroscopic measurements in conjunction with single-molecule fluorescence microscopy. Fluorescence emission of the conjugated samples decreased slightly as a function of dye mixing ratio, which, in combination with a negligible change in fluorescence lifetime, was attributed to static quenching of the dye by the AuMPCs. From the single-molecule fluorescence measurements, it was observed that luminescent conjugates could still be detected, and, at all loading ratios, almost all of the dye-particle conjugates photobleached in either a single- or double-step process, with a small subpopulation exhibiting more than two photobleaching events. Beyond simple, irreversible photobleaching, no additional blinking dynamics were detected at the single-molecule level within the time resolution of the experiment. Emission intensities of coupled fluorophores were comparable with those measured

of dye molecules that had not been attached to the AuMPCs, suggesting that the statically quenched fluorophores are entirely nonemissive, whereas the remaining dyes are essentially unquenched. These results are discussed in the context of other dye−AuMPC coupled systems described in the literature.

5.2 Introduction

The rapid development of nanotechnology over the past several decades has opened new possibilities for investigating interactions between photoexcited molecules and metal surfaces. When located in close proximity to metallic surfaces, photoexcited molecules can exhibit strong changes in electronic and optical properties, likely a result of the mixing of molecular and metallic electronic energy levels. Reports of both fluorescence quenching and emission enhancement have been reported in a wide range of metal-fluorophore conjugate systems (for a recent review see ref 1), along with extensive attempts to explain and model this behaviour. While the majority of efforts to date have been directed at understanding spectroscopic behaviour in planar systems (i.e., metallic films), there is an increasing interest in characterizing similar interactions between metal nanoparticles that are covalently linked with fluorophores, in part because of potential use of these systems for imaging, photoswitching, light harvesting, and biosensing applications.[2-4]

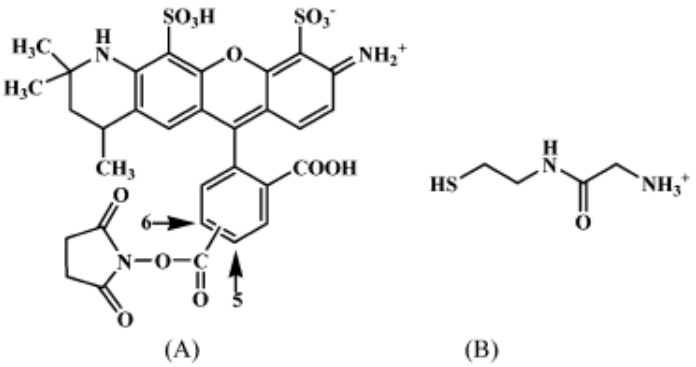

Figure 5-1. (A) Chemical structure of AF514 carboxylic acid, succinimidyl ester (mixed isomers with active ester on both position “5” and “6”). For subsequent figures, only the isomer with the active ester localized on position 5 will be shown. (B) Chemical structure of glycine-cysteamine.

A common theme that has been observed in a number of covalently linked dye-AuMPC systems is a strong quenching of fluorescence emission upon dye coupling.[1,5-7] In some cases, fluorescence deactivation has been attributed to a combination of energy and electron transfer from the photoexcited species to the tethered particle,[1,8] as well as through coupling of the exciton into the surface plasmon band of the nanoparticle and radiative rate depression.[1,5,8,9] In other cases, the covalent linkage of organic moieties to AuMPCs (and nanostructured films) can affect optical properties of linked fluorophores through modulation of the surface plasmon absorption band of the particle, or by causing adjacent, linked fluorophore units to self-aggregate.[1,8,10,11] In still other situations, more subtle effects are important; for example, Jennings, et al. have investigated the behavior of the molecular dye Cy5 coupled to 1.5 nm gold nanoparticles, and observed significant fluorescence quenching, as manifested by both a decrease in photoluminescence intensity and as a decrease in fluorescence lifetime.[12] These results were explained via a so-called nanosurface energy transfer (NSET) model, in which the photoexcited dye donates energy to the Au nanosurface according to a distance-dependent oscillator coupling ($1/d^4$, where d is the fluorophore-Au NP separation distance). These results are somewhat surprising as the surface plasmon resonance of 1.5 nm particles is weak (or nonexistent) and will not play a role in the energy transfer process, though the results can still be well rationalized through the intensity quenching mechanism described by Persson, et al. for bulk metal films.[13]

In addition to standard ensemble electronic spectroscopy characterization tools, single-molecule fluorescence spectroscopy has also been demonstrated as a useful and insightful method for probing photoexcitation quenching in dye-AuMPC systems, as this approach allows detection of phenomena that are blurred by traditional ensemble averaging measurements.[14,15] In a seminal work in this area, Anger, et al. modeled and systematically measured the dependence of fluorescence emission rate on the separation distance between laser-irradiated, 80 nm Au nanoparticles and individual dye molecules.[16] Both fluorescence enhancement (via local field amplification) and quenching (via nonradiative energy transfer) were observed in the same experiment, depending upon the Au nanoparticle-fluorophore separation. Cannone, et al.[3] have explored the influence of coupling metal nanoparticles (diameters ranging from 5-20 nm) on the emission of a fluorescein derivative by single-molecule fluorescence spectroscopy. They observed complex millisecond time-scale fluorescence blinking dynamics for the dye-AuMPC system, which had a strong dependence on the size of the particles; average blinking on-times

decreased with increasing particle diameters, whereas off-times increased with increasing particle diameter. They attributed the blinking dynamics to energy coupling between the photoexcited fluorophore and the substantial plasmon features of the AuMPCs.

We seek to further explore photoexcitation quenching and energy transfer processes in covalently linked dye-AuMPC systems through a combination of ensemble and single-molecule fluorescence measurements. Of particular interest to these investigations is the role played by the AuMPC surface Plasmon band in the quenching process; it might reasonably be anticipated that in smaller AuMPCs in which plasmon bands are vanishingly small (<2 nm), quenching should be substantially reduced, and at suitable dye-AuMPC separations, even negligible. It should be noted, however, that a recent time-dependent density functional theory study by Munoz-Losa, et al.[17] has suggested that nonplasmonic particles may, in fact, be effective excitation energy transfer agents, and exploring this effect experimentally is of significant value. The synthesis and characterization of nearly monodisperse, water-soluble AuMPCs, in which the monolayer protection group is composed of glycine-cysteamine (Gly-CSA) has recently been described,[18,19] and these particles appear well suited for this purpose; the average composition of (Gly-CSA) MPCs employed in our study is Au_{201}Gly-CSA_{71} with an average diameter of 1.8 $\pm$ 0.4 nm in diameter. Alex Fluor 514 (AF514, part A of Figure 5-1), an excellent fluorophore (high absorption cross-section, quantum yield, and comparatively low photobleaching quantum yield), which can be detected at the single-molecule level with excellent sensitivity, was chosen for preparing the dye-coupled MPCs. The fluorophores were linked to the AuMPCs through amide conjugation between the carboxylic group from dye molecules and the terminal free amine groups on the Au surface.

In this article, we describe the chemical synthesis and optical spectroscopic characterization of plasmon band free, labelled dye-AuMPC conjugates. By examining the spectroscopic properties of these labeled materials using a combination of steady-state and time-resolved methods, information about the extent of fluorescent-labeling, degree of fluorescence quenching, as well as the influence of the AuMPC on excited-state lifetime and single-molecule blinking dynamics has been obtained. Results are discussed in context of the recent literature and compared with those from closely related systems.

5.3 Experimental Section

5.3.1 Synthesis of Gly-CSA protected AuMPCs

Synthesis of Gly-CSA protected AuMPCs was carried out as outlined in Figure 5-2, following established procedures previously reported by Leontowich et al.[19] From TEM and TGA investigations, the general composition of the AuMPCs was determined to be $Au_{201}(Gly\text{-}CSA)_{71}$, and mean particle diameters were 1.8 ± 0.4 nm.

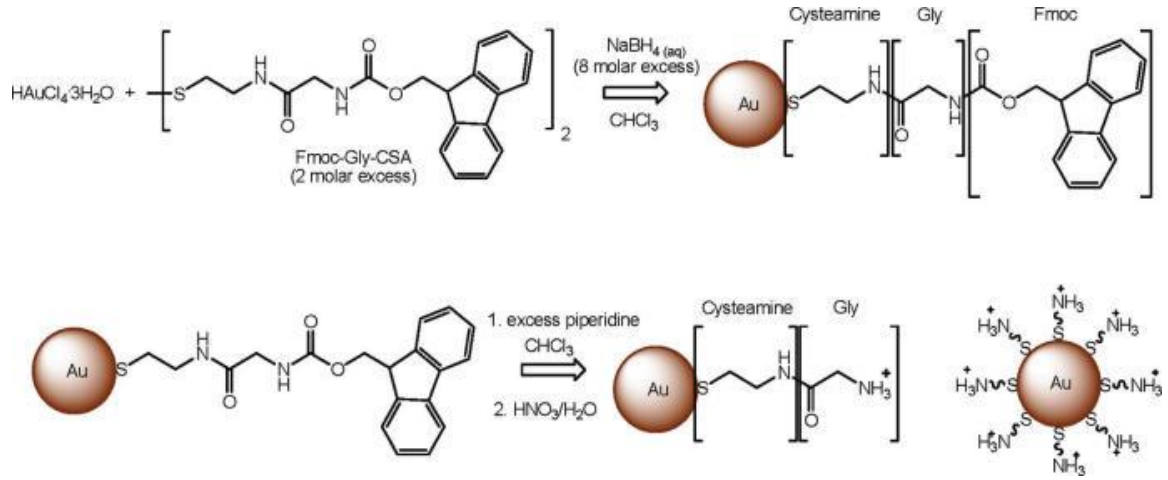

Figure 5-2. Synthetic preparation scheme for the Gly-CSA-functionalized AuMPCs.

5.3.2 Conjugation of Gly-CSA AuMPCs with AF514

The Gly-CSA AuMPCs were conjugated with AF514 carboxylic acid succinimdyl ester (Invitrogen) through the formation of an amide bond between the amine group on the Gly-CSA moiety and the carboxylic group of AF514 (structure shown in Figure 5-1).[18] Because formation of the amide bond is favourable under slightly basic conditions, the AuMPCs were dissolved in a $NaHCO_3$ buffer solution (0.010 M, pH 9.0) to produce a 1.0 mg/mL stock solution. For all aqueous solutions, ultrapure water (Millipore, resistivity 18.2 $M\Omega \cdot cm$) was used. The AF514 stock solution was prepared at a concentration of 1.40×10^{-4} M in DMSO. The dye to AuMPC mixing ratio was controlled by varying the volumes of the Gly-CSA AuMPC stock solution added to a fixed volume of dye solution. The $NaHCO_3$ buffer solution was then added to make a fixed total volume for all mixtures. The reactants were left stirring overnight under an N_2 atmosphere. Finally, the conjugates were dialyzed for 5 days against an acidic HNO_3 solution (pH 4.0) under N_2 to remove any unreacted dye.

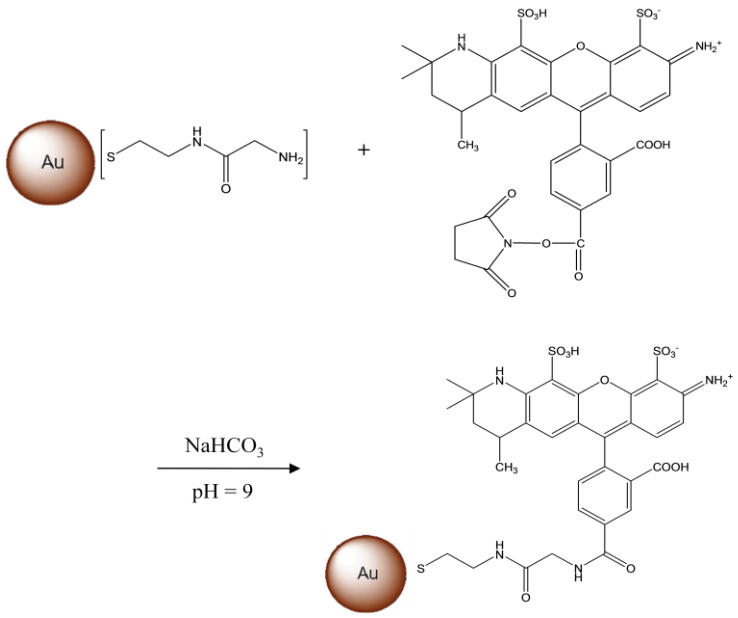

Figure 5-3. Schematic illustration of the conjugation reaction between Gly-CSA AuMPCs and AF514 carboxylic acid succinimidyl ester.

5.3.3 Ensemble spectroscopy measurements

The emission spectra of Gly-CSA AuMPCs and AF514 mixtures at different mixing ratios were collected both before and after the conjugation reaction. The solutions were degassed with N_2, placed in quartz cuvettes and the emission spectra were measured on a PTI QuantaMaster Luminescence Fluorometer (Photon Technology International). The control samples were measured under the same conditions. Fluorescence lifetimes were measured using the method of time-correlated single-photon counting (TCSPC). Excitation was performed with the output from a mode-locked, frequency-doubled femtosecond Ti-sapphire laser at 492 nm, with an emission wavelength of 556 nm collected at the magic angle. Fluorescence decay profiles were fit using a nonlinear least-squares reconvolution procedure based on the Marquardt algorithm. The quality of fit was assessed through the value of the reduced χ^2 and through the distribution of weighted residuals.

5.3.4 Single-molecule epifluorescence microscopy measurements

After dialysis, the conjugates were diluted 100× with ultrapure water. Samples for single-molecule microscopy measurements were prepared by first spin-casting 120 μL of the diluted conjugate solution onto a cleaned glass coverslide, followed by a layer of dilute polymer (2% w/v poly(vinyl alcohol) in ultrapure water) to minimize the effect of oxygen-induced

photobleaching of fluorescence. Control samples of AuMPCs that had not been mixed with AF514, as well as bare coverslides, coverslides that had been dosed with ultrapure water, and polymer coated coverslides showed no significant fluorescent impurities when examined under single-molecule imaging conditions.

For ensemble and single-molecule fluorescence imaging experiments, a home-built, wide-field epifluorescence microscope was used.[20] The output from a tunable argon-ion laser with a wavelength of 514 nm was passed through a spatial filter, collimated, and then focused by means of a 500 mm focal length lens onto the back focal plane of a 60×, 1.4 NA oil-immersion objective lens (PlanApo, Nikon). Fluorescence emission from the sample was collected through two long-pass filters (540LP, Omega Optical) to remove residual excitation light and directed onto a wide-area, front-illuminated electron multiplying CCD camera (Cascade 512F, Photometrics). A data collection rate of 1 frame per 100 ms was used.

5.4 Result and Discussion

5.4.1 Steady-state absorption and emission spectra

Steady-state spectra of the unconjugated AuMPCs and AF514 were collected and are shown in Figure 5-4, along with a transmission electron micrograph taken from a typical sample of AuMPCs. Absorbance spectra of the AuMPCs consisted of a single, decreasing shoulder across the measured spectral range, with no additional spectral features present. The AuMPCs do not exhibit a characteristic plasmon resonance absorption band, as was anticipated from the particle size determined from electron microscopy (1.8 ± 0.4 nm). The emission spectrum of AF514 consisted of a single broad band (emission maximum of 537 nm), which is comparable with that provided by the manufacturer, except for a small blue shift (~ 6 nm) in the emission maximum, which may be due to the slightly basic buffer solution used in these experiments. Given that AuMPCs with an average diameter that is less than 2 nm do not exhibit significant characteristic plasmon resonance absorption, the spectral overlap between the absorption of AuMPCs and the fluorescence emission is very limited. Thus, quenching of fluorescence emission due to coupling into the plasmon band is anticipated to be minimal.

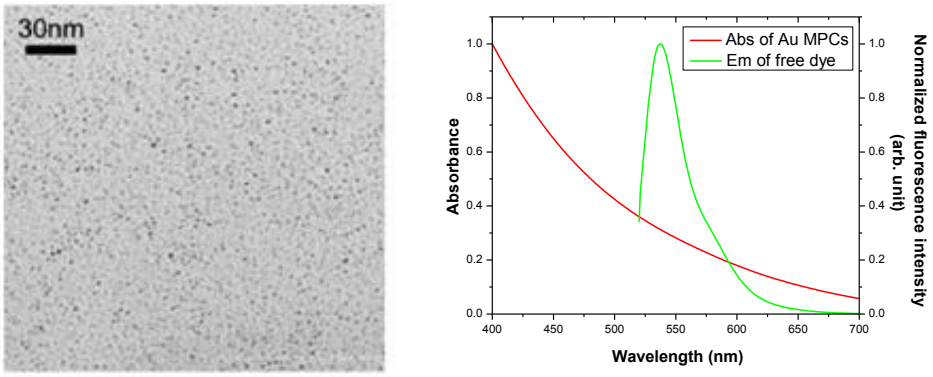

(A) **(B)**

Figure 5-4. (A) Transmission electron micrograph of Gly-CSA functionalized AuMPCs and (B) extent of spectral overlap of the absorption spectra of AuMPCs and the emission spectra of AF514 (sample excited at 514 nm in order to reproduce imaging conditions used in subsequent single-molecule fluorescence microscopy experiments).

Both absorption and emission spectra were collected for the dye-AuMPC particle conjugates prepared at different dye-AuMPC mixing ratios (moles of dye to moles of AuMPC; ratios adjusted by changing the amount of AuMPCs in the mixture). The absorbance spectra of the conjugates (not shown) were simply summations of the dye and AuMPC spectra without any additional features due to the conjugation reaction. Fluorescence emission spectra of the AF514 before and after conjugation were identical in shape and position of emission maxima, though a decrease in the overall fluorescence intensity was observed when increasing the concentration of AuMPCs in the mixture (shown in Figure 5-5). For comparison purposes, a series of emission spectra of mixtures of dye and AuMPCs immediately after mixing were collected and are also shown in Figure 5-5.

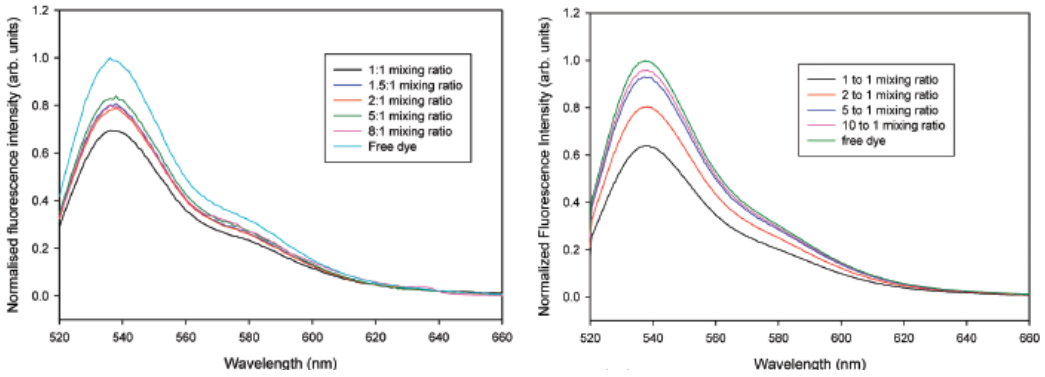

(A) **(B)**

Figure 5-5. Fluorescence emission spectra showing fluorescence intensity as a function of the AF514 to Gly-CSA AuMPC mixing ratio: (A) immediately after mixing, and (B) after overnight conjugation.

Comparison of parts A and B of Figure 5-5 indicates that there is little difference between the trends in fluorescence intensities of the AF514-AuMPC mixtures before and after the overnight conjugation period. This suggests that the conjugation reaction reaches completion shortly after mixing. However, the mixtures from both sets of reaction conditions do exhibit significantly lower fluorescence intensities in comparison with the dye alone, particularly at low dye to AuMPC mixing ratios. When the dye to AuMPC mixing ratio exceeds 2, the decrease in emission intensity that is caused by the presence of AuMPCs is negligible. This effect is explored in further detail, in conjunction with fluorescence lifetime measurements, in subsequent sections of this article.

Measurements were taken to examine the influence, if any, of free (unreacted) dye on the emission spectra of the mixtures through dialysis-based purification experiments. In these experiments, the dye to AuMPC mixing ratio was again adjusted by maintaining a fixed concentration of dye but changing the amount of AuMPCs in the mixture. After mixing, samples were extensively dialyzed to remove any unreacted dye. As a control experiment, a sample of free dye alone was also included. Emission spectra collected from the dialyzed mixtures and the control sample are shown in Figure 5-6. The fluorescence intensity of the mixtures decreased with increasing dye-AuMPC mixing ratio, which is the exact opposite of the observations from the unpurified conjugates. These results are consistent with only a small fraction of the fluorophores conjugating with the AuMPCs (typically around ~ 1-5 fluorophores per AuMPC).

That is, the majority of the dye that is mixed with the system does not react and is removed by dialysis; control samples of pure dye alone are only weakly fluorescent indicating that free dye is removed very efficiently. The decrease in fluorescence signal at high dye loading occurs because the majority of dye does not react with the particles and is removed by the purification step. The overall fluorescence signal is simply proportional to the quantity of labeled AuMPCs in the system, which increases with decreasing dye-AuMPC mixing ratio. While we cannot completely discount the possibility of low levels of desorbed Gly-CSA-dye linkages from the AuMPC surface (for recent reports of ligand exchange and desorption from AuMPCs see Ionita et al.[21,22]), we do note that the samples were synthesized, dialyzed, and examined under inert nitrogen atmosphere; previous work in our groups have shown that thiol desorption/oxidation on MPCs is more prominent in air and examinations of the Gly-CSA MPCs have shown that they are quite stable under inert atmosphere conditions.[19,23] Recent fluorescence correlation spectroscopy measurements by Navarro et al.[24] have been used to distinguish between desorbed dye molecules and those coupled with AuMPCs via determination of diffusion coefficients, and this approach might be of use in the future to quantify any contribution to the overall signal from desorbed dye.

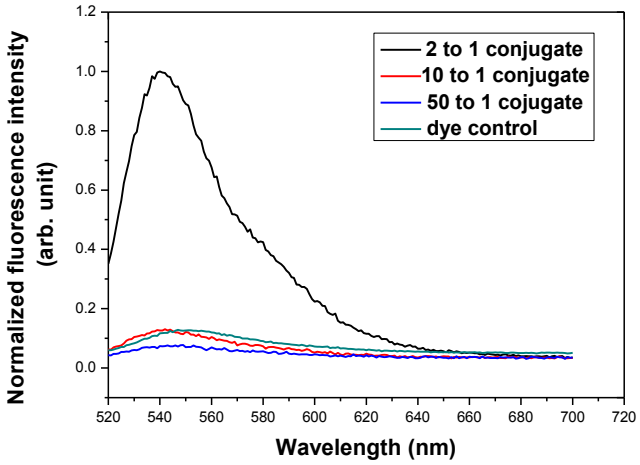

Figure 5-6. Fluorescence emission spectra for a series of dye-Au MPC mixtures and pure dye control sample after dialyzing for 5 days.

5.4.2 Lifetime measurement (TCSPC)

To gain further insight into the spectral properties of AF514 after its conjugation with AuMPCs, fluorescence lifetimes of dye-AuMPC conjugates (mixing ratios ranging from 1:1 to

5:1) were measured. Control measurements were also carried out for the free dye prepared in buffer solution. As shown in Table 5-1, fluorescence lifetimes of the conjugates were measured after dialysis, and showed no significant difference in comparison with the free dye prepared in buffer solution. Both free dye and conjugate samples were well fit well by a double-exponential decay (equation (5-1)) in which none of the fitting parameters (lifetimes or pre-exponential factors) were fixed.

$$I(t) = \alpha_1 e^{-t/\tau_1} + \alpha_2 e^{-t/\tau_2} \qquad (5\text{-}1)$$

Curving fitting of all samples indicated the presence of two distinct components, a long-lived component with a lifetime of 4.0 ns and a short-lived component with lifetime of 0.1 ns. For conjugates with different dye-particle mixing ratios, the pre-exponential factors of both long-lived and short-lived species remain unchanged within our ability to measure: 60% of fluorophores decay with the long lifetime and the remaining 40% decay with short lifetime. However, the 40% short-lived species could only contribute to ~ 2% of the overall fluorescence intensity. The overwhelming majority of the fluorescence emission is attributed to the fluorescence species with longer lifetime. These results are also comparable to the fitting data from the free dye samples prepared under the same solution conditions. We note that it is not immediately clear why all samples of AF514 (including the free dye) decay according to a two-component model; for a simple fluorophore in aqueous solution, a single-exponential decay is clearly the expected result. A number of chemical or photophysical effects may be at work here (e.g., aqueous equilibria, excited state processes, etc., for an example of another simple fluorophore system that shows multiexponential decay kinetics, see the work by Klonis[25]), though the presence of two components in the lifetime decay does not alter the principal result that the lifetimes are essentially unaltered by conjugation with the AuMPC.

Sample	Fitting parameters (two-component)				
	α_1	τ_1 (ns)	α_2	τ_2 (ns)	χ^2
dye blank (buffer)	0.62	4.1	0.37	0.2	1.1
dye/Au MPC (1:1)	0.59	4.1	0.41	0.1	1.1
dye/Au MPC (1.5:1)	0.67	4.1	0.33	0.2	1.2
dye/Au MPC (2:1)	0.48	4.1	0.52	0.1	1.0
dye/Au MPC (5:1)	0.65	4.1	0.35	0.2	1.0

Table 5-1. Fluorescence lifetime determined by single and double-exponential decay fits of the fluorescence decay profiles of samples prepared at different dye-AuMPC mixing ratios

The decrease in fluorescence intensity as a function of dye mixing ratio (Figure 5-5) is not trivial to reconcile with the lifetime data, as fluorescence quenching is often (though not always) associated with a change in the observed fluorescence lifetime. We can think of three possible mechanisms that give rise to this effect: (i) compensating changes in radiative and nonradiative decay rates, (ii) static quenching, and (iii) trivial inner filter effects. For case (i), the rate of fluorescence (k_f) can be written as a sum of radiative and nonradiative decay rates (k_{rad}, k_{nr}), and τ is the observed fluorescence lifetime:

$$k_f = \tau^{-1} = k_{rad} + k_{nr} \qquad (5\text{-}2)$$

If conjugation of the fluorophore to the AuMPC resulted in changes to both decay rates that were approximately equal in magnitude but opposite in direction changes, then the net fluorescence intensity of the fluorophore could be decreased with negligible (within the ability to deconvolute) changes to the measured lifetime. It seems highly unlikely for such an exact, coincidental change to occur, however, and mechanisms (ii) and (iii) seem significantly more plausible.

Static quenching typically results from the formation of a nonfluorescent complex between fluorophore and quencher. Chemical species in systems exhibiting static quenching will be complexed with a quencher and nonemissive, or will not be complexed and emissive with a lifetime equal to that of the system in the absence of quencher.[26] In some cases, static quenching can be recognized through subtle changes in absorption spectra caused by formation of a quenched complex; as noted previously, we observed no changes in the absorption spectra

(plotted on a linear energy scale to aid in comparison) upon conjugation. However, we have also performed a Stern-Volmer analysis to aid in mechanistic interpretation of the data. A standard Stern-Volmer analysis for simple static quenching indicates that quenching efficiency (ratio of fluorescence intensities for the quenched and unquenched system) should be linearly related to the quencher concentration [Q] (taken as the concentration of the AuMPCs):

$$Q_{eff} = \frac{F_0}{F} = 1 + K_S[Q] \qquad (5\text{-}3)$$

where F_0 and F are the fluorescence signal intensity for the unquenched and quenched species respectively, and K_s is the static quenching constant. To account for inner filter effects (photon reabsorption by the mixture components) we have applied the simple correction factor proposed previously by Lakowicz:[26]

$$F_{corrected} = F_{obs}C_1C_2 = F_{obs}10^{A_{ex}+A_{em}/2} \qquad (5\text{-}4)$$

where F_x are the fluorescence intensities for the corrected and observed signals, C_1 and C_2 are the first- and second-order inner filter correction factors, and A_{ex} and A_{em} are the solution absorbances at the excitation and emission wavelengths, respectively. Figure 5-7 shows the Stern-Volmer plot using fluorescence intensities corrected with equation 5-4, along with a linear fit based on equation 5-3. Clearly, the data is very well represented by the static quenching model, suggesting that quenching in this system can be attributed to the formation of quenched complexes between the fluorophore and AuMPC. A static quenching constant of K_s = 2.1 × 10^5 M^{-1} was calculated from the experimental data (R^2 = 0.9979).

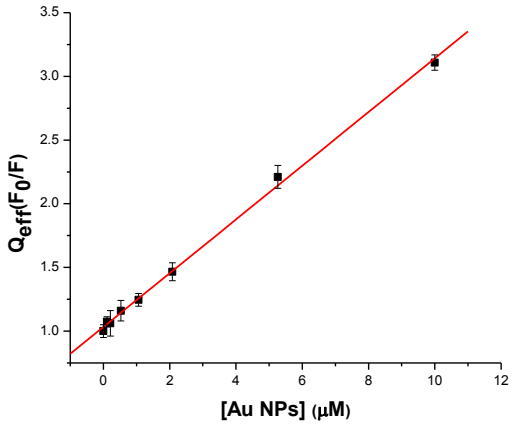

Figure 5-7. Stern-Volmer plot showing dependence of fluorescence quenching on concentration of AuMPCs, corrected for inner filter effects. The fitted static quenching constant is K_s = 2.1 × 10^5 M^{-1}.

It is of interest to compare the static quenching constant determined here with that obtained from a closely related system in which the fluorophore has not been covalently coupled to the particle. While it is difficult to find systems that are readily compared with the one described in this manuscript (particle sizes, compositions and fluorophores differ significantly), Cheng et al.[27] have reported on the quenching between tiopronin-decorated AuMPCs of a similar size to those reported here, and $[Ru(bpy)_3]^{2+}$ that was electrostatically associated with AuMPCs. Cheng et al. have reported static quenching constants of $\sim 5.9 \times 10^7$ M^{-1} for this system, with quenching constants increasing as a function of particle diameter. The approximately 2 orders of magnitude difference between quenching constants for comparable diameter particle suggests that the nature of the linker unit between fluorophore and AuMPC plays a crucial role in inhibiting quenching for the conjugated system. Presumably, for the quenched complex to form, the fluorophore and AuMPC must be in close proximity (and perhaps of the correct mutual orientation) and it seems highly likely that the short, rigid Gly-CSA linker hinders this association.

It is also worth noting that this result provides direct experimental support of the work by Munoz-Losa et al., in which it is suggested that effective excitation energy transfer between fluorophores and AuMPCs does not necessarily require the existence of surface plasmons, and, in some situations, can take place with comparable efficiency.[17] While the significant differences between the experimental system explored here and that described by Munoz-Losa (particle shape, nature of the fluorophore, separation, and geometry of fluorophore-quencher pair) preclude quantitative comparison, the qualitative agreement between the two approaches is excellent and highlights the importance of nonplasmonic particles when considering excitation energy transfer processes.

To summarize the results of the ensemble spectroscopy experiments, the measurements indicate that the conjugated fluorophores exist in one of two states: efficiently quenched through interaction with the AuMPCs or strongly emissive. The remainder of this investigation makes use of single-molecule fluorescence measurements to provide further evidence that this is the case.

5.4.3 Single-molecule fluorescence microscopy

To further explore the influence on fluorophore emission played by conjugation to Au MPCs, single-molecule fluorescence measurements were carried out via epifluorescence imaging of highly diluted ($\sim 10^{-8}$ M) dye-particle conjugates deposited on glass coverslips. Images consisted

of a series of discrete, brightly luminescent entities on a dark background, with the entities having diameters that were comparable to the diffraction limit of the excitation light (~ 300 nm). Because of the rigorous control experiments described in the Experimental Section, in combination with the fact that all of the dye-AuMPC conjugates had undergone extensive dialysis (the efficacy of which was demonstrated earlier in this manuscript) followed by 100-fold dilution in pure solvent, all of the fluorescent entities that were imaged could reasonably be attributed to AF514 molecules that were covalently bound to the AuMPCs. On a few occasions, extremely bright entities that were considerably larger than the ~ 300 nm diffraction limited size were observed. The source of these unusually large, emissive entities is currently unclear, though they likely consist of aggregated AuMPCs. These entities were excluded in subsequent data analysis.

In conventional single-molecule imaging experiments, fluorophores typically exhibit single-step photobleaching in their fluorescence time trajectories (integrated fluorescence emission intensity as a function of time) upon continuous illumination, as expected from the photodegradation of a discrete emitter.[15] For the systems studied here, fluorescence time trajectories that contained both individual photobleaching steps, as well as multiple, sequential photobleaching steps were observed. Several representative time trajectories that show the different types of photobleaching are shown in parts A-C of Figure 5-8 (single-step, two-step, and three-step photobleaching). It should be noted that the entities exhibited negligible repeated on-off blinking within the time resolution of the experiment, an effect that has been observed in a number of other single-molecule systems (see Ref 28 for example), regardless of the number of photobleaching steps. After a fluorophore underwent photobleaching, it was permanently nonemissive.

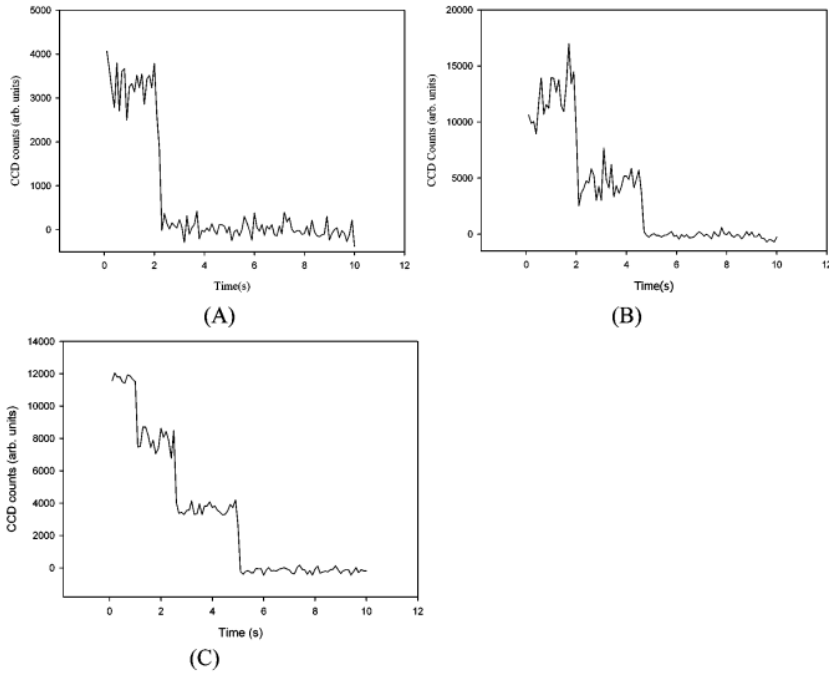

Figure 5-8. Representative fluorescence time trajectories of dye-AuMPC conjugates exhibiting (A) single-step photobleaching, (B) two-step photobleaching, and (C) three-step photobleaching collected by single-molecule microscopy (excitation intensity) 0.9 kW/cm^2 at 514 nm) of highly diluted ($\sim 10^{-8}$ M) samples.

Fluorescence time-trajectories were classified into four different subgroups according to the number of discrete photobleaching steps they exhibited (samples having one, two, three, and four well-defined steps were observed). The fraction of the total measured samples (over 200 particles measured per group) in each subgroup is summarized in Table 5-2 for four different dye-AuMPC loading ratios and the free dye alone. As shown in Table 5-2, at low dye-loading ratios, approximately >90% of the sample population photobleached in either a single or double step, with single-step photobleaching occurring slightly more frequently than double-step (a small fraction of free dye molecules showed two steps, but the vast majority photobleached in a single step). The remaining ~ 3-4% of the population photobleached in three discrete steps. As the dye-loading ratio was increased, there was a slight shift in favour of the formation of the double-step photobleaching, and at the 5:1 dye-AuMPC ratio, the three-step photobleaching frequency increased. Four-step photobleaching was only observed in samples prepared with this higher dye-loading ratio. The results of these single-molecule measurements are in excellent general agreement with the ensemble results, which indicated the average coordination number of dye on

each Au particle is between 1 and 2. While the use of higher dye-loading ratios resulted in a slight increase in the number of AuMPCs that were labeled with more than two fluorophores, the effect was quite small, indicating that saturation of the available conjugation sites had already occurred. The number of dye molecules that can be covalently bound to the AuMPC is surprisingly low, given that the entire particle surface is functionalized with reactive amine groups and an excess of reactive dye was used in the chemical synthesis. Of course, a fraction of the bound dye molecules will be statically quenched and nonemissive, but the combination of ensemble and single-molecule measurements provides compelling evidence that there is simply a small number of dye molecules bound to the AuMPCs. It seems plausible that the small particle diameters in combination with the relatively bulky fluorophore (long axis of the AF514 fluorophore is ~ 1.8 nm, as determined by MMFF molecular modeling calculations, Spartan '08) results in significant steric crowding, making the coupling of more than a few fluorophores problematic.

dye/AuMPCs	single step	two step	three step	four step
1 to 1	53%	43%	4%	0%
1.5 to 1	48%	48%	4%	0%
2 to 1	57%	40%	3%	0%
5 to 1	45%	46%	8%	1%
free dye	91%	9%	0%	0%

Table 5-2. Percentage distribution in number of step in photobleaching for the 1:1, 1.5:1, 2:1, 5:1 dye-AuMPC mixing ratios samples, as well as a free dye control sample

To further elucidate the influence of the AuMPC on fluorophore emission and to explore the nature of the static quenching process at the single-molecule level, an analysis of single-molecule fluorescence intensities of the photobleaching steps was carried out. Figure 5-9 shows histograms of fluorescence intensities taken from two dye-loading ratios, 1:1 to 5:1 (results from intermediate dye-loading ratios were comparable). Because of the appearance of multiple photobleaching steps, analysis of both the total fluorescence intensity of the entire entities, as well as the fluorescence intensity of each individual decay step in the multistep decays was carried out. Serving as a reference, the fluorescence intensity distributions of monomer AF514

were also measured under the same imaging conditions, and are included in Figure 5-9 for comparison. As seen via the histograms, the total fluorescence intensity showed minimal changes as a function of dye loading, indicating that the average compositions of the dye-particle conjugates are similar for all ratios. Again, this is the expected result from the ensemble measurements, which showed that only a small number of fully fluorescent molecules (~ 1-2) are present, regardless of the amount of dye used in the coupling reaction. The fluorescence intensity of the photobleaching steps also showed negligible differences between samples prepared at different dye-loading ratios, nor was there any indication that the fluorescence intensity of any individual photobleaching step in the multiple bleaching event decay curves varied significantly from the others. We interpret these results to mean that the fluorescence intensities of individual dye molecules bound to the AuMPC were essentially independent of the amount of dye present.

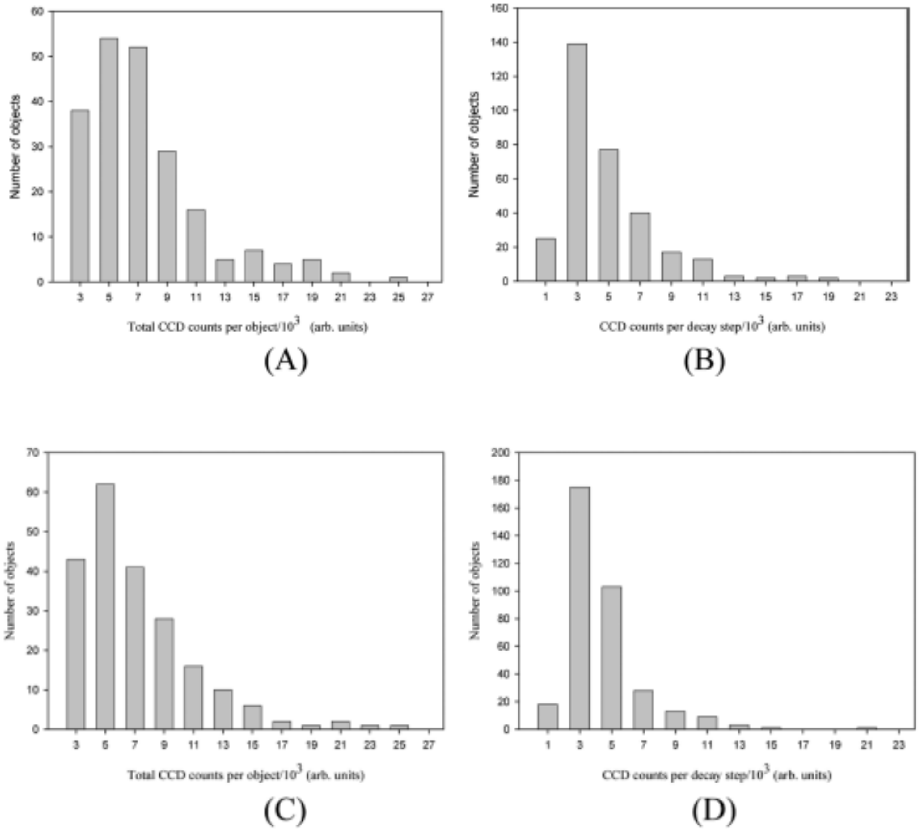

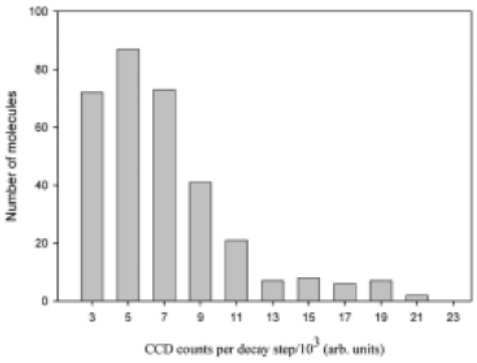

(E)

Figure 5-9. Histograms of fluorescence intensities from single-molecule measurements. (A) Total fluorescence intensity for entire entity, 1:1 dye-loading ratio, (B) fluorescence intensity of individual photobleaching steps, 1:1 dye-loading ratio, (C) total fluorescence intensity for entire entity, 5:1 dye-loading ratio, (D) fluorescence intensity of individual photobleaching steps, 5:1 dye loading ratio, (E) AF514 dye. (Excitation intensity in all cases was 0.9 kW/cm^2 at 514 nm).

It should be noted that there was a small but detectable difference in terms of fluorescence intensity between the pure dye control sample and dye-conjugated samples, with the mean fluorescence intensity of the control sample being marginally greater than that measured for the AuMPC-coupled fluorophores (mean ~ 4800 CCD counts/100 ms versus ~ 4500 CCD counts/100 ms). At present, it is difficult to rationalize this small difference in emission intensity with the available data; certainly, the ensemble data indicates that the small changes in fluorescence emission is from static quenching, and as such, we expected the individual molecules to exhibit the same fluorescence emission intensity as that measured for the coupled dye molecules. It is possible that there are purely single-molecule effects at work that cannot readily be detected using the relatively simple epifluorescence microscope system used in these experiments. Spectral wandering, for example, shifts in fluorescence emission spectra that are often seen in single-molecule experiments, could result in significant movement of the emission spectrum to shorter wavelengths where the optical filters of the microscope act to reduce net fluorescence signals. Subtle changes to fluorescence lifetime might also be taking place, though at present, limitations in instrumentation prevent us from probing these effects further. Efforts to refine our instrumental setup an enable these measurements at the single-molecule level are ongoing.

5.5 Conclusion

The fluorescent molecule AF514 was covalently coupled to monodisperse, 1.8 nm diameter AuMPCs, and the optical spectroscopy properties of the dye-AuMPC conjugate were examined through a combination of ensemble and single-molecule fluorescence measurements. It was observed that after coupling, the AF514 exhibits only minimal fluorescence quenching, with the reduced fluorescence intensity attributed to static quenching of some fraction of AuMPC-bound fluorophores in conjunction with self-absorption (inner filter) effects. Only a small number of fluorophores could be coupled to the AuMPCs, because the size of the AF514 molecules are comparable to that of the AuMPCs and steric hindrance prevents greater extents of dye loading. Single-molecule measurements verified these observations, with fluorescence time trajectories consisting of either single- or multiple-step sequential photobleaching, corresponding to the photobleaching of a small number of discrete, but strongly emissive fluorophores tethered to the AuMPC surface. The results in combination indicate that there are two populations of tethered fluorophores on the AuMPC surface, those that are efficiently quenched through interaction with the AuMPCs, and a separate population that remains strongly emissive and essentially unquenched.

5.6 Acknowledgments

Funding for this work was provided by the Natural Sciences and Engineering Research Council of Canada (NSERC), the Canada Foundation for Innovation (CFI), the Province of Saskatchewan and by the University of Saskatchewan. The Saskatchewan Structural Sciences Centre and Professor Ron Steer are acknowledged for providing access to the TCSPC equipment, and Dr. Sophie Brunet is thanked for providing assistance with lifetime measurements. Christina Calver is thanked for providing assistance with chemical synthesis.

5.7 References

1. Thomas, K. G.; Kamat, P. V. *Accounts of Chemical Research* **2003**, *36*, 888-898.

2. Aslan, K.; Perez-Luna, V. H. *Journal of Fluorescence* **2004**, *14*, 401-405.
3. Cannone, F.; Chirico, G.; Bizzarri, A. R.; Cannistraro, S. *Journal of Physical Chemistry B* **2006**, *110*, 16491-16498.
4. Chhabra, R.; Sharma, J.; Wang, H. N.; Zou, S. L.; Lin, S.; Yan, H.; Lindsay, S.; Liu, Y. *Nanotechnology* **2009**, *20*.
5. Mayilo, S.; Kloster, M. A.; Wunderlich, M.; Lutich, A.; Klar, T. A.; Nichtl, A.; Kurzinger, K.; Stefani, F. D.; Feldmann, J. *Nano Letters* **2009**, *9*, 4558-4563.
6. Nerambourg, N.; Werts, M. H. V.; Charlot, M.; Blanchard-Desce, M. *Langmuir* **2007**, *23*, 5563-5570.
7. Pons, T.; Medintz, I. L.; Sapsford, K. E.; Higashiya, S.; Grimes, A. F.; English, D. S.; Mattoussi, H. *Nano Letters* **2007**, *7*, 3157-3164.
8. Adams, D. M.; Brus, L.; Chidsey, C. E. D.; Creager, S.; Creutz, C.; Kagan, C. R.; Kamat, P. V.; Lieberman, M.; Lindsay, S.; Marcus, R. A.; Metzger, R. M.; Michel-Beyerle, M. E.; Miller, J. R.; Newton, M. D.; Rolison, D. R.; Sankey, O.; Schanze, K. S.; Yardley, J.; Zhu, X. Y. *Journal of Physical Chemistry B* **2003**, *107*, 6668-6697.
9. Dulkeith, E.; Ringler, M.; Klar, T. A.; Feldmann, J.; Javier, A. M.; Parak, W. J. *Nano Letters* **2005**, *5*, 585-589.
10. Ipe, B. I.; Thomas, K. G.; Barazzouk, S.; Hotchandani, S.; Kamat, P. V. *Journal of Physical Chemistry B* **2002**, *106*, 18-21.
11. Kamat, P. V.; Barazzouk, S.; Hotchandani, S. *Angewandte Chemie-International Edition* **2002**, *41*, 2764.
12. Jennings, T. L.; Singh, M. P.; Strouse, G. F. *Journal of the American Chemical Society* **2006**, *128*, 5462-5467.
13. Persson, B. N. J.; Lang, N. D. *Physical Review B* **1982**, *26*, 5409-5415.
14. Moerner, W. E.; Fromm, D. P. *Review of Scientific Instruments* **2003**, *74*, 3597-3619.
15. Moerner, W. E.; Orrit, M. *Science* **1999**, *283*, 1670-1676.
16. Anger, P.; Bharadwaj, P.; Novotny, L. *Physical Review Letters* **2006**, *96*.
17. Munoz-Losa, A.; Vukovic, S.; Corni, S.; Mennucci, B. *Journal of Physical Chemistry C* **2009**, *113*, 16364-16370.
18. Dasog, M.; Kavianpour, A.; Paige, M. F.; Kraatz, H. B.; Scott, R. W. J. *Canadian Journal of Chemistry-Revue Canadienne De Chimie* **2008**, *86*, 368-375.

19. Leontowich, A. F. G.; Calver, C. F.; Dasog, M.; Scott, R. W. J. *Langmuir* **2010**, *26*, 1285-1290.
20. Bagh, S.; Paige, M. F. *Canadian Journal of Chemistry-Revue Canadienne De Chimie* **2005**, *83*, 435-442.
21. Ionita, P.; Volkov, A.; Jeschke, G.; Chechik, V. *Analytical Chemistry* **2008**, *80*, 95-106.
22. Ionita, P.; Wolowska, J.; Chechik, V.; Caragheorgheopol, A. *Journal of Physical Chemistry C* **2007**, *111*, 16717-16723.
23. Dasog, M.; Scott, R. W. J. *Langmuir* **2007**, *23*, 3381-3387.
24. Navarro, J. R. G.; Plugge, M.; Loumaigne, M.; Sanchez-Gonzalez, A.; Mennucci, B.; Debarre, A.; Brouwer, A. M.; Werts, M. H. V. *Photochemical & Photobiological Sciences*, *9*, 1042-1054.
25. Klonis, N.; Sawyer, W. H. *Photochemistry and Photobiology* **2003**, *77*, 502-509.
26. Lakowicz, J. *Principles of fluorescence spectrosopy*; 2nd ed.; Kluwer Academic: New York, 1999.
27. Cheng, P. P. H.; Silvester, D.; Wang, G. L.; Kalyuzhny, G.; Douglas, A.; Murray, R. W. *Journal of Physical Chemistry B* **2006**, *110*, 4637-4644.
28. Clifford, J. N.; Bell, T. D. M.; Tinnefeld, P.; Heilemann, M.; Melnikov, S. M.; Hotta, J.; Sliwa, M.; Dedecker, P.; Sauer, M.; Hofkens, J.; Yeow, E. K. L. *Journal of Physical Chemistry B* **2007**, *111*, 6987-6991.

CHAPTER 6

CONCLUSIONS AND FUTURE WORK

6.1 Conclusions

In this PhD thesis, single-molecule (SM) fluorescence spectroscopy was used as a tool to probe the photophysical properties of a number of different fluorescent systems. By visualizing the fluorescence emission of individual molecules, spectroscopic studies at the SM level allow one to probe unexpected fluctuations and heterogeneities in a number of photophysical parameters, such as fluorescence intensities, photobleaching times, emission spectra, and fluorescence polarization. As an important addition to conventional ensemble measurements, SM techniques allow for the construction of frequency histograms of values for any measurable parameter. The new information that SM measurement provide enable us to probe the properties and processes (usually involves in electron, energy transfer and change in molecular conformation) which could not be fully understood from the bulk measurements.

The first part of the thesis focused on a characterization and comparison study of two closely-related calcium-ion indicators, Calcium-Green 1(CG-1) and Calcium-Green 2 (CG-2) using a combination of ensemble and SM optical microscopy. In terms of ensemble measurements, both indicators exhibited a strong increase in fluorescence intensity as a function of increasing [Ca^{2+}] below saturation conditions. Fluorescence lifetime measurements indicated that both CG-1 and CG-2 had two chemical forms co-existing in the solution: the long-lived specie corresponding to the highly-fluorescent Ca^{2+}-bound form, and the short-lived specie corresponding to the weakly-fluorescent Ca^{2+}-free form of the dye. From the SM measurements, it was found that the fluorescence intensity and photobleaching time of either CG-1 or CG-1 molecule was invariant with [Ca^{2+}]. Changes in ensemble fluorescence intensities could be simply correlated with the number of highly fluorescent dye molecules in solution.

Previous work [1] on CG-2 indicates that in Ca^{2+}-free solution, CG-2 exists primarily as a highly quenched dimer by forming an intramolecular exciton, where the molecular planes of two

fluorophores are parallel to each other. However, when bound to Ca^{2+}, the molecule adopts an extended and highly-fluorescent conformation with the molecular planes of the two fluorophores making an angle of ~ 120 ° to each other. The presence of two distinct peaks in absorption spectra of CG-2 at low [Ca^{2+}] demonstrates the excitonic splitting between the two fluorophores in CG-2 molecules in absence of calcium ion. However, the monomeric variant, CG-1, was expected to operate via a different mechanism (photoinduced electron transfer, PET). When CG-1 associates with Ca^{2+}, the PET process is retarded due to the significant increase in the oxidation potential of the Ca^{2+} binding site. The observations from both ensemble and SM measurements indicate that CG-1 molecule operates via PET. Comparison of the absorption spectra of CG-1 and CG-2 allowed for the definitive assignment of the two distinct peaks in CG-2 spectra at low [Ca^{2+}], which furthermore reinforced the previously proposed mechanism. In addition, the fluorescence intensity of a single CG-1 molecule was found to have half of the emission intensity of CG-2. This is another expected result, simply because CG-2, with two identical fluorophore in one molecule, will have an absorption cross-section that is approximately twice as large as CG-1.

To gain further insight into the molecular conformation of CG-2 upon binding with Ca^{2+}, modifications were made to convert the original epifluorescence microscope into a dual-polarization microscope. The new setup was used to characterize CG-2 at the SM level by comparing the fluorescence intensity of each CG-2 molecule in two mutually orthogonal polarization image channels. By constructing a frequency distribution of fluorescence polarization of CG-2, we were capable of extracting information on the relative orientation of the two fluorophores. Experimental results were compared with those predicted from a geometric model of randomly-orientated dimeric molecules. The results provided additional support that the molecular conformation of CG-2 changes when binding with calcium ion, such that the molecular plane of the two fluorophore will form an angle of ~ 120 °. In addition, further development of the geometric model demonstrates that the shape of the frequency diagram of fluorescence polarization is highly dependent on the relative angle between the two molecular planes of the dimeric system. This allows the further application of dual-polarization fluorescence imaging in studying of transition dipole orientations in other multifluorophoric molecules.

The solvatochromic behaviour of a lipid-sensitive dye, Nile Red (NR), which had been incorporated into a phase-separated Langmuir-Blodgett (LB) film, was investigated by ensemble and single-molecule spectroscopy. The film system used in this study was a mixture composed of two surfactants, perfluorotetradecanoic acid (PA) and arachidic acid (AA). Based on previous investigations by atomic force microscopy (AFM), the film phase-separates into discrete, micron-sized hexagonal domains (discontinuous domain) that are almost exclusively comprised of AA, and the surrounding continuous domain enriched in PA (occasionally contains small deposits of residual hydrocarbon). NR was spin-cast onto the LB films that contain two physically and chemically distinct regions (the hydrogenated and perfluorinated regions).[7,8] During the ensemble measurement, we simultaneously characterized the brightness of the fluorescence signal in different sample regions, and measured the emission spectra of NR in the different domains. The former was performed using epifluorescence microscopy, while the latter was characterized via fluorescence confocal spectromicroscopy. The results showed that NR preferentially associated with the hydrogenated domains with only a small subpopulation localized in the perfluorinated continuous domains. While the emission spectra of NR in different domains of the LB film displayed solvatochromism, its effect on generating the overall image contrast were negligible. The SM fluorescence imaging measurements indicated that the subpopulation of NR in the continuous domain was not spectroscopically distinguishable from that associated with the discontinuous domain, which further reinforced the idea that the image contrast for the system arises from stain accumulation in specific sample regions.

In the last sub-project, the fluorescence quenching of a strongly fluorescent probe, AlexaFluor 514 (AF514), was investigated when it was covalently bound to a gold metal protected cluster (AuMPC) with a negligible plasmon band. The quenching of fluorescence in conjugated systems of this type can often be attributed to either energy or electron transfer between the dye molecule and the nearby gold particle.[9-12] In most cases, the linker (covalent bond in our case) between the quencher and the photoexcited specie plays a very important role in the emission behaviour of the fluorophore.

In our system, only minimal fluorescence quenching was observed in the ensemble measurements at low dye/ AuMPC loading ratios due to the limited spectral overlap between the absorption spectrum of the acceptor (AuMPC) and the emission spectrum of the donor (AF514).

Furthermore, time-resolved measurements indicated that the fluorescence lifetime of AF514 remained invariant at different dye/AuMPC ratios. This result, in conjunction with the fluorescence emission spectra of conjugated samples after correction by inner filter effects, demonstrated a static quenching of the dye by the AuMPCs. From the SM fluorescence measurements, the luminescent conjugates could still be observed at all loading ratios. The majority of the fluorescence time-trajectories decayed to the background via either a single- or double-step photobleaching. However, the fluorescent species in conjugated dye samples were not spectroscopically distinguishable from the free, unbound AF514 molecules. On the basis of the observations, we concluded that the dye only reacted with the AuMPC at low ratios (between 1 and 2 fluorophores per AuMPC), and the fluorophores that are tethered to the gold particles will either become entirely non-fluorescent due to the static quenching, or stay strongly emissive and essentially unquenched.

6.2 Future Work

It is proposed that further investigations of the previous systems (including CG-1, CG-2, NR, AF514-AuMPC conjugate) could be carried out using the newly-constructed confocal spectromicroscope with single-molecule sensitivity. Through the use of this approach, one is able to measure the fluorescence trajectory and the emission spectra of the same fluorescent molecule in the same measurement, enabling a detailed spectroscopic analysis, which should provide complementary information to that already obtained.

The spectral properties of each individual molecule (including variations in spectral position, shape, width, and time dependence) can provide invaluable insight into heterogeneity in the molecular environment and local interactions. For immobilized SM samples in which lateral diffusion is negligible, emission spectra can be correlated with variations in transition dipoles, the conformational changes in molecules and the interaction between the fluorophore and the environment.

For the calcium-ion indicators, SM spectromicroscopy will allow characterization of the spectral properties of individual CG-1/CG-2 molecules upon excitation. As mentioned in the previous chapter, at zero calcium concentration, both CG-1 and CG-2 samples were not entirely free of fluorescence entities. The fluorescence emission at nominal $[Ca^{2+}]_{free}=0$ could be observed at both ensemble and single molecule level. It remains unclear that whether those fluorescent signals should be attributed to the trace amount of free Ca^{2+} ion in the solution or the distribution of the "highly-quenched" molecular conformation from the dye. By measuring the SM fluorescence emission spectra, one can construct frequency histograms of the emission maxima as a function of wavelength. The shape of the distribution is crucial in determining how many fluorescent species contribute to the overall emission intensity in the CG-1 and CG-2 systems.

For the NR system, by focusing the laser beam onto individual molecules in the different phase-separated regions, the NR molecules doped in both continuous and discontinuous domains of the LB film could be examined. As a result, the frequency histograms (of both fluorescence intensity and on-times) and the emission spectra of NR molecules could be obtained for different domains separately. By conducting these measurements, the detailed variation of NR in two significantly different micropolarities could be observed.

Furthermore, the APD detector which is used for SM spectromicroscopy has high temporal resolution and sensitivity, which will help us characterize events that are beyond the time resolution of the epifluorescence microscope. This would help us to determine whether there is any sub-millisecond photo-blinking taking place in the dye-Au MPC system due to the interaction between AF514 and gold nanosurface. Meanwhile, by characterizing the spectral dispersion of AF514 before and after conjugated with gold particles, we will gain further understanding on the underlying quenching mechanism.

In addition to the confocal spectromicroscope, other microscopic techniques could also be applied to gain further insight into the systems of our interests. For example, simultaneous atomic force and fluorescence microscopy could be applied to collect both morphological and fluorescence images of the same sample region. This could assist us to obtain further understanding of the relations between the photophysical property of a fluorophore and its surrounding. Such measurement will be of great significance for the phase-separated LB film

system, since the sample morphology (molecular height difference) is closely related to the nano-polarity.

Total internal reflection fluorescence microscopy (TIRF) could also provide some complementary information of the dye molecules regarding their relative depths in the specimen. The penetration depth of the evanescence wave will selectively illuminate and excite fluorophore in a restricted region on the sample surface. As a result, we are capable of localizing the fluorophores: whether they are floating on the top or penetrating into the sample matrix.

Furthermore, fluorescence lifetime imaging microscopy (FLIM) is an imaging technique for producing an image based on the difference in the exponential decay rate of the fluorescence in different sample regions. Serving as an important addition to the spectral detections, it could be used to recognize the variance of fluorescence lifetime of the same fluorophore in chemically and physically distinct nano-environments.

6.3 References

1. Bagh, S.; Paige, M. F. *Journal of Physical Chemistry A* 2006, *110*, 7057-7066.
2. de Silva, A. P.; Gunaratne, H. Q. N. *Journal of the Chemical Society-Chemical Communications* 1990, 186-188.
3. de Silva, A.; Gunnlaugsson, T.; Rice, T. *Analyst* 1996, *121*, 1759-1762.
4. Hou, Y. W.; Bardo, A. M.; Martinez, C.; Higgins, D. A. *Journal of Physical Chemistry B* 2000, *104*, 212-219.
5. Dutta, A. K.; Kamada, K.; Ohta, K. *Journal of Photochemistry and Photobiology A-Chemistry* 1996, *93*, 57-64.
6. Sarkar, N.; Das, K.; Nath, D. N.; Bhattacharyya, K. *Langmuir* 1994, *10*, 326-329.
7. Qaqish, S. E.; Paige, M. F. *Langmuir* 2007, *23*, 10088-10094.
8. Qaqish, S. E.; Paige, M. F. *Langmuir* 2007, *23*, 2582-2587.
9. Thomas, K. G.; Kamat, P. V. *Accounts of Chemical Research* 2003, *36*, 888-898.

10. Adams, D. M.; Brus, L.; Chidsey, C. E. D.; Creager, S.; Creutz, C.; Kagan, C. R.; Kamat, P. V.; Lieberman, M.; Lindsay, S.; Marcus, R. A.; Metzger, R. M.; Michel-Beyerle, M. E.; Miller, J. R.; Newton, M. D.; Rolison, D. R.; Sankey, O.; Schanze, K. S.; Yardley, J.; Zhu, X. Y. *Journal of Physical Chemistry B* 2003, *107*, 6668-6697.
11. Ipe, B. I.; Thomas, K. G.; Barazzouk, S.; Hotchandani, S.; Kamat, P. V. *Journal of Physical Chemistry B* 2002, *106*, 18-21.
12. Kamat, P. V.; Barazzouk, S.; Hotchandani, S. *Angewandte Chemie-International Edition* **2002**, *41*, 2764.

SPRINGER LICENSE
TERMS AND CONDITIONS

Oct 22, 2010

This is a License Agreement between Yin Lu ("You") and Springer ("Springer") provided by Copyright Clearance Center ("CCC"). The license consists of your order details, the terms and conditions provided by Springer, and the payment terms and conditions.

All payments must be made in full to CCC. For payment instructions, please see information listed at the bottom of this form.

License Number	2534490615588
License date	Oct 22, 2010
Licensed content publisher	Springer
Licensed content publication	Journal of Fluorescence
Licensed content title	An Ensemble and Single-molecule Fluorescence Spectroscopy Investigation of Calcium Green 1, a Calcium-ion Sensor
Licensed content author	Yin Lu
Licensed content date	Jan 1, 2007
Volume number	17
Issue number	6
Type of Use	Thesis/Dissertation
Portion	Full text
Number of copies	1
Author of this Springer article	Yes and you are the editor of the new work
Order reference number	
Title of your thesis / dissertation	Single-Molecule Fluorescence Microscopy Studies of Fluorescent Probes in Thin Films and on Nanoparticle Surfaces
Expected completion date	January 2011
Estimated size(pages)	120
Total	0.00 USD

Dear Yin,

Thank you for your email.
We hereby grant permission for the requested use expected that due credit is given to the original source. Please note that the author's permission is also required.

Name of the requestor: Yin Lu
Organization Name: University of Saskatchewan
Address: 110 Science Place, Saskatoon, SK, S7N 4X2
Country: Canada
Contact: +1(306) 966-1441
Type of use: Thesis/Dissertation
Title of the thesis: Single-molecule Fluorescence Microscopy Studies of Fluorescent Probes in Thin Films and on Nanoparticle Surfaces
Product Title: ChemPhysChem

You may use the version of the contribution as originally submitted for publication for an electronic presentation of the thesis. The contribution may not be updated or replaced with the published version. The version posted must contain a legend as follows: This is the pre-peer reviewed version of the following article: FULL CITE.

With kind regards,

Bettina
****

Bettina Loycke
Senior Rights Manager
Wiley-VCH Verlag GmbH & Co. KGaA
Boschstr. 12
69469 Weinheim, Germany

Phone: +49 (0) 62 01- 606 - 280
Fax: +49 (0) 62 01 - 606 - 332
E-mail: rights@wiley-vch.de

SPRINGER LICENSE
TERMS AND CONDITIONS

Jan 31, 2011

This is a License Agreement between Yin Lu ("You") and Elsevier ("Elsevier") provided by Copyright Clearance Center ("CCC"). The license consists of your order details, the terms and conditions provided by Elsevier, and the payment terms and conditions.

All payments must be made in full to CCC. For payment instructions, please see information listed at the bottom of this form.

Supplier	Elsevier Limited The Boulevard,Langford Lane Kidlington,Oxford,OX5 1GB,UK
Customer name	Yin Lu
Customer address	110 Science Place Saskatoon, SK, S7N 5C9, Canada
License Number	2599531319884
License Date	Jan 31st, 2011
Licensed content publisher	Elsevier
Licensed content publication	Spectochimica Acta Part A: Molecular and Biomolecular Spectroscopy
Licensed content title	An ensemble and single-molecule fluorescence microscopy investigation of phase-separated monolayer films stained with Nile Red
Licensed content author	Yin Lu, Robyn Porterfield, Terri Thunder, Matthew F. Paige
Licensed content date	January 2011
Licensed content volume number	78
Licensed content issue number	1
Number of pages	8
Start Page	216
End Page	223
Type of Use	reuse in a thesis/dissertation
Intended publisher of new work	other
Portion	full article

Format	both print and electronic
Are you author of this Elsevier article?	Yes
Will you be translating?	No
Order reference number	
Title of your thesis/dissertation	Single-molecule Fluorescence Microscopy Studies of Fluorescent Probes in Thin Films and on Nanoparticle Surfaces
Expected completion date	Jan 2011
Estimated size (number of pages)	120
Elsevier VAT number	GB 494 6272 12
Permission price	0.00 USD
Value added tax 0.0%	0.0 USD/0.0 GBP
Permissions price	0.00 USD
Total	0.00 USD

AMERICAN CHEMICAL SOCIETY LICENSE
TERMS AND CONDITIONS

Oct 22, 2010

This is a License Agreement between Yin Lu ("You") and American Chemical Society ("American Chemical Society") provided by Copyright Clearance Center ("CCC"). The license consists of your order details, the terms and conditions provided by American Chemical Society, and the payment terms and conditions.

All payments must be made in full to CCC. For payment instructions, please see information listed at the bottom of this form.

License Number	2534481037477
License date	Oct 22, 2010
Licensed content publisher	American Chemical Society
Licensed content publication	The Journal of Physical Chemistry C
Licensed content title	Fluorescently Labeled Gold Nanoparticles with Minimal Fluorescence Quenching
Licensed content author	Yin Lu et al.
Licensed content date	Oct 1, 2010
Volume number	114
Issue number	41
Type of Use	Thesis/Dissertation
Request type	Not specified
Format	Both print and electronic
Portion	Full article
Author of this ACS article	Yes
Title of your thesis / dissertation	Single-molecule Fluorescence Microscopy Studies of Fluorescent Probes in Thin Films and on Nanoparticle Surfaces
Expected completion date	January 2011
Estimated size(pages)	120
Billing type	Invoice
Billing address	110 Science Pl. Department of Chemistry Saskatoon, SK S7N 5C9 Canada
Total	0.00 USD

AMERICAN INSTITUE OF PHYSICS LICENSE TERMS AND CONDITIONS

Oct 19, 2010

This is a License Agreement between Yin Lu ("You") and American Institute of Physics ("AIP") provided by Copyright Clearance Center ("CCC"). The license consists of your order details, the terms and conditions provided by American Institute of Physics, and the payment terms and conditions.

All payments must be made in full to CCC. For payment instructions, please see information listed at the bottom of this form.

License Number	2532290701893
License date	Oct 19, 2010
Licensed content publisher	American Institute of Physics
Licensed content publication	Review of Scientific Instruments
Licensed content title	Methods of Single-Molecule Fluorescence Spectroscopy and Microscopy
Licensed content author	W. E. Moerner, David P. Fromm
Licensed content date	Aug 1, 2003
Volume number	74
Issue number	8
Type of Use	Thesis/Dissertation
Requestor type	Student
Format	Print and electronic
Portion	Figure/Table
Number of figures/tables	1
Title of your thesis / dissertation	Single-Molecule Fluorescence Microscopy Studies of Fluorescent Probes in Thin Films and on Nanoparticle Surfaces
Expected completion date	January 2011
Estimated size(pages)	120
Total	0.00 USD

NRC RESEARCH PRESS LICENSE
TERMS AND CONDITIONS

Oct 19, 2010

This is a License Agreement between Yin Lu ("You") and NRC Research Press ("NRC Research Press") provided by Copyright Clearance Center ("CCC"). The license consists of your order details, the terms and conditions provided by NRC Research Press, and the payment terms and conditions.

All payments must be made in full to CCC. For payment instructions, please see information listed at the bottom of this form.

License Number	2532310945112
License date	Oct 19, 2010
Licensed content publisher	NRC Research Press
Licensed content publication	Canadian Journal of Chemistry
Licensed content title	Construction and Application of a Single-Molecule Fluorescence Microscope
Licensed content author	Sangram Bagh and Matthew F. Paige
Licensed content date	May 1, 2005
Volume number	83
Issue number	5
Type of Use	Thesis/Dissertation
Requestor type	Academic
Format	Print and electronic
Portion	Figure/Table
Number of figures/tables	1
Order reference number	
Title of your thesis / dissertation	Single-molecule Fluorescence Microscopy Studies of Fluorescent Probes in Thin Films and on Nanoparticle Surfaces
Expected completion date	January 2011
Estimated size(pages)	120
Total	0.00 USD

AMERICAN INSTITUTE OF PHYSICS LICENSE TERMS AND CONDITIONS

Feb 04, 2011

This is a License Agreement between Yin Lu ("You") and American Institute of Physics ("AIP") provided by Copyright Clearance Center ("CCC"). The license consists of your order details, the terms and conditions provided by American Institute of Physics, and the payment terms and conditions.

All payments must be made in full to CCC. For payment instructions, please see information listed at the bottom of this form.

License Number	2597851246751
License date	Jan 28, 2011
Licensed content publisher	American Institute of Physics
Licensed content publication	Review of Scientific Instruments
Licensed content title	Time-resolved Detection and Identification of Single Analyte Molecules in Microcapillaries by Time-correlated Single-photon Counting (TCSPC)
Licensed content author	W. Becker, H. Hickl, C. Zander, et al
Licensed content date	Dec 31, 1999
Volume number	70
Issue number	3
Type of Use	Thesis/Dissertation
Requestor type	Student
Format	Print and electronic
Portion	Figure/Table
Number of figures/tables	1
Title of your thesis / dissertation	Single-Molecule Fluorescence Microscopy Studies of Fluorescent Probes in Thin Films and on Nanoparticle Surfaces
Expected completion date	January 2011
Estimated size(pages)	120
Total	0.00 USD

Dear Yin Lu,

you are welcome to use the figure.

Best regards

Wolfgang Becker
Becker & Hickl GmbH
Nahmitzer Damm 30
12277 Berlin
Tel. +49-30-787 56 32
Fax +49-30-787 57 34
becker@becker-hickl.com
http://www.becker-hickl.com
==========

Hello,

I am writing this E-mail to apply for your permission to reuse one of the figure in your TCSPC handbook in my PhD. thesis. My personal information is as follow,

Name: Yin Lu
Address: 110 Science Place, Department of Chemistry, University of Saskatchewan, Saskatoon, SK, S7N 4X2, Canada
Contact: +1 (306) 966-1441
Title of my thesis: Single-molecule Fluorescence Microscopy Studies of Fluorescent Probes in Thin Films and on Nanoparticle Surfaces
Name of the figure: Fig. 1 TCSPC Measurement Principle

If you need any other information regarding myself or my thesis, please let me know.

Regards,

Dr. Yin Lu
Department of Chemistry
University of Saskatchewan
Saskatoon, SK, S7N 4X2
Tel: +1(306)966-1441